

THE ADVANCEMENT OF COOLING
ABSORBERS IN COSY INFINITY

We'll have to come up with a better title

BY
JOSIAH D. KUNZ

Submitted in partial fulfillment of the
requirements for the degree of
Doctor of Philosophy in Physics
in the Graduate College of the
Illinois Institute of Technology

Approved _____
Advisor

Chicago, Illinois
May 2016

ACKNOWLEDGMENT

It goes without saying that I am grateful to God, who has guided me in my academic path and has allowed me to fulfil my dream of getting my Ph.D. in physics.
I would also like to thank my wife, Meredith Kunz, who has been by my side even before graduate school. I am very fortunate to have an advisor like Pavel Snopok, who puts in so much time and thought on my behalf. Pavel has worked with me on every turn, and has even allowed me to live in Indiana with my wife while finishing up graduate school. I could be no luckier than to have an advisor like him.

I would like to acknowledge the committee for their valuable time and selflessness: Dan Kaplan, Linda Spentzouris, Yagmur Torun, Jinqiao Duan, and of course Pavel Snopok. The Department of Energy is also acknowledged for funding me through Pavel.

On a less serious note, I would like to thank my late cat Scout, who slept on my lap through many of my COSY days. Although he did not make it to see the end result, he will not be forgotten. I would also like to thank my puppy Oliver for his patience with me while writing my thesis, and for keeping my mind fresh with breaks for playtime.

TABLE OF CONTENTS

	Page
ACKNOWLEDGEMENT	iii
LIST OF TABLES	vi
LIST OF FIGURES	ix
LIST OF SYMBOLS	x
ABSTRACT	xv
CHAPTER	
1. INTRODUCTION	1
1.1. Muon-based Accelerators	1
1.2. COSY Infinity	2
1.3. Introduction to Matter-Dominated Lattices	5
2. STOCHASTIC PROCESSES IN ICOOL	19
2.1. Straggling	19
2.2. Scattering	32
3. STOCHASTIC PROCESSES IN G4BEAMLINE	41
3.1. Straggling	41
3.2. Scattering	44
4. STOCHASTIC PROCESSES IN COSY INFINITY	48
4.1. Straggling	48
4.2. Scattering	51
4.3. Transverse Displacement	68
4.4. Temporal Displacement	69
5. RESULTS	72
5.1. Benchmark Against Other Codes	72
5.2. Validation	84
5.3. The Muon Ionization Cooling Experiment	87
6. SUPPLEMENTAL INFORMATION	92
6.1. A Brief Review of Particle Physics	92
6.2. Explicit Forms of the Dirac Gamma Matrices and Pauli Matrices	94

6.3. Proofs of Useful Dirac Gamma Matrix Trace Identities	95
6.4. Scattering Amplitude from Figure 4.2	99
BIBLIOGRAPHY	101

LIST OF TABLES

Table	Page
-------	------

LIST OF FIGURES

Figure	Page
1.1 The current model of particle physics. Image courtesy of [2].	1
1.2 Phase space vector \mathbf{Z} . Coordinates are transverse positions (x, y) , time-of-flight in units of length (l), transverse angles w.r.t. the reference particle (a, b) , and kinetic energy deviations w.r.t. the reference particle (δ) . The 0 subscript in the definitions denotes the reference particle's properties.	4
1.3 The reference orbit.	4
1.4 Example of some map \mathcal{M} creating a bijection from s_0 to s_1	5
1.5 Example of two maps $\mathcal{M}(s_0, s_1)$ and $\mathcal{M}(s_1, s_2)$. These two maps may be multiplied together to reduce to a single map, $\mathcal{M}(s_0, s_2)$	5
1.6 Classical muon-target interaction model courtesy of [7].	7
1.7 Quantum muon-target interaction model. The incoming particle wavefunction is represented as a plane wave and is scattered locally as a spherical wave. Image courtesy of [6].	8
1.8 Proposed muon accelerator shematics.	9
1.9 Cartoon of a cooling channel.	10
1.10 Vectoral depiction of ionization cooling in Figure 1.9.	11
1.11 Left: example beam with no x - θ correlation. Right: example beam with significant x - θ correlation.	12
1.12 Stopping power curve for antimuons on copper, courtesy of [13].	16
1.13 Energy loss table for muons in iron. Table courtesy of [14].	17
2.1 Plot of $\int w(u)(1 - e^{-pu})du$	29
2.2 Example of the Landau function.	31
2.3 Quantum scattering model.	34
2.4 Two parts of Green's function with their poles at $s = \pm k$, altered to be closed via semicircle at $ s = \pm\infty$	37
4.1 λ_{max} vs. $\langle \lambda \rangle$ over a variety of liquid hydrogen absorber lengths and initial beam momenta. The black line is the fitted curve (see Eqn. 4.2) and the pink line is the form given by Geant 3 (see Eqn. 4.1).	50

4.2	Feynman diagram for electron-muon scattering. P_1 and P_2 are the incoming four-momenta for the electron and muon and P_3 and P_4 are the outgoing four-momenta. Q represents the four-momentum carried by the virtual photon.	52
4.3	COSY treatment of muon-electron scattering. Since the routines are called separately, the model assumes no straggling while scattering.	59
4.4	Example of the cumulative angular distribution function for muons of 200 MeV/c through 1 mm of liquid hydrogen. Note that the y-axis is log scaled due to the very sharp peak. Furthermore, note that u_0 is greatly exaggerated, since its actual value for these parameters is 0.9999992.	63
4.5	Example of the first iteration of the algorithm to obtain the true u (in green). The true G is chosen uniformly from $G \in [0, G_{max}]$. If $G < G_0$, then the tail is sampled via bisection method. In this case, since $\bar{G} < G$, \bar{u} is the new u_{min} and \bar{u} is calculated again.	65
4.6	Example of a muon entering an absorber (purple) with some nonzero initial angle θ_o . The muon then scatters an angle θ_s with respect to its initial momentum \vec{p} . The scattering distribution $g(u)$ assumes a straight, on-axis particle ($x = y = p_x = p_y = 0$), and so is in the rotated frame, represented by T_R, z_R	67
4.7	Two examples of true paths which a particle might take when traversing a medium. Note that both the red path and green path have the same final scattered angle but different transverse positions.	69
5.1	MuScat results for 109 mm of liquid hydrogen compared against COSY (red), G4BL (green), and ICOOL (blue).	85
5.2	MuScat results for 159 mm of liquid hydrogen compared against COSY (red), G4BL (green), and ICOOL (blue).	86
5.3	MuScat results for 3.73 mm of beryllium compared against COSY (red), G4BL (green), and ICOOL (blue).	87
5.4	MICE Stage III cell. Left: rotated such that the y-axis points out of the page. Right: rotated such that the x-axis points into the page.	88
5.5	Diagram of obtaining a vector of rank SIZE via 2^n method. Typically 2^n is either much less than or much greater than the intended SIZE	91
6.1	Feynman diagram for electron-muon scattering. P_1 and P_2 are the incoming four-momenta for the electron and muon and P_3 and P_4 are the outgoing four-momenta. Q represents the four-momentum carried by the virtual photon.	100

6.2 Mathematical interpretation the three branches of the Feynman diagram in Figure 6.1. The top part is the muon flow, the middle is the virtual photon, and the bottom is the electron flow.	100
--	-----

LIST OF SYMBOLS

Symbol	Definition
$g(u)$	Angular distribution function
θ_0	Angular distribution Gaussian width
s	Arc length coordinate
Z	Atomic charge
N	Atomic density
N_A	Avagadro's Number
(px, py, pz)	Beamline momentum coordinate system
(x, y, z)	Beamline position coordinate system
u_0	Characteristic cosine variable
Q_i	Charge number of particle i
π	Circle constant
$*$	Complex conjugate
K	Constant (context dependent)
$u = \cos \theta$	Cosine variable (context dependent; see also 'Dummy variable')
ζ	COSY amplitude of scattering tail
b_c	COSY offset of scattering tail
Σ	Cross section
δ	Density correction parameter (straggling; see also 'Dirac function')
\checkmark δ	Dirac function (see also 'density correction parameter')
γ^α	Dirac gamma matrix

f	Distribution function (general; context dependent)
h	Distribution function (general; context dependent)
F	Distribution function antiderivative (general; context dependent)
H	Distribution function antiderivative (general; context dependent)
u	Dummy variable (context dependent; see also ‘Cosine variable’)
z_{ch}	Electric charge
N_{el}	Electron density
e^-, e^+	Electron or antielectron
m_e	Electron mass
$\nu_e, \bar{\nu}_e$	Electron neutrino or electron antineutrino
r_e	Electron radius
ϵ	Emittance (see also ‘energy loss fluctuation’)
E	Energy (general; context dependent)
$g(E)$	Energy loss distribution function
$\Delta E = \epsilon$	Energy loss fluctuation (see also ‘emittance’)
$\langle dE/dx \rangle$	Energy loss per unit length, mean (Bethe Bloch)
C_{Euler}	Euler’s constant (≈ 0.577)
P	Four-momentum
\checkmark	e Fundamental charge (such that $z_{ch} = eQ$)
a, b_r, d_r, p_g, q_g	GEANT4 angular parameters
z_g	Geometric path length

\dagger	Hermitian conjugate (see also ‘transpose conjugate’)
h_i	Highland corrections ($i = 1, 2$)
b	Impact parameter
I	Ionization energy (mean)
λ	Landau parameter
ϕ	Laplace transformed function
P_k	Legendre polynomials
L	Length (of absorber or step size)
γ	Loretnz factor
m	Mass (general; context dependent)
\mathcal{M}	Matrix element (scattering) (see also ‘Scattering amplitude’)
T_{max}	Maximum transferrable kinetic energy
μ	Mean (context dependent; see also ‘Muon’)
η	Minkowski metric
M	Moments of a function
p	Momentum (total)
μ	Muon (context dependent; see also ‘Mean’)
m_μ	Muon mass
ν_μ	Muon neutrino
C, C_i	Normalization constant (see also ‘Shell correction parameter’)
f_i	Oscillator strengths
σ^j	Pauli matrices

h	Planck's constant
\hbar	Planck's constant divided by 2π
X_0	Radiation length
θ	Scattered angle
\mathcal{M}	Scattering amplitude (context dependent; see also 'transfer map')
$g(u)$	Scattering function
C	Shell correction parameter (for straggling; see also 'Normalization constant')
Ω	Solid angle
c	Speed of light in a vacuum
U	Spinor
σ	Standard deviation
$g(E)$	Straggling function
t	Time (variable)
ℓ	Time-of-flight in units of length (COSY coordinate)
λ_k	Transport free mean paths, k^{th} value
\dagger	Transpose conjugate (see also 'Hermitian conjugate')
T	Transpose of a matrix
T	Transverse coordinate
t_z	True path length
I_j	Unit matrix of rank j
\vec{v}	Unit vector

λ_v	Vavilov parameter
κ	Vavilov limit parameter
v	Velocity
ψ	Wavefunction, time-independent component
w	Weight for a distribution function (context dependent)

ABSTRACT

Abstract goes here!

CHAPTER 1

INTRODUCTION

1.1 Muon-based Accelerators

Muons (μ) were first discovered experimentally in 1947 by Powell et. al [1] who were looking for the Yukawa meson. It is now known that muons in fact fit into a fundamental particle group called leptons, and fit into the standard model as shown in Figure 1.

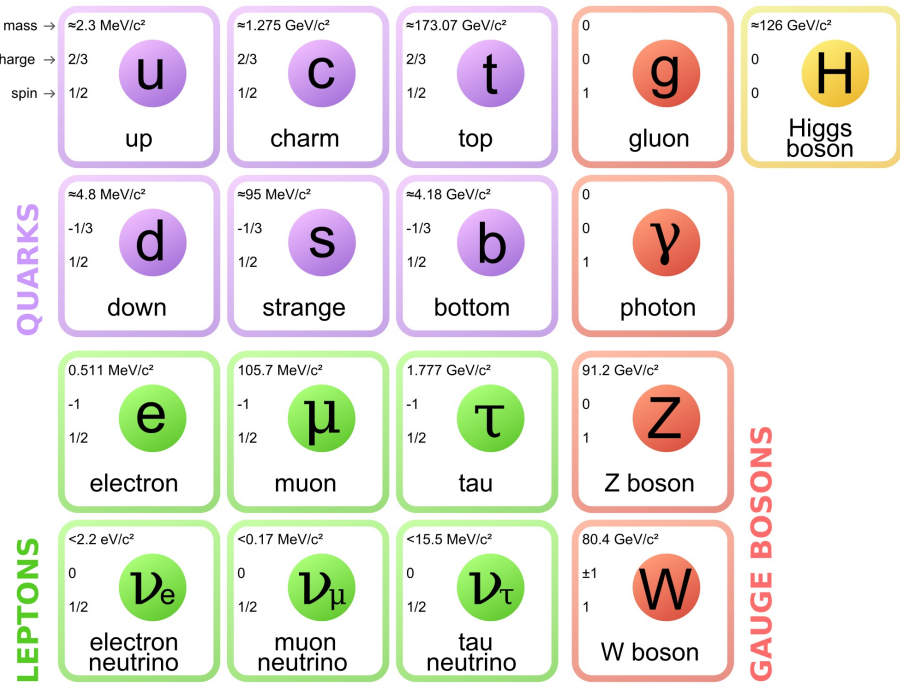


Figure 1.1: The current model of particle physics. Image courtesy of [2].

Similar to the electron (e), the muon carries a fundamental charge of ± 1 , a spin of $1/2$, and observes the electromagnetic and weak forces. Moreover, the muon also has a corresponding neutrino: the muon neutrino (ν_μ). However, the muon (mass = $105.7 \text{ MeV}/c^2$) is about 200 times heavier than the electron (mass = $0.511 \text{ MeV}/c^2$).

Indeed, sometimes it is useful to think of a muon simply as a heavy electron, but the mass implies several unique characteristics. One of these are the instability of muons, since the following process is not forbidden by mass, charge, or lepton number conservation:

$$\mu \rightarrow e + \bar{\nu}_e + \nu_\mu.$$

*bar should be over ν only, not the combination $\bar{\nu}_e$
($\bar{J}_e \rightarrow \bar{J}_e$)*

✓

This is quite interesting, as it means muons are a double-edged sword. On the one hand, their fundamentality means that the muon collisions will be clean. This is (what is "clean collision", etc) a great advantage over baryon collisions, since baryons are composed of three quarks and therefore their collisions are not clean? why? how? (e.g. protons, neutrons). Consequently, any data from muon interactions will have relatively little noise and will not require the burden of jet analysis (as is sometimes the advantage of linear electron colliders). Yet unlike the electron, the muon does not emit a large amount of synchrotron radiation as it is accelerated. For this reason, it is possible to have a circular muon accelerator, and one far smaller than the equivalent baryon accelerator due to its small comparative mass. On the other hand, a rest frame lifetime of $2 \mu\text{s}$ requires the muons to be accelerated fast before they decay. This is a challenge for circular colliders which require a high luminosity beam.

*"overall" or "thus"**↳ define the term*

Now, it appears that there are several good advantages and only one disadvantage: the $2 \mu\text{s}$ mean rest frame lifetime of the muon. However, this is only a disadvantage for muon colliders. Another application which turns the moderately short lifetime into an advantage is that of a neutrino factory. The concept of a muon storage ring has existed since 1960 [3], and its list of advantages only grows with time.

1.2 COSY Infinity

COSY Infinity is a beamline simulations tool used in the design, analysis, and optimization of particle accelerators [4]. To do this, COSY uses the transfer map approach, which evaluates the overall effect of a system on a beam of particles using

(*) we'll have to modify this: usually people talk about "hadron" colliders even though what's really meant is "protons or antiprotons", no one is accelerating neutrons or pions
I'd say, since you are giving an example, say "proton colliders" or "hadron colliders", and leave out what's in parentheses, or say "(e.g. protons)"

differential algebra) involving multivariate Taylor polynomials up to arbitrary order).

While a transfer map is technically not a nonlinear matrix, it is sometimes helpful to think of them as one in the same. Along with the evaluation of particles through a lattice, COSY also has a plethora of analysis and optimization tools, including (but not limited to) lattice aberration and correction tools, support for Twiss parameters, support for tunes and nonlinear tune shifts, built-in optimizers (for lattice design), and spin tracking.

COSY is particularly advantageous to use when considering the efficient use of computational time. This is due to the transfer map methods that COSY employs.

Given some initial phase space vector $\mathbf{Z}(s_0)$ (see Figure 1.2), the transfer map \mathcal{M} will uniquely predict the time evolution of \mathbf{Z} . This is because most beam elements follow Maxwell's equations, which yield unique solutions that are dependent on initial conditions. Mathematically, this relationship is $\mathbf{Z}(s) = \mathcal{M}(s_0, s) * \mathbf{Z}(s_0)$. Here, the independent variable s is understood as the reference orbit (the zero point of a beam of particles in some comoving reference frame—see Figure 1.3). An example of this relationship can be seen in Figure 1.4. The initial phase space occupied by the beam of particles is at the coordinate s_0 . Physically, there exists some deterministic beamline element. This element can be represented by the map \mathcal{M} , which creates a bijection for the phase space vectors $Z(s_0)$ and $Z(s)$ between the initial coordinate s_0 and an arbitrary final coordinate s .

Valid elements are any beamline tools which are deterministic. Elements used in this study are magnetic multipoles (dipoles, quadrupoles, etc.), RF cavities, and drifts. Currently supported elements in COSY include but are not limited to: various magnetic and electric multipoles (with fringing effects), homogeneous and inhomogeneous bending elements, Wien filters, wigglers and undulators, cavities, cylindrical

What about solenoids? we don't really use any dipoles and quads, but those should work out of the box, of course, so just mention solenoids along with multipoles

This will have to be rephrased, otherwise it is not clear why you need to even talk about Fig. 1.3, co-moving frame, beam size, etc.

to preserve uniqueness

electromagnetic lenses, general particle optical elements, and deterministic polynomial absorbers of arbitrary order, with the last element being of particular interest.

$$\mathbf{Z} = \begin{pmatrix} x \\ y \\ l = k(t - t_0) \\ a = p_x/p_0 \\ b = p_y/p_0 \\ \delta = (E - E_0)/E_0 \end{pmatrix}$$

→ you've mentioned it, so you should probably explain your interest, however briefly, before getting back to transfer maps? Or are you building up suspense?

Figure 1.2: Phase space vector \mathbf{Z} . Coordinates are transverse positions (x, y), time-of-flight in units of length (l), transverse angles w.r.t. the reference particle (a, b), and kinetic energy deviations w.r.t. the reference particle (δ). The 0 subscript in the definitions denotes the reference particle's properties. Introduce k

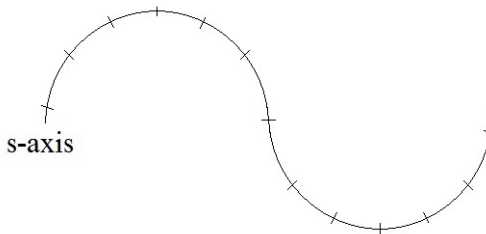


Figure 1.3: The reference orbit.

either add a ref. to martin's lectures, or redo the picture yourself (and potentially add either a few trajectories or some beam envelope)

Now, the composition of two maps yeilds another map: $\mathcal{M}(s_1, s_2) \times \mathcal{M}(s_0, s_1) = \mathcal{M}(s_0, s_2)$. Therefore, it is possible to "cut out" the middle part s_1 . "two single right quotes"

This we will need to rethink
a bit, so that
it mentions "building up a transfer map of the system from the transfer map of components or subsections"
physical lattice corresponds to some transfer map, it is possible to construct a single map that represents many individual lattices. An example of this can be seen in Figure 1.5. Computationally this is advantageous because once calculated, it is much faster

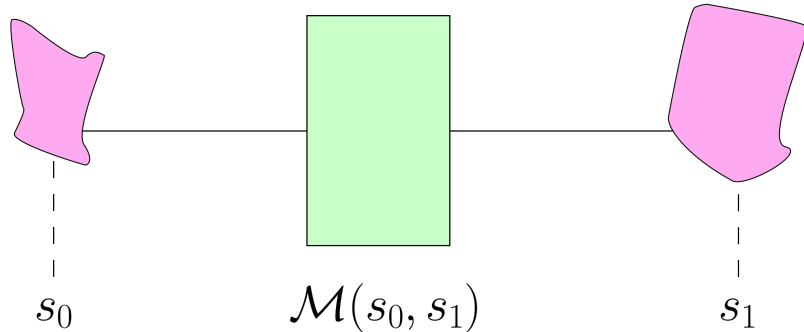


Figure 1.4: Example of some map \mathcal{M} creating a bijection from s_0 to s_1 .

to apply a single transfer map to a distribution of particles than to simulate that same distribution through many meters of lattices, elements, individual

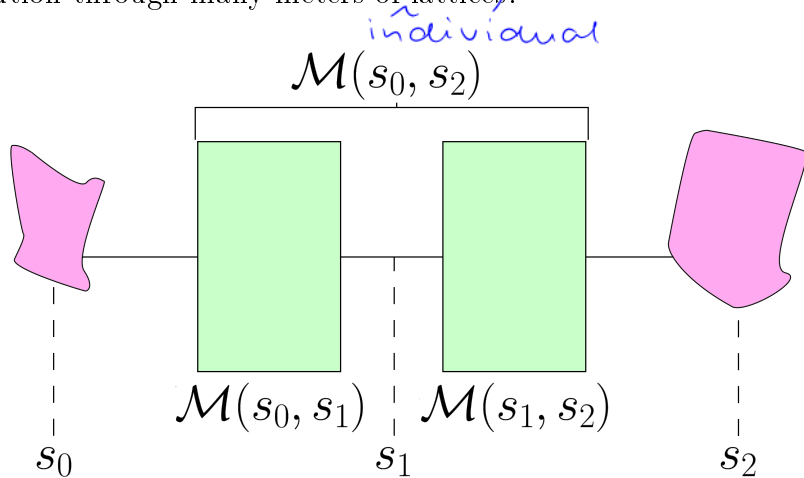


Figure 1.5: Example of two maps $\mathcal{M}(s_0, s_1)$ and $\mathcal{M}(s_1, s_2)$. These two maps may be multiplied together to reduce to a single map, $\mathcal{M}(s_0, s_2)$.

☞ careful here, it's only "multiplied" if M is a linear map. I'd use "combined"

1.3 Introduction to Matter-Dominated Lattices

1.3.1 Introduction to Stochastic Effects.

This whole passage is unnecessarily complicated and I'm sure by the end of it the reader is lost.
 Should be rephrased in a more straight-forward fashion.
 Writing center might help? or just some victim of a friend, maybe?

This next section introduces stochastic effects, or effects which are intrinsically random. These are not to say effects which are deterministic, but approximated as random, as is the case in classical thermodynamics. In classical thermodynamics, a system has a very large number of particles. These particles and their evolution through time may be kept track of by a set of deterministic interactions (computational biophysics does this well with protein folding), but classically they are approximated simply as a random set. In this sense, the large thermodynamic system is not stochastic, since it fails to be *intrinsically* random. This is not the case with computational beam physics, as the models involved typically require close range, dissipative forces, and quantum effects. It's not that the interactions are deterministic but difficult to keep track of, for that would require better bookkeeping or more precise measurements; rather the interactions are random by nature, deterministically unpredictable by no fault of the observer.

As discussed in the next section, this work is concerned with the interactions between a muon beam and some stationary target called the 'absorber'—typically a cylinder or wedge filled with liquid hydrogen. The simplest model of a beam interacting with some stationary target can be found in several textbooks [5,6], but perhaps the most helpful model comes from [7] in Figure 1.6.

Here b is referred to as the impact parameter and is measured with respect to the particle's initial trajectory. For a beam of noninteracting particles and a perfectly stationary target, classical mechanics suggest that this is a purely deterministic problem (see, e.g., 'hard-sphere scattering' in [6]); the particle with a smaller impact parameter b will deflect more than its neighbor with a slightly larger impact parameter of $b + db$. This model is entirely based on initial conditions, and if this were reality it would be relatively easy to implement these effects into the map methods of COSY Infinity. However, reality does not follow the model of Figure 1.6. A more

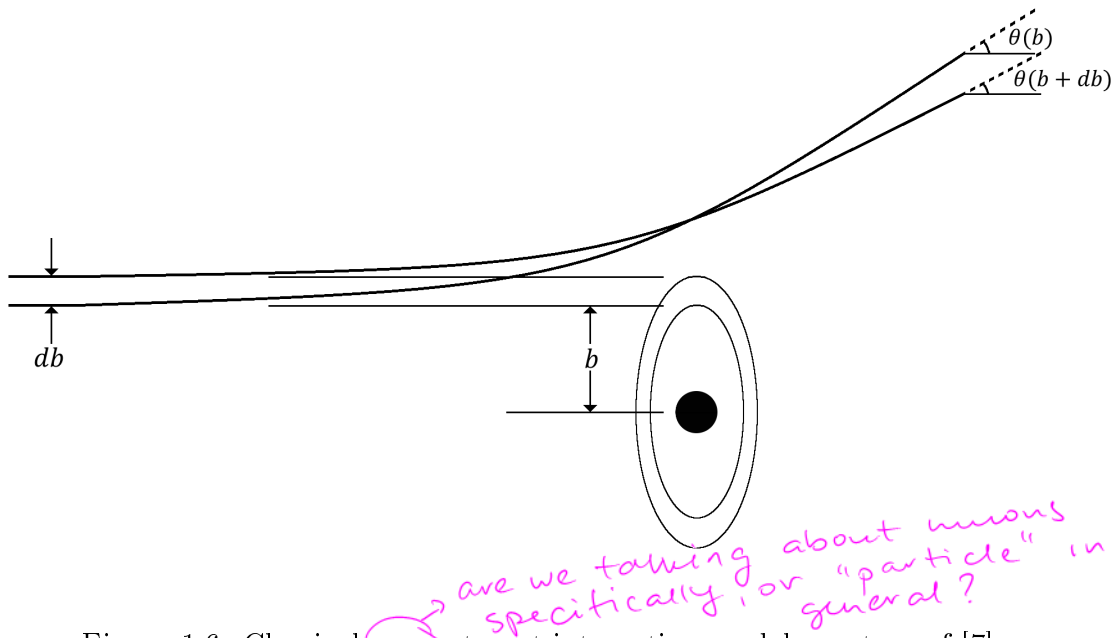


Figure 1.6: Classical muon-target interaction model courtesy of [7].

accurate model is illustrated by Figure 1.7. Here the target is still approximated as fixed, but the incident particle is now approximated as a travelling plane wave and the scattered particle is approximated as a spherical wave (at least locally). It will be shown later that this model predicts

1. a spectrum of energy loss $\omega(\epsilon)$ which yields the probability of losing an amount of energy ϵ (see Section 2.1), and
2. a scattering amplitude which gives the form of the probability of scattering in a given direction θ (see Section 2.2).

✓ Hence, quantum theory suggests that even if two identical particles have identical initial conditions their final conditions will not be the same. I'm pretty sure there are other disadvantages too, so I

1.3.2 Muon Ionization Cooling. In Section 1.1, the only real disadvantage would not be so to any muon-based accelerator was the mean muon rest frame lifetime ($2 \mu\text{s}$). This is expected to be far too short of a timespan to be useful in a traditional acceler-

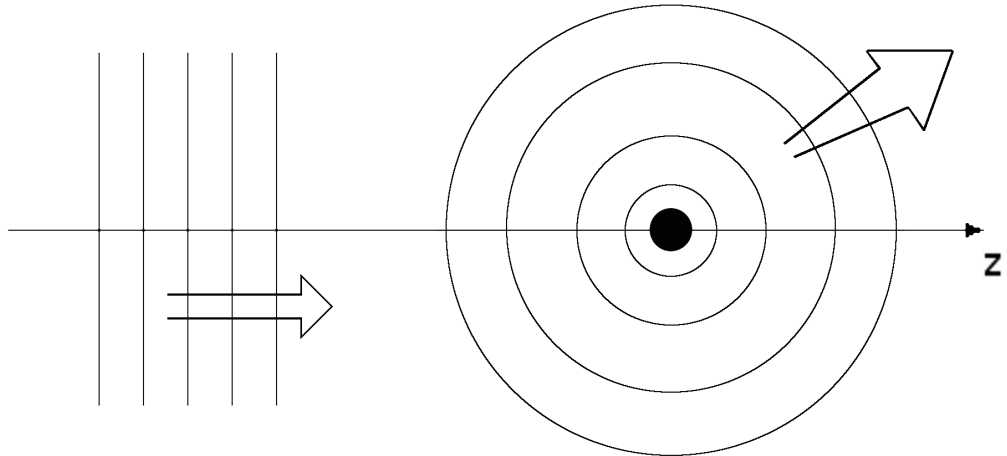


Figure 1.7: Quantum muon-target interaction model. The incoming particle wavefunction is represented as a plane wave and is scattered locally as a spherical wave. Image courtesy of [6]. This diagram is rather useless without more explanation, and potentially adding something to the figure itself.

ator scheme. For the moment, observe the two proposed schematics in Figure 1.8. [Reference map]

The section labelled ‘Proton Driver’ produces the source protons, which will eventually yield (avoid repetition) either “is the source” or “produces protons” which? target (which must be optimized to produce the highest yield), resulting in a spray of protons, muons, electrons, and pions (even shorter-lived particles consisting of a quark-antiquark pair). To further optimize this process, it is advantageous to let the resulting ensemble pions decay into muons via $\pi^\pm \rightarrow \mu^\pm + \nu_\mu$. The large assemblage of muons is then split up into bunches and propagated through the phase rotator. The next section is either explain what it is where all of the interesting physics lies, and is the topic of this entire thesis. For now, briefly, focal point? or drop it altogether it will be simply addressed as the ‘cooling channel’ and delved into later. Cooling the beam reducing beam simply means to reduce the bunch’s transverse phase space—that is, it means to limit not necessarily, there is limiting the beam’s immediate physical size and possible future physical size in the transverse em-dash, no space longitudinal cooling and 6D cooling as well. Suggest dropping “transversal” momentum components are reduced, and it takes some distance for that to translate into beam size reduction. (You can find better ways to describe cooling in various sources)

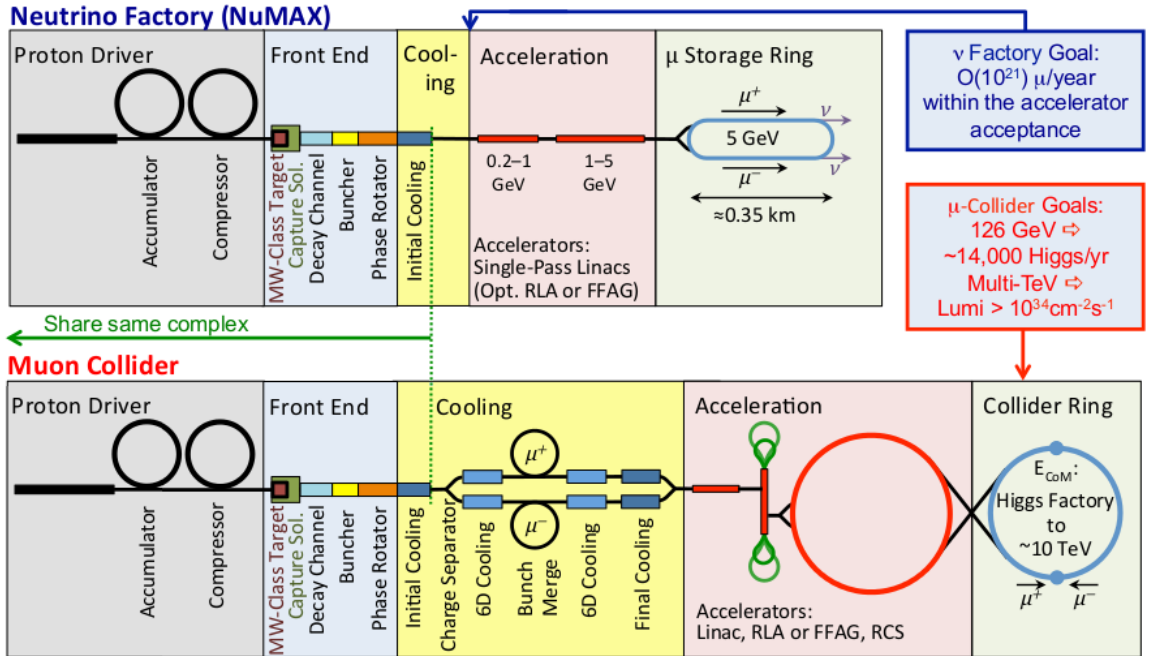


Figure 1.8: Proposed muon accelerator shematics.

of what? not quite: in the long run –
direction. The purpose of this is to increase the luminosity of the resulting beam; for a collider, this means more collisions; for a neutrino factory, this means more neutrino counts in the detectors (since neutrinos are neutral, the ν beam would otherwise tend to disperse). After this critical step, the beam accelerates to an appropriate energy. For a neutrino factory, this is 5 GeV, and the muon and antimuon beams are allowed to decay in a storage ring. For a muon collider, the center-of-momentum energy is 126 GeV for a Higgs factory or up to 10 TeV with current technology for high energy studies.

more sure these are on the same line (remember, large-aperture magnets are expensive)? why "otherwise", it'll disperse no matter what, but with more muons to begin with, there will be more J's, indeed stochastic cooling,

Suggest dropping, we have not demonstrated feasibility, so it's a bit premature. The cooling channel is the crux of the entire operation for either purpose. Traditional cooling methods (e.g. FODO, electron cooling, etc.) are expected to take far too long to allow a significant portion of the muon beam to survive. For example, for 1 TeV muons the mean muon lifetime in the lab frame is $\bar{t} = 2.2 \mu\text{s} \cdot 1 \text{ TeV}/105.7 \text{ MeV} \approx 0.02 \text{ s}$. However, ionization cooling is a much faster method. Ionization cooling requires the beam to deposit its energy in matter, thus ionizing the matter.

what's a FODO cooling method?

Drop this example altogether, not a good illustration, we don't cool at 1 TeV, just say "muon lifetime at rest is $\tau = 2.2 \text{ ms}$ "

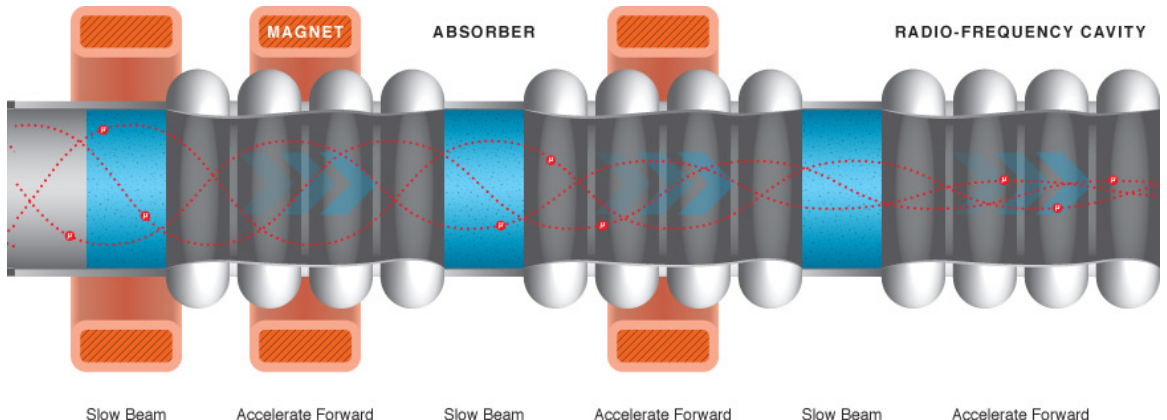


Figure 1.9: Cartoon of a cooling channel.

*Image courtesy
of MAP.*

This reduction of total energy in the beam diminishes its phase space in all three directions: (x, P_x) , (y, P_y) , and (z, P_z) . For this reason, it is sometimes also called 6D cooling. *reduction, let alone in 6D. In fact, if you just pass through an absorber, your longitudinal emittance will likely increase.*

While the idea of ionization cooling has been around since at least 1956 [8,9], it did not appear to be a viable option until roughly 1970 [10]. It was believed that the multiple scattering effect would mask any cooling benefits. Scattering is a quantum effect which deflects two objects when they are in close proximity at high energies, and hence is intrinsically random. This means that while the energy deposition reduced

the beam's phase space, the beam would also grow in the transverse direction due to this multiple scattering. *This phenomenon is now known as phase space exchange or*

Nope! Let's discuss.

Now, this seems to be quite the opposite of what is intended; ionization cooling produces a *slow, yes, if there is no RF, which you explain in the next paragraph, but not necessarily fat, depends on the absorber material, so "fat" is misleading.* Fortunate, there exists a schematic that solves both of these problems simultaneously. *Physically, it is represented in Figure 1.9 and it is vectorally depicted in Figure 1.10.*

What you show is artistic interpretation only, so I would stay away from terms like "physical", sounds misleading.

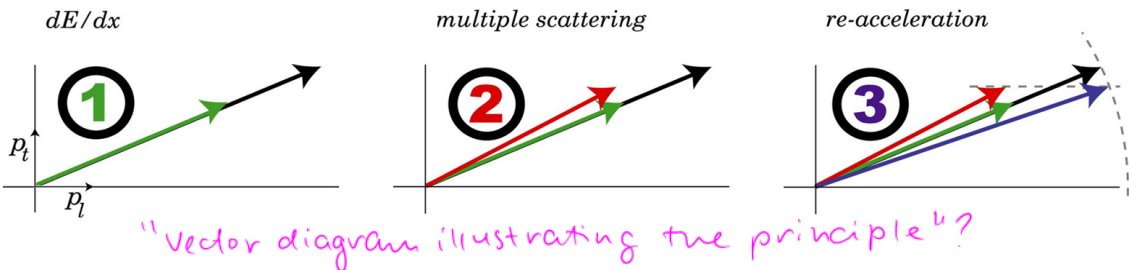


Figure 1.10: Vectoral depiction of ionization cooling in Figure 1.9.

The key is to use a cell which contains both the ionizing material and a radio frequency cavity. It is clear why this solves the latter problem: after the beam loses energy, it gains that much energy again, and so the Lorentz boost stays roughly constant. However, to understand why this solves the former problem it is necessary to observe Figure 1.10. In Figure 1.10, the longitudinal momentum (p_l) is plotted against the transverse momentum (p_t). *but only in the longitudinal direction, "on average", or "after each cell" so the ratio between trans. and long. emittance changes.*

1. Beam deposits energy in material, reducing the momentum in both directions. *"all"? (given that there are two transverse directions, "both" is a bit misleading)*
2. Multiple scattering effects are observed. The transverse direction increases (or "heats up"). *"direction" cannot "increase", emittance can, but maybe not as much as it was reduced, depending on material*
3. The beam is re-accelerated by the RF cavity, increasing the longitudinal momentum only. The result is a reduction in transverse momentum (i.e. blue vector compared to black vector). *if multiple scattering does not prevail*

1.3.3 Emittance. Often, it is advantageous to represent the volume of phase space occupied by the beam as the emittance, ϵ . Moreover, this volume should be normalized by the usual relativistic factors, γ and β . For the relevant transverse emittance, *term in the previous section, saves a lot of trouble and long words. Suggest switching the order of sections.*

$$\epsilon_x^N = \beta \gamma \epsilon_x = \beta \gamma \sqrt{\langle x^2 \rangle \langle \theta^2 \rangle - \langle x\theta \rangle^2}. \quad (1.1)$$

You talk a lot about the term

You haven't why is that, quite the reader wonders?

defined yet. Tell the reader what emittance is, what types of emittances are commonly considered and why. Introduce all the variables in Eq. (1.1)

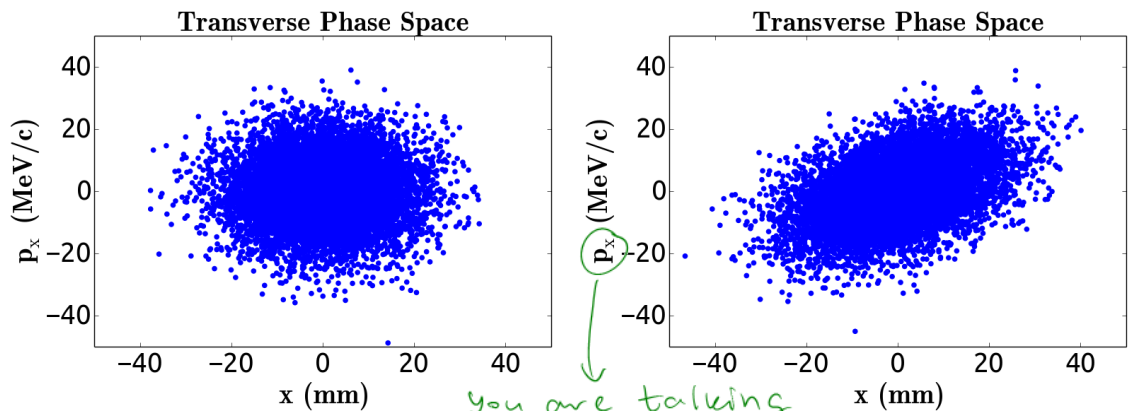


Figure 1.11: Left: example beam with no $x\theta$ correlation. Right: example beam with significant $x\theta$ correlation.

? why do we need that line that

Here, azimuthal symmetry is assumed, and so x represents the general transverse position, and θ is the projection of the divergence angle of the particle trajectory onto the $x\theta$ plane.

↙ What's θ ?

It is conceptually easy to understand why this represents a volume of phase

space. Since the 'beam' is a collection of particles, its full width is not simply defined. For this reason, the width of the beam is represented as the beam's RMS. Provided that the beam is nearly Gaussian, if there existed no cross-dependence in x and θ ,

then the picture should look like the left side of Figure 1.11. Then the volume of this bivariate Gaussian is proportional to $\sqrt{\langle x^2 \rangle \langle \theta^2 \rangle}$. However, if there is some cross-dependence (right side of Figure 1.11) then this must be accounted for by subtracting the cross term from the RMS terms.

↙ why does that produce the desired result, i.e.

Now it is possible to derive the effect of cooling absorbers on emittance as it describes tilted ellipse?

pertains to muon ionization cooling. Closely following [11], Eqn. 1.1 is differentiated

by z :

$$\frac{d\epsilon_x^N}{dz} = \epsilon_x \frac{d(\beta\gamma)}{dz} + \beta\gamma \frac{d\epsilon_x}{dz}, \quad (1.2)$$

⊗ In all likelihood, we can simply derive emittance evolution formula in its explicit form, thus avoiding lengthy discussion of cooling/heating terms in the next few pages. Let's talk

It will soon be shown that the first term represents ‘cooling’ and the second term represents ‘heating’ in the transverse plane. Starting with the heating term,

$$\frac{d\epsilon_x^N}{dz}(\text{heat}) = \beta\gamma \frac{d\epsilon_x}{dz}. \quad \begin{matrix} \text{fragment, rephrase,} \\ \text{even "start with" may work} \end{matrix}$$

Why?

It can be assumed that the cooling is taking place near the beam waist (that

sloppy statement

is, the part of the trajectory where the beam is smallest). For this case, it is a reasonable approximation that the transverse phase space looks more similar to the left side of Figure 1.11, and so the $\langle x\theta \rangle$ term may be neglected. Furthermore, with strong focusing it is possible to neglect the rate of position growth of the beam (this is cited in ?? provided the conditions that $\sigma_{xo}^2 \gg \theta_c^2 L / 2\omega^2$ and $\sigma_{xo}^2 \gg \theta_c^2 / 4\omega^3$, where L is the absorber length, ω is the focusing strength parameter, σ_{xo} is the original beam size incident upon the absorber, and θ_c is the coefficient of the RMS scattering angle given in [12]). Using these two approximations, the only derivative in the heating term is that by $\langle \theta^2 \rangle$:

$$\frac{d\epsilon_x^N}{dz}(\text{heat}) \approx \beta\gamma \frac{d}{dz} \sqrt{\langle x^2 \rangle \langle \theta^2 \rangle} \approx \frac{\beta\gamma}{2\epsilon_x} \langle x^2 \rangle \frac{d}{dz} \langle \theta^2 \rangle.$$

true?

From betatron focusing theory, $\langle x^2 \rangle$ may be rewritten as $\beta_\perp \epsilon_x$. Moreover, using [12] $\langle \theta^2 \rangle$ can be written as $h(z)/\beta^2 E$. Here, $h(z)$ is the Highland z -dependence, the form of which many theories disagree. However, the first order term of $h(z)$ is generally not model-dependent, and so this becomes

$$\langle \theta^2 \rangle \approx \frac{E_s}{\beta^2 E} \sqrt{\frac{z}{X_0}},$$

where E_s is some characteristic energy ($\approx 14 \text{ MeV}$) and X_0 is the radiation length of the given material. Then

$$\frac{d\epsilon_x^N}{dz}(\text{heat}) \approx \beta\gamma \frac{\beta_\perp}{2} \frac{d}{dz} \left(\frac{E_s}{\beta^2 E} \sqrt{\frac{z}{X_0}} \right),$$

$$\frac{d\epsilon_x^N}{dz}(\text{heat}) \approx \frac{\beta_\perp}{2} \frac{E_s^2}{\beta^3 E mc^2} \frac{1}{X_0}. \quad (1.3)$$

Now it is clearer why this is referred to as the heating term. Since the derivative of emittance is positive, this part represents emittance growth. Moreover, to reduce this growth it is necessary to have highly energetic particles through a material with a large radiation length (typically $X_0 \propto Z$ (nuclear charge)).

Observe the cooling term of Eqn. 1.2:

$$\frac{d\epsilon_x^N}{dz}(\text{cool}) = \epsilon_x \frac{d(\beta\gamma)}{dz} = \epsilon_x \cdot (\beta \frac{d\gamma}{dz} + \gamma \frac{d\beta}{dz}).$$

First,

$$\frac{d\beta}{dz} = \frac{d}{dz}(1 - \gamma^{-2})^{\frac{1}{2}} = \frac{1}{\beta\gamma^3} \frac{d\gamma}{dz},$$

and then,

$$\frac{d\gamma}{dz} = \frac{\gamma}{E} \frac{dE}{dz},$$

with E as the total energy of the muon beam. Finally,

$$\frac{d\epsilon_x^N}{dz}(\text{cool}) = \epsilon_x \cdot (\beta \frac{d\gamma}{dz} + \gamma \frac{1}{\beta\gamma^3} \frac{d\gamma}{dz}) = \epsilon_x \cdot \frac{d\gamma}{dz} \beta \left(1 + \frac{1}{\beta^2\gamma^2}\right) \frac{d\epsilon_x^N}{dz}(\text{cool}) = \epsilon_x \frac{dE}{dz} \frac{\gamma}{E\beta}.$$

Normalizing the emittance by first multiplying and then dividing by $\beta\gamma$ results in

$$\frac{d\epsilon_x^N}{dz}(\text{cool}) = \frac{1}{\beta} \frac{dE}{dz} \frac{\epsilon_x^N}{E}$$

However, there are two notations which should be observed. First, even for a perfect monoenergetic pencil beam energy loss is stochastic, not deterministic. Two muons with identical initial conditions will likely lose different amounts of energy as they pass through the same medium. Since emittance is a collective effect, is it more appropriate to talk about an average energy loss, which turns $\frac{dE}{dz}$ into $\langle \frac{dE}{dz} \rangle$. The second observation is with regard to sign convention. Typically, one refers to energy loss as a positive quantity (e.g. the beam lost 10 MeV from point A to point B), even though it is clear that $\frac{dE}{dz}$ is a negative quantity. For this reason, the energy loss term must again be changed from $\langle \frac{dE}{dz} \rangle$ to $-\left| \langle \frac{dE}{dz} \rangle \right|$. This leaves the full cooling term as

$$\frac{d\epsilon_x^N}{dz}(\text{cool}) = -\frac{1}{\beta} \left| \left\langle \frac{dE}{dz} \right\rangle \right| \frac{\epsilon_x^N}{E}. \quad (1.4)$$

Similar to the heating term, it is now understandable why this is referred to as the cooling term. The rate of change of the normalized transverse emittance is negative, and so the transverse phase space shrinks. However, at this point Eqn. 1.4 does not explain precisely how the rate changes, and so is purely conceptual for the time being. The shape of the cooling term is determined by the average energy loss, $|\langle \frac{dE}{dz} \rangle|$. However, usually it is not $|\langle \frac{dE}{dz} \rangle|$ that is measured, but rather the stopping power $S(E) = -\frac{1}{\rho} \langle \frac{dE}{dx} \rangle$, typically in units of $MeV \cdot cm^2/g$. A good example of a stopping power curve can be seen in Figure 1.12 [13]. For this example, there are several effects noted in Figure 1.12, and one may be tempted to think that based on 1.4 the most cooling should occur in the Anderson-Ziegler regime at $\beta\gamma \sim 0.01$ (since there is a $1/E$ dependence in Eqn. 1.4, the high energy part of the curve does no good). Indeed, for $\rho = 8.92 \text{ g/cm}^3$ it is easy to see that at $\beta\gamma = 0.01$ then $\frac{de_x^N}{dz}(\text{cool}) \approx -900 \text{ cm}^{-1} \cdot \epsilon_x^N$.

However, the correct strategy is just the opposite –one should endeavor to build a cooling cell with the minimum ionization point in mind (in the Bethe regime, where $\beta\gamma \sim 2$). At the peak ($\beta\gamma \sim 0.01$), the muon beam slows down quite a bit through a single cooling cell and one is at risk of losing their beam to decay. Moreover, Figure 1.12 only depicts the stopping power, not the actual energy loss that individual particles experience. The individual energy loss is a stochastic effect, and the distribution of energy losses broadens with decreasing beam energy. This means that for lower energies, there will be more particles which stop completely. Further, with a higher beam energy the stochastic energy loss profile is more sharply peaked, and so there are fewer decays and more particles which fall into the RF bucket. (Remember, the longitudinal emittance is observed by the RF cavities, as seen in Figure 1.9. The longitudinal emittance increases with energy loss according to [11].) Finally, it is apparent in Eqn. 1.3 that higher energies are better, since they reduce the heating term. For these reasons, it is apparent that a muon cooling cell

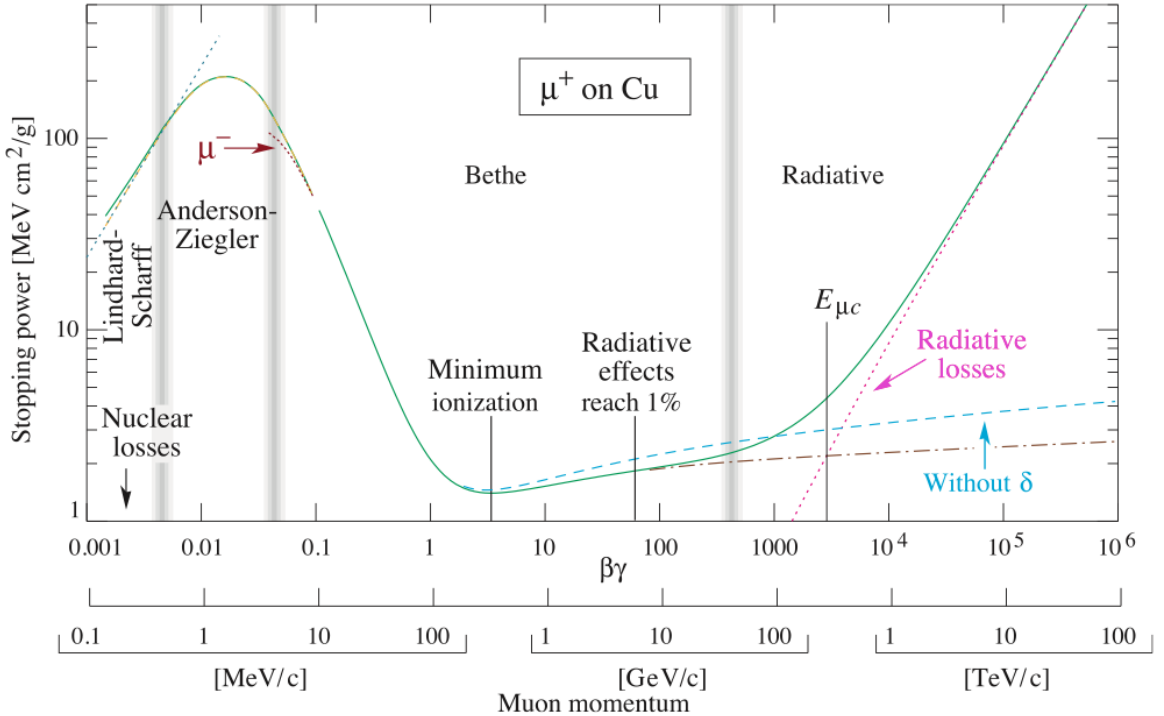


Figure 1.12: Stopping power curve for antimuons on copper, courtesy of [13].

should be made of low Z materials such as liquid hydrogen or lithium hydride and operate anywhere between $100 \text{ MeV}/c$ to $400 \text{ MeV}/c$.

When particles impinge upon a fixed target, they lose some of their energy. For massive particles like muons, there are four major effects which contribute to this energy loss: ionization, bremsstrahlung radiation, pair production, and photonuclear interactions. However, it is important to note that in the muon cooling regime only ionization contributes significantly to the energy loss. To see this, take for an example the relatively heavy element of iron (iron is chosen because it is a fairly relatable element to those who are not experts in this field). In Figure 1.13, the energy loss contributions of these four effects can be seen. However, the non-ionization effects only start to contribute at an initial beam kinetic energy of 1.40 GeV – far outside of the muon cooling regime.

Muons in iron (Fe)									
Z 26 (Fe)	A [g/mol] 55.845 (2)	ρ [g/cm ³] 7.874	I [eV] 286.0	a 0.14680	k = m_s 2.9632	x ₀ -0.0012	x ₁ 3.1531	\overline{C} 4.2911	δ_0 0.12
T	p [MeV/c]	Ionization	Brems	Pair prod [MeV cm ² /g]	Photonucl	Total	CSDA range [g/cm ²]		
10.0 MeV	4.704×10^1	5.494				5.494	1.025×10^0		
14.0 MeV	5.616×10^1	4.321				4.321	1.854×10^0		
20.0 MeV	6.802×10^1	3.399				3.399	3.437×10^0		
30.0 MeV	8.509×10^1	2.654				2.654	6.812×10^0		
40.0 MeV	1.003×10^2	2.274				2.274	1.091×10^1		
80.0 MeV	1.527×10^2	1.717				1.717	3.178×10^1		
100. MeV	1.764×10^2	1.616				1.616	4.382×10^1		
140. MeV	2.218×10^2	1.516				1.516	6.950×10^1		
200. MeV	2.868×10^2	1.463				1.463	1.099×10^2		
274. MeV	3.642×10^2	1.451			0.000	1.451	Minimum ionization		
300. MeV	3.917×10^2	1.452			0.000	1.453	1.787×10^2		
400. MeV	4.945×10^2	1.467	0.000		0.000	1.467	2.472×10^2		
800. MeV	8.995×10^2	1.548	0.000		0.000	1.548	5.124×10^2		
1.00 GeV	1.101×10^3	1.581	0.001		0.000	1.582	6.402×10^2		
1.40 GeV	1.502×10^3	1.635	0.001	0.000	0.001	1.637	8.885×10^2		

Figure 1.13: Energy loss table for muons in iron. Table courtesy of [14].

This is a good example because all of the cooling materials currently being considered have less muon stopping power than iron. This means that iron represents the maximum contribution of non-ionization energy loss per initial beam energy; that is, the non-ionization effects begin to emerge at much higher energies for lighter elements such as liquid hydrogen. Note that Figure 1.12 may also be useful when discussing this subject.

Here, *ionization* refers to both true ionization (the production of δ rays) and excitation (the promotion of an inner electron to a higher shell). To reiterate a previous section, the term ‘straggling’ refers to the fluctuation about some mean energy loss. That is to say, the amount of energy that a particle will lose is intrinsically random –there exists some distribution with some average value, and when the particle of interest transverses a length of matter the amount of energy that this particle loses is selected from this distribution. This intrinsic randomness can be attributed to

quantum-like behaviors (e.g. the energy loss cross section which comes from the wave nature of the particle in question).

CHAPTER 2

STOCHASTIC PROCESSES IN ICOOL

2.1 Straggling

ICOOL [15] employs four levels of straggling models, three of which were used in these muon simulations studies. They are

1. Gaussian (Bohr),
2. Landau distribution, and
3. Vavilov distribution (with appropriate limits).

The fourth model is “restricted energy fluctuations from continuous processes with energy below DCUTx” and was not used for this study.

2.1.1 Gaussian (Bohr).

The first model uses a Guassian function to model the energy loss distribution. Recall that Gaussian distributions can be determined from two parameters: the mean μ and the standard deviation σ . The first of these comes from the Bethe-Bloch equation, which will be derived here and yeilds Eqn. 2.4.

Classical Derivation

The model begins with a particle of charge e moving into a volume of electrons. It is assumed that the mass of the incoming particle is much greater than the mass of the electron since there will be no scattering in this derivation. Moreover, the electron must either be at rest and fixed into place (which is nonphysical) or the collision time of the particle and electron is very small compared to the electron

orbital time. The z -axis is aligned with the particle's velocity such that $v_x = v_y = 0$. The momentum transfer Δp is sought, and the first observation is that the change in longitudinal momentum is zero (i.e. $\Delta p_z = 0$). This is true since the particle feels a force "forwards" just as much as it feels a force "backwards". Since this model bars scattering, the change in momentum must be interpreted as energy imparted upon the electron. Then:

$$\begin{aligned}\Delta p_x &= \int_{-\infty}^{\infty} F_x dt = \int_{-\infty}^{\infty} F_x \frac{dz}{v} = \int_{-\infty}^{\infty} F \cos \theta \frac{dz}{v} \\ &= \int_{-\infty}^{\infty} \frac{e^2}{r^2} \frac{b}{r} \frac{dz}{v} = \int_{-\infty}^{\infty} \frac{e^2}{z^2 + b^2} \frac{b}{\sqrt{z^2 + b^2}} \frac{dz}{v} \\ &= \frac{e^2 b}{v} \int_{-\infty}^{\infty} \frac{1}{(z^2 + b^2)^{3/2}} dz,\end{aligned}$$

where b is the impact parameter (the closest distance between the particle and the electron). By substitution of the following

$$z = b \tan \theta,$$

$$dz = b \sec^2 \theta d\theta,$$

$$z = \infty \rightarrow \theta = \frac{\pi}{2},$$

$$z = -\infty \rightarrow \theta = \frac{-\pi}{2},$$

the integral becomes

$$\begin{aligned}\Delta p_x &= \frac{e^2 b}{v} \int_{-\pi/2}^{\pi/2} \frac{b \sec^2 \theta d\theta}{(b^2(\tan^2 \theta + 1))^{3/2}} \\ &= \frac{e^2 b}{v} \int_{-\pi/2}^{\pi/2} \frac{d\theta}{b^2 |\sec \theta|} \\ &= \frac{2e^2}{vb}.\end{aligned}$$

The non-relativistic approach yeilds the energy loss for the interaction between a muon and a single electron:

$$\epsilon = \frac{\Delta p^2}{2m_e} = \frac{2e^4}{v^2 b^2 m_e} \quad (2.1)$$

Here, it is useful to note that if the interaction of the muon with the nucleus was desired, ϵ for a single interaction would be proportional to Z^2/m_{nuc} and would be added on to the above term. However, since $1/m_e \gg 1/m_{nuc}$ the second term will be disregarded.

For multiple electrons, the average electron density is $N_{el} = N_A \cdot Z\rho/A$. The cylindrical symmetry of the system is exploited by integrating the single electron interaction in cylindrical coordinates, with the cylindrical angle as θ , radius as b (the impact parameter), and length as z . The bounds on b are some $[b_{min}, b_{max}]$ which will be discussed shortly. Then

$$\begin{aligned}\langle \epsilon \rangle &= \int_{b_{min}}^{b_{max}} \int_0^L \int_0^{2\pi} \frac{2e^4}{v^2 b^2 m_e} N_{el} d\theta dz b db \\ &= \frac{4\pi N_A e^4}{v^2 m_e} \frac{Z\rho L}{A} \int_{b_{min}}^{b_{max}} \frac{db}{b}\end{aligned}\quad (2.2)$$

It is known that b_{min} comes from the maximum amount of energy (T_{max}) which a muon may impart upon an electron. This quantity is derived later and can be seen in Eqn. 2.8, but is only symbolic here. Similarly, the minimum transferrable energy is simply the (mean) ionization energy, I , which is usually taken as an empirical value. Any energy below this value will not transfer, since this is the minimum amount of energy to free the electron from its orbit. Then

$$\begin{aligned}\epsilon_{max} &= \frac{2e^4}{v^2 b_{min}^2 m_e} = T_{max} \\ b_{min} &= \frac{e^2}{v} \sqrt{\frac{2}{m_e T_{max}}}\end{aligned}$$

$$\begin{aligned}\epsilon_{min} &= \frac{2e^4}{v^2 b_{max}^2 m_e} = T_{min} = I \\ b_{max} &= \frac{e^2}{v} \sqrt{\frac{2}{m_e I}}.\end{aligned}$$

Now that the bounds have been acquired, the integral in Eqn. 2.2 is solvable.

$$\begin{aligned}\langle \epsilon \rangle &= \frac{4\pi N_A e^4}{v^2 m_e} \frac{Z\rho L}{A} \int_{b_{min}}^{b_{max}} \frac{db}{b} \\ \langle \epsilon \rangle &= \frac{4\pi N_A e^4}{v^2 m_e} \frac{Z\rho L}{A} \ln \frac{b_{max}}{b_{min}} \\ \langle \epsilon \rangle &= \frac{2\pi N_A e^4}{v^2 m_e} \frac{Z\rho L}{A} \ln \frac{T_{max}}{I}.\end{aligned}\quad (2.3)$$

Modern Corrections

There are a number of corrections to the Bethe-Bloch equation. The first is a correction under the logarithm due to the relativistic flattening of the incoming particle's electric field. This factor is $2m_e\beta^2\gamma^2/I$. Another correction is known as the density correction parameter δ and arises due to polarization. This is important for high energies and may or may not be useful for these medium energy studies. The last correction is the shell correction parameter C and accounts for the fact that the electron is not at rest (or the interaction time is not much faster than the electron orbit). This is important for low energies and may or may not be useful for these medium energy studies. Finally, in its more familiar form, the constants in front are condensed into a single constant $K = \frac{2\pi e^4 N_A}{m_e} \approx 15.4$ (MeV · cm³)/(m · g). Since the model assumes natural units of light (i.e. $c = 1$), v^2 is usually replaced with β^2 . Moreover, to avoid confusion $\langle \epsilon \rangle$ is given a negative sign in order to emphasize energy loss.

The final result is the Bethe-Bloch equation for the average energy lost by a particle traversing some medium with correction factors (with correction factors according to [4]):

$$\langle \epsilon \rangle = -\frac{K}{\beta^2} \frac{Z\rho L}{A} \left(\ln \frac{2m_e\beta^2\gamma^2 T_{max}}{I^2} - 2\beta^2 - \delta - 2\frac{C}{Z} \right). \quad (2.4)$$

According to the Particle Data Group [13], this equation is generally accurate for intermediate Z materials (up to a few % when compared to experimental data)

in the energy regime of $0.1 \lesssim \beta\gamma \lesssim 1000$. The lower limit of this equation is when the incoming particle's velocity is comparable to the atomic electron velocities and the upper limit is due to radiative effects, as well as both limits having some Z dependence. Figure 1.12 depicts this region approximately with muons on copper. Clearly, the region for muon ionization cooling ($100\text{MeV}/c < p_\mu < 1000\text{MeV}/c$) falls in the middle of the Bethe region, with the Anderson-Ziegler region as the low cutoff and radiative losses coming into effect at the high cutoff.

As previously stated, the first energy loss model from ICOOL selects an energy loss from a Gaussian profile with mean $\mu = \langle \epsilon \rangle$ (Eqn. 2.4) and standard deviation according to [16]:

$$\sigma^2 = 2\pi e^2 N_A T_c \frac{Z\rho L}{A} \frac{1 - \beta^2/2}{\beta}, \quad (2.5)$$

where T_c is the cut kinetic energy of δ -electrons.

Derivation of T_{max}

Although T_{max} does have symbolic meaning in many equations, here it will be derived explicitly from a relativistic point of view. This derivation yields Eqn. 2.8 and works in natural light units such that $c = 1$. Conservation of energy for a muon incident upon an electron at rest requires that

$$\begin{aligned} E_\mu + m_e &= E_{\mu,f} + E_e, && \text{or} \\ \sqrt{p_\mu^2 + m_\mu^2} + m_e &= \sqrt{p_{\mu,f}^2 + m_\mu^2} + T_e + m_e, && \text{or} \\ p_{\mu,f}^2 &= p_\mu^2 + T_e^2 - 2T_e \sqrt{p_\mu^2 + m_\mu^2} \end{aligned} \quad (2.6)$$

with

$$\begin{aligned} E_e &= T_e + m_e = \sqrt{p_e^2 + m_e^2}, && \text{or} \\ p_e^2 &= (T_e + m_e)^2 - m_e^2 \end{aligned} \quad (2.7)$$

where T_e is the final kinetic energy of the electron, p_μ is the initial muon momentum, m_μ is the mass of the muon, and $p_{\mu,f}$ is the final muon momentum.

Conservation of momentum requires that

$$\vec{p}_\mu = \vec{p}_{\mu,f} + \vec{p}_e, \quad \text{or}$$

$$p_{\mu,f}^2 = p_\mu^2 + p_e^2 - 2p_\mu p_e \cos \theta.$$

Using Eqn. 2.7 for p_e on the right side this becomes

$$p_{\mu,f}^2 = p_\mu^2 + (T_e + m_e)^2 - m_e^2 - 2p_\mu \cos \theta \sqrt{(T_e + m_e)^2 - m_e^2}$$

Now substitution of Eqn. 2.6 for $p_{\mu,f}^2$ on the left side yields

$$p_\mu^2 + T_e^2 - 2T_e \sqrt{p_\mu^2 + m_\mu^2} = p_\mu^2 + (T_e + m_e)^2 - m_e^2 \sqrt{(T_e + m_e)^2 - m_e^2}$$

For maximum energy (i.e. to attain $T_e = T_{max}$), $\cos \theta = 1$, which is representative of a head-on collision. Then

$$T_{max}^2 - 2T_{max} \sqrt{p_\mu^2 + m_\mu^2} = T_{max}^2 + 2T_{max}m_e - 2p_\mu \sqrt{T_{max}^2 + 2T_{max}m_e}$$

$$-2T_{max}(\sqrt{p_\mu^2 + m_\mu^2} + m_e) = -2p_\mu \sqrt{T_{max}^2 + 2T_{max}m_e}$$

$$\sqrt{p_\mu^2 + m_\mu^2} + m_e = p_\mu \sqrt{1 + \frac{2m_e}{T_{max}}}.$$

Substituting the initial muon energy $E_\mu = \sqrt{p_\mu u^2 + m_\mu^2} = \gamma m_\mu$ and the initial muon momentum $p_\mu^2 = E_\mu^2 - m_\mu^2 = m_\mu^2(\gamma^2 - 1) = m_\mu^2 \gamma^2 \beta^2$ results in

$$\gamma m_\mu + m_e = m_\mu \gamma \beta \sqrt{1 + \frac{2m_e}{T_{max}}}$$

$$(\gamma m_\mu + m_e)^2 = m_\mu^2 \gamma^2 \beta^2 \left(1 + \frac{2m_e}{T_{max}}\right).$$

Finally, solving for the maximum transferrable energy from an incident muon to an electron at rest is

$$T_{max} = \frac{2m_e \beta^2 \gamma^2}{1 + 2\gamma \frac{m_e}{m_\mu} + \left(\frac{m_e}{m_\mu}\right)^2}. \quad (2.8)$$

2.1.2 Landau.

The second ICOOL straggling model selects an energy loss from a Landau distribution [17]. This derivation is particularly important since it is the same model that COSY uses. Landau begins the derivation by stipulating that this theory assumes fast particles ("so that the usual ionisation theory may be applied", here taken as particles whose energy is in the Bethe regime in Figure 1.12). Moreover, the thickness of the absorber should be small enough such that the energy loss is small compared to the initial energy. This is so that the weight function ($w(E, u)$; the probability per unit length of an energy loss u) may be written simply as $w(u)$. Another way of describing this constraint is that the total energy of the particle is roughly constant while traversing the medium.

Let $f(L, \epsilon)$ be desired distribution function for this energy loss. This means that the particle will lose an amount of energy between ϵ and $\epsilon + d\epsilon$ while traversing an absorber of length L . Then on one hand

$$\text{change in } f \text{ per unit length} = \frac{\partial f(L, \epsilon)}{\partial L}.$$

On the other hand, the change in f may also be expressed as the difference in two f functions: one at a length L with possible energy losses between ϵ and $\epsilon + d\epsilon$ and another at length L and with possible energy losses between $\epsilon - u$ and $\epsilon + d\epsilon - u$, with u accounting for the infinitesimal change in length. Then

$$\text{change in } f \text{ per unit length} = \left[\int_0^\infty w(u)f(L, \epsilon - u)du \right] - f(L, \epsilon).$$

Often referred to as the integral transport equation, the two previous definitions of the change in f per unit length may be combined as

$$\frac{\partial f(L, \epsilon)}{\partial L} = \left[\int_0^\infty w(u)f(L, \epsilon - u)du \right] - f(L, \epsilon). \quad (2.9)$$

Since L and ϵ are independent and implicit variables, this allows for a Laplace transformation. Take the transformed function with respect to ϵ as

$$\phi(p, L) = \int_0^\infty e^{-p\epsilon} f(\epsilon) d\epsilon.$$

(Note that p is simply a dummy variable and not the momentum.) Then the inverse transformation gives

$$f(L, \epsilon) = \frac{1}{2\pi i} \int_{K-i\infty}^{K+i\infty} \phi(p, L) e^{p\epsilon} dp \quad (2.10)$$

Observe here that $K > 0$ and so the integral is happening just to the right of the imaginary axis. This is the desired distribution function, and so will be useful later. However, without the form of ϕ it is not useful. The goal then will be to find a closed form of ϕ .

Multiplying both sides of Eqn. 2.9 by $e^{-p\epsilon}$ and integrating with respect to $d\epsilon$ yields

$$\int_0^\infty \frac{\partial f}{\partial L} e^{-p\epsilon} d\epsilon = \int_0^\infty \left[\int_0^\infty w(u) f(L, \epsilon - u) du \right] e^{-p\epsilon} d\epsilon - \int_0^\infty f(L, \epsilon) e^{-p\epsilon} d\epsilon.$$

On the left side, the operations of partial derivative and integration are commutable, and are therefore switched. On the right side, the first term has commutable integrations and so the order is switched. For the second term, note that $w(u)$ is normalized, so that adding the integral of $w(u)$ over all u changes nothing. Then

$$\frac{\partial}{\partial L} \int_0^\infty e^{-p\epsilon} f(\epsilon) d\epsilon = \int_0^\infty \left[\int_0^\infty e^{-p\epsilon} f(\epsilon - u) d\epsilon \right] w(u) du - \int_0^\infty \left[\int_0^\infty e^{-p\epsilon} f(\epsilon) d\epsilon \right] w(u) du.$$

The left side and the second term on the right side may be substituted for ϕ directly, while the first term on the right side should be shifted by $-u$, resulting in

$$\frac{\partial}{\partial L} \phi(p, L) = \int_0^\infty \left[\int_{-u}^\infty e^{-p(\epsilon+u)} f(\epsilon) d\epsilon \right] w(u) du - \int_0^\infty \phi(p, L) w(u) du.$$

Now recall that $f(\epsilon)$ is the desired function for energy loss. Therefore, $f(\epsilon < 0) = 0$ (i.e. the particle cannot gain energy while traversing a medium), and so

$$\begin{aligned}\frac{\partial}{\partial L} \phi(p, L) &= \int_0^\infty e^{-pu} \left[\int_0^\infty e^{-p\epsilon} f(\epsilon) d\epsilon \right] w(u) du - \phi(p, L) \int_0^\infty w(u) du \\ &= \phi(p, L) \int_0^\infty w(u) (e^{-pu} - 1) du.\end{aligned}$$

This differential equation is a first-order, undriven normal linear ODE (ordinary differential equation) [18]. Let prime (') denote a partial derivative with respect to L . Then the treatment is to define a function $h(L)$ as

$$h(L) = - \int_0^\infty w(u) (e^{-pu} - 1) du$$

and its antiderivative as

$$H(L) = \int h(L) dL = L \int_0^\infty w(u) (1 - e^{-pu}) du.$$

Then

$$\phi' + \phi \cdot h(L) = 0. \quad (2.11)$$

Since $(e^{H(L)})' = e^{H(L)} \cdot H'(L) = e^{H(L)} \cdot h(L)$, it is useful to multiply both sides of the ODE in Eqn. 2.11 by $e^{H(L)}$, resulting in

$$\phi' \cdot e^{H(L)} + \phi \cdot h(L) \cdot e^{H(L)} = 0$$

$$(\phi \cdot e^{H(L)})' = 0.$$

Integrating both sides yields

$$\begin{aligned}\phi \cdot e^{H(L)} &= K_1 \\ \phi &= K_1 e^{-H(L)} \\ \phi(p, L) &= K_1 \exp \left[-L \int_0^\infty w(u) (1 - e^{-pu}) du \right].\end{aligned}$$

This differential equation is now solvable provided that there are initial conditions. The first observation is that for $L = 0$, the only possible energy loss is zero.

Mathematically, this means that $f(0, \epsilon) = \delta(\epsilon)$; that is, the probability of energy loss is 100% for an energy loss of zero and 0% for all other energy losses. Then the boundary condition on ϕ is

$$\begin{aligned}\phi(p, 0) &= \int_0^\infty \delta(\epsilon) e^{-p\epsilon} d\epsilon \\ \phi(p, 0) &= e^{p \cdot 0} \\ \phi(p, 0) &= 1 = K_1 \exp[0].\end{aligned}$$

Then

$$\phi(p, L) = \exp \left[-L \int_0^\infty w(u)(1 - e^{-pu}) du \right].$$

Now using Eqn. 2.10, the energy loss distribution function f in terms of $w(u)$ is

$$f(L, \epsilon) = \frac{1}{2\pi i} \int_{K-i\infty}^{K+i\infty} \exp \left[p\epsilon - L \int_0^\infty w(u)(1 - e^{-pu}) du \right] dp. \quad (2.12)$$

In principle, this is the general solution to the energy loss profile for a particle traversing some medium. In practice, the only thing which is inhibiting implementation is an algorithm to generate a number from this distribution (which will be discussed in a later chapter) and the function $w(u)$. Once $w(u)$ is obtained, the integral may be theoretically found using numeric integration, provided that it is not computationally expensive.

Livingston and Bethe [19] derived the form of $w(u)$ in 1937, and is

$$w(u) = \frac{\xi}{L} \frac{1}{u^2},$$

where

$$\xi = \frac{2\pi r_e^2 m_e N_A Z \rho L}{\beta^2 A}. \quad (2.13)$$

Given this, the form of $w(u)(1 - e^{-pu})$ may now be seen in Figure 2.1. Clearly, the most important values of p are those where $pu_{min} \ll 1$ and $1 \ll pu_{max}$ since values of $pu \approx 1$ will tend to vanish.

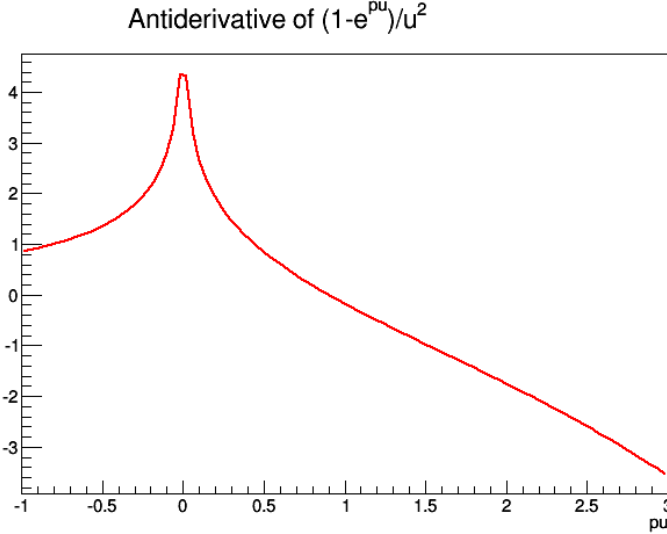


Figure 2.1: Plot of $\int w(u)(1 - e^{-pu})du$.

Now consider a certain energy u_1 such that $u_{min} \ll u_1$ and $pu_1 \ll 1$. Then the integral in the exponent of Eqn. 2.12 has the form

$$L \int_0^\infty w(u)(1 - e^{-pu}) du = \xi \left(i \int_0^{u_1} \frac{1 - e^{-pu}}{u^2} du + \int_{u_1}^\infty \frac{1 - e^{-pu}}{u^2} du \right).$$

Since the first integral is over the small values, it is possible to write $1 - e^{-pu} \approx 1 - (1 - pu) = pu$. Furthermore, the minimum energy loss is not 0 but rather u_{min} . Then

$$\begin{aligned} \frac{L}{\xi} \int_0^\infty w(u)(1 - e^{-pu}) du &= \int_{u_{min}}^{u_1} p u du + \int_{u_1}^\infty \frac{1 - e^{-pu}}{u^2} du \\ &= p \int_{u_{min}}^{u_1} \frac{1}{u} du + \int_{u_1}^\infty \frac{1 - e^{-pu}}{u^2} du \\ &= p \ln \frac{u_1}{u_{min}} + \int_{u_1}^\infty \frac{1 - e^{-pu}}{u^2} du. \end{aligned}$$

For the second term, integration by parts and evaluation at the boundaries gives

$$\frac{L}{\xi} \int_0^\infty w(u)(1 - e^{-pu}) du = p \ln \frac{u_1}{u_{min}} + \frac{1 - e^{-pu_1}}{u_1} + p \int_{u_1}^\infty \frac{e^{-pu}}{u} du.$$

Recalling that u_1 was chosen such that $pu_1 \ll 1$, the exponential in the second term may be approximated as $e^{-pu_1} \approx 1 - pu_1$. Then

$$\frac{L}{\xi} \int_0^\infty w(u)(1 - e^{-pu}) du = p \ln \frac{u_1}{u_{min}} + p + p \int_{u_1}^\infty \frac{e^{-pu}}{u} du. \quad (2.14)$$

The final integral may be evaluated first by letting $K_2 = pu$:

$$\begin{aligned}
\frac{L}{\xi} \int_{u_1}^{\infty} \frac{e^{-pu}}{u} du &= \int_{pu_1}^{\infty} \frac{e^{-K_2}}{K_2} dK_2 \\
&= \int_{pu_1}^{\infty} \frac{e^{K_2}}{K_2} dK_2 + \int_{pu_1}^1 \frac{dK_2}{K_2} - \int_{pu_1}^1 \frac{dK_2}{K_2} \\
&= \int_{pu_1}^1 \frac{e^{K_2}}{K_2} dK_2 + \int_1^{\infty} \frac{e^{K_2}}{K_2} dK_2 + \int_{pu_1}^1 \frac{dK_2}{K_2} - \int_{pu_1}^1 \frac{dK_2}{K_2} \\
&= \int_{pu_1}^1 \left(\frac{e^{K_2}}{K_2} - \frac{1}{K_2} \right) dK_2 + \int_1^{\infty} \frac{e^{K_2}}{K_2} dK_2 + \int_{pu_1}^1 \frac{dK_2}{K_2} \\
&= \int_{pu_1}^1 \frac{dK_2}{K_2} + \left[\int_{pu_1}^1 \frac{e^{-K_2} - 1}{K_2} dK_2 + \int_1^{\infty} \frac{e^K}{K_2} dK_2 \right].
\end{aligned}$$

The first term is easily evaluated, and the second term in brackets is approximately¹ the negative of Euler's constant, $-C_{Euler}$. Putting this back into Eqn. 2.14 yields

$$\begin{aligned}
\frac{L}{\xi} \int_0^{\infty} w(u)(1 - e^{-pu}) du &= p \ln \frac{u_1}{u_{min}} + p(1 - C_{Euler} - \ln pu_1) \\
&= p(1 - C_{Euler} - \ln pu_{min}).
\end{aligned}$$

Now Eqn. 2.12 may be rewritten as

$$\begin{aligned}
f(L, \epsilon) &= \frac{1}{2\pi i} \int_{K-i\infty}^{K+i\infty} \exp \left[p\epsilon - L \int_0^{\infty} w(u)(1 - e^{-pu}) du \right] dp \\
&= \frac{1}{2\pi i} \int_{K-i\infty}^{K+i\infty} \exp \left[p\epsilon - p\xi(1 - C_{Euler} - \ln pu_{min}) \right] dp.
\end{aligned}$$

If a unitless variable of integration is desired, then $p \rightarrow p/\xi$, and

$$f(\xi, \epsilon) = \frac{1}{2\pi i \xi} \int_{K-i\infty}^{K+i\infty} \exp \left[p \frac{\epsilon}{\xi} - p(1 - C_{Euler} - \ln \frac{u_{min}}{\xi}) + p \ln p \right] dp,$$

or simply

$$f(\lambda) = \frac{1}{2\pi i \xi} \int_{K-i\infty}^{K+i\infty} \exp \left[p \ln p + \lambda p \right] dp, \quad (2.15)$$

where evidently

$$\lambda = \frac{\epsilon}{\xi} - 1 + C_{Euler} + \ln \frac{\xi}{u_{min}}.$$

¹This expression would be exactly $-C_{Euler}$ if $pu_1 = 0$.

However, typically the Landau function is evaluated for the desired *fluctuation about the mean energy loss*, not the energy loss itself. Because of this, λ must be shifted by the mean, $\langle \epsilon \rangle$. Furthermore, a correction of $-\beta^2$ is added and $u_{min} \rightarrow T_{max}$, resulting in the final form of the Landau parameter:

$$\lambda \equiv \frac{\epsilon - \langle \epsilon \rangle}{\xi} - (1 - C_{Euler}) - \beta^2 - \ln(\xi/T_{max}). \quad (2.16)$$

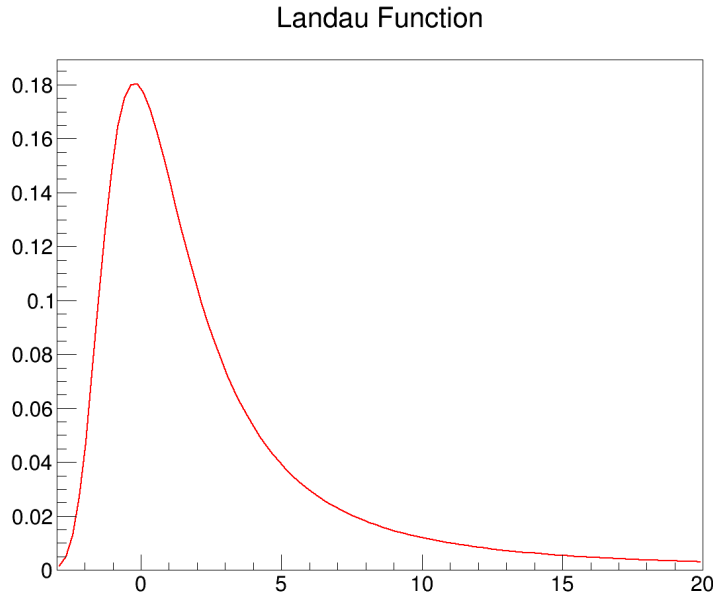


Figure 2.2: Example of the Landau function.

In summary, the ICOOL Landau model uses the mean energy loss from the Bethe-Bloch equation (Eqn. 2.4). The routine then adds noise from the Landau function (see, e.g., Figure 2.2), which has a mode of zero. This value is then accepted as the total energy loss of the particle.

2.1.3 Vavilov.

The Vavilov model [20] is similar to the Landau model, except that the thickness of the absorber is not required to be small enough such that the energy loss is small compared to the initial energy. The derivation is also similar, except that Vav-

Vavilov introduced a limit on the maximum transferable energy due to a single collision (recall that in Landau theory the upper limit was ∞). The result is

$$f(\lambda_v, \kappa, \beta^2) = \frac{1}{\xi} \phi_v(\lambda_v, \kappa, \beta^2), \quad (2.17)$$

where

$$\begin{aligned} \phi_v(\lambda_v, \kappa, \beta^2) &= \frac{1}{2\pi i} \int_{K+i\infty}^{K-i\infty} \phi(p, \kappa, \beta^2) e^{\lambda p}, \\ \phi(p, \kappa, \beta^2) &= \exp[\kappa(1 + \beta^2 \gamma)] \exp[\psi(p, \kappa, \beta^2)], \\ \psi(p) &= p \ln \kappa + (p + \beta^2 \kappa)[\ln(p/\kappa) + E_1(p/\kappa)] - \kappa e^{-p/\kappa}, \\ E_1(p) &= \int_{\infty}^z \frac{e^{-u}}{u} du \quad (\text{the exponential integral}), \\ \lambda_v &= \kappa \left(\frac{\epsilon - \langle \epsilon \rangle}{\xi} - (1 - C_{Euler}) - \beta^2 \right) = \kappa(\lambda + \ln \kappa), \text{ and} \\ \kappa &= \xi/T_{max}. \end{aligned}$$

While this function in theory is universal for the needs of this study, clearly such a distribution function requires numeric methods, and as such is more costly than the Landau method. Fortunately, the Vavilov distribution converges to either the Landau distribution (for $\kappa \rightarrow 0$) or a Gaussian distribution (for $\kappa \rightarrow \infty$) at its extrema. The cutoffs for these extrema in practice are

$$\phi_v = \begin{cases} \text{Landau via Eqn. 2.15} & \kappa \leq 0.01 \\ \text{Vavilov via Eqn. 2.17} & 0.01 < \kappa < 10 \\ \text{Gaussian via } Gaus(\langle \epsilon \rangle, \sigma) \text{ in Eqns. 2.4 and 2.5} & 10 \leq \kappa \end{cases} \quad 10 \leq \kappa$$

2.2 Scattering

ICOOL version 3.30 [15] boasts a total of seven models of multiple scattering:

1. Gaussian (σ determined by Rossi-Greisen model),

2. Gaussian (σ determined by Highland model),
3. Gaussian (σ determined by Lynch-Dahl model),
4. Bethe version of Molière distribution with Rutherford limit,
5. Rutherford,
6. Fano with Rutherford limit, and
7. Tollestrup with Rutherford limit.

The scattering model used in this work is Fano with Rutherford limit, which is also the default scattering model in ICOOL. The following is a derivation of the Rutherford model accompanied by a few words on the Fano model. Unless otherwise stated, the derivation of the Rutherford model closely follows [6].

The Rutherford model is used in part in four out of the seven models because it is so robust. The derivation can be done using the Coulomb potential, classical mechanics, the Born approximation, and quantum field theory, with the quantum mechanics Born approximation being the weapon of choice here. Recall that the quantum model used is represented by Figure 2.3. Here there is an incoming wave (mathematically represented by e^{ikz}) and a spherical wave (represented by e^{ikr}/r). r and z are coordinates, i is the imaginary unit, and k is the wave number, classically related to the energy as $k = \sqrt{2mE}/\hbar$. Then basic quantum mechanics suggests that the solution to the Schrödinger equation has the form

$$\psi(r, \theta) \approx A(e^{ikz} + f(\theta) \frac{e^{ikr}}{r}), \quad (2.18)$$

where A is the total amplitude and $f(\theta)$ is the scattering amplitude. The probability of the particle scattering in a particular direction is given by the amplitude squared,

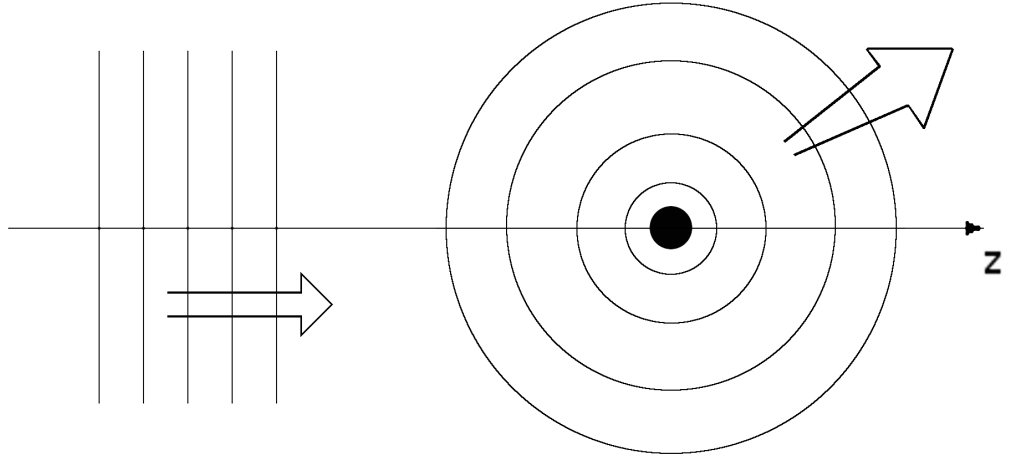


Figure 2.3: Quantum scattering model.

$|f(\theta)|^2$, and is the object of this derivation. Now, ψ solves the differential (time-independent) Schrödinger equation, which usually has the form

$$-\frac{\hbar^2}{2m}\nabla^2\psi + V\psi = E\psi,$$

where V is the system potential and E is the energy of the wavefunction. This can be expressed alternatively by assigning $Q \equiv V\psi \cdot 2m/\hbar^2$ and recalling that $k = \sqrt{2mE}/\hbar$. Then

$$(\nabla^2 + k^2)\psi = Q. \quad (2.19)$$

From Eqn. 2.18 it is clear that it is advantageous to solve Eqn. 2.19 for ψ , and if Eqn. 2.19 is solved for ψ then it suggests that ψ will be in integral form (note: it does not matter at this point that Q is a function of ψ , since the task will be to compare the integrated solution of Eqn. 2.19 with that of Eqn. 2.18). Observe then that Eqn. 2.19 may again be rewritten as

$$(\nabla^2 + k^2)\psi(\vec{r}) = Q(\vec{r}) = \int \delta^3(\vec{r} - \vec{r}_0)Q(\vec{r}_0)d^3\vec{r}_0.$$

Now it is natural to guess that there exists some function $G(\vec{r})$ such that

$$\psi(\vec{r}) = \int G(\vec{r} - \vec{r}_0) Q(\vec{r}_0) d^3 \vec{r}_0, \quad (2.20)$$

in which case

$$\begin{aligned} (\nabla^2 + k^2)\psi(\vec{r}) &= (\nabla^2 + k^2) \int G(\vec{r} - \vec{r}_0) Q(\vec{r}_0) d^3 \vec{r}_0 \\ &= \int [(\nabla^2 + k^2)G(\vec{r} - \vec{r}_0)] Q(\vec{r}_0) d^3 \vec{r}_0 \\ &= \int \delta^3(\vec{r} - \vec{r}_0) Q(\vec{r}_0) d^3 \vec{r}_0 = Q(\vec{r}), \end{aligned}$$

and so one comes to the conclusion that

$$(\nabla^2 + k^2)G(\vec{r}) = \delta^3(\vec{r}). \quad (2.21)$$

If Eqn. 2.21 seems familiar, it is because this is the Helmholtz equation with a delta function source. $G(\vec{r})$ is Green's function for the Helmholtz equation, and in this case is the response to the delta function source. Now, if one accepts that there exists a well-known particular solution for Eqn. 2.21, then one could skip forward to the solution in Eqn. 2.24; however, it will also be derived subsequently.

The usual strategy in solving systems like Eqn. 2.21 is to Fourier transform both the Green's function and the delta function. Then creating the dummy variable \vec{s} , the transform yields

$$G(\vec{r}) = \frac{1}{(2\pi)^{\frac{3}{2}}} \int e^{i\vec{s}\cdot\vec{r}} g(\vec{s}) d^3 \vec{s},$$

and

$$\delta^3(\vec{r}) = \frac{1}{(2\pi)^3} \int e^{i\vec{s}\cdot\vec{r}} d^3 \vec{s}.$$

Then from Eqn. 2.21,

$$\frac{1}{(2\pi)^{\frac{3}{2}}} \int (k^2 e^{i\vec{s}\cdot\vec{r}} - s^2 e^{i\vec{s}\cdot\vec{r}}) g(\vec{s}) d^3 \vec{s} = \frac{1}{(2\pi)^3} \int e^{i\vec{s}\cdot\vec{r}} d^3 \vec{s},$$

it is clear that $g(\vec{s}) = 1/(2\pi)^{3/2}(k^2 - s^2)$. Now all that is left is to find $G(\vec{r})$ from its transformation:

$$G(\vec{r}) = \frac{1}{(2\pi)^3} \int e^{i\vec{s}\cdot\vec{r}} \frac{d^3\vec{s}}{k^2 - s^2}$$

$$G(\vec{r}) = \frac{1}{(2\pi)^3} \int_0^\infty \frac{s}{k^2 - s^2} \left(\int_0^\pi e^{isr \cos \theta} \sin \theta d\theta \right) ds \int_0^{2\pi} d\phi.$$

The integration over ϕ is trivial, and the integration over θ can be done via u substitution. The last integral is over s , and is

$$G(\vec{r}) = \frac{1}{2\pi^2 r} \int_0^\infty \frac{s \sin sr}{k^2 - s^2} ds = \frac{1}{4\pi^2 r} \int_{-\infty}^\infty \frac{s \sin sr}{k^2 - s^2} ds.$$

This integral is not simple to solve, but it does have two poles at $s = k$ and $s = -k$, which implies the technique of choice should be to use Cauchy's integral formula for simple poles²:

$$\oint \frac{f(z)}{z - z_0} dz = 2\pi i f(z_0), \quad (2.22)$$

where the integral is done over some path in the complex plane and z_0 is the pole of interest which lies in the enclosed path (note: the integral is zero if there exist no poles in the enclosed path). It follows then that $f(z)$ is not simply any function, but a necessarily complex function which is closed. For this reason, the (strictly real) Green's function integral should be split up into two (strictly complex) functions, as depicted by Figure 2.4. This can be done by expanding the $\sin sr$ term and factoring $k^2 - s^2$:

$$G(\vec{r}) = \frac{i}{8\pi^2 r} \left[\int_{-\infty}^\infty \frac{se^{isr}}{(s - k)(s + k)} ds - \int_{-\infty}^\infty \frac{se^{-isr}}{(s - k)(s + k)} ds \right]. \quad (2.23)$$

Observe that in Eqn. 2.23 the path integrals at $|s| = \pm\infty$ have been left out. This is because they do not contribute to the integral, since the first integrand

²This touches an area of mathematics known as the calculus of residues, and is based on the Laurent series.

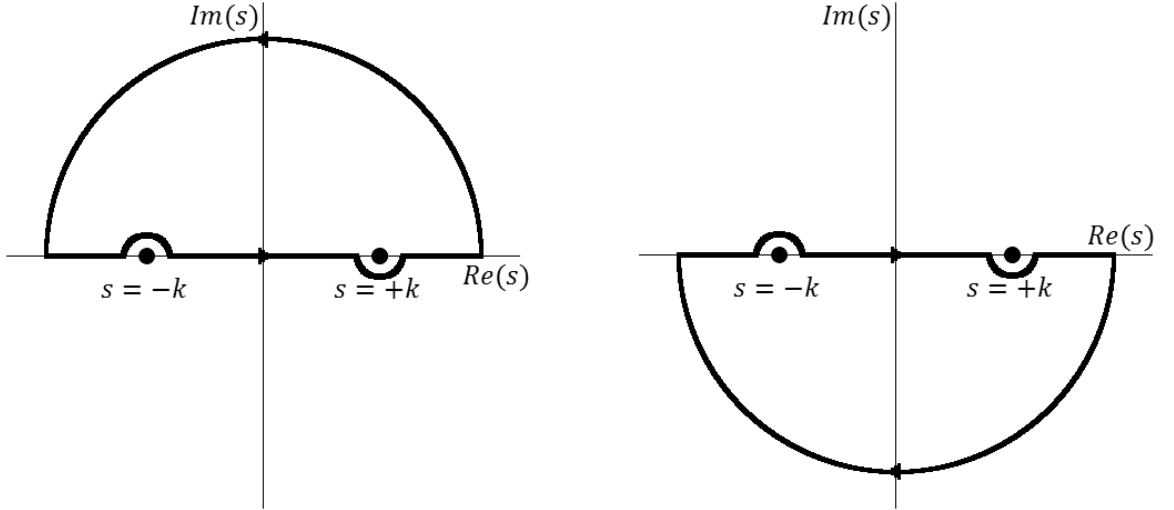


Figure 2.4: Two parts of Green's function with their poles at $s = \pm k$, altered to be closed via semicircle at $|s| = \pm \infty$.

corresponds to the left side of Figure 2.4 and goes like e^{isr} , hence going to zero at large positive imaginary numbers. Similarly, the second integrand goes like e^{-isr} and goes to zero at large negative imaginary numbers.

Combining Eqns. 2.22 and 2.23, it can be seen that

$$G(\vec{r}) = \frac{i}{8\pi^2 r} [(i\pi e^{ikr}) - (-i\pi e^{ikr})] = -\frac{e^{ikr}}{4\pi r}.$$

This is a particular solution to the Helmholtz equation. To get a general solution, the solution to the homogeneous Helmholtz equation must be added:

$$G(\vec{r}) = G_0(\vec{r}) - \frac{e^{ikr}}{4\pi r}; \quad (2.24)$$

that is, $G_0(\vec{r})$ solves $(\nabla^2 + k^2)G_0(\vec{r}) = 0$.

Using Eqn. 2.20 in conjunction with Eqn. 2.24 gives rise to the *integrated* time-independent Schrödinger equation:

$$\psi(\vec{r}) = \psi_0(\vec{r}) - \frac{m}{2\pi\hbar^2} \int \frac{e^{ik|\vec{r}-\vec{r}_0|}}{|\vec{r}-\vec{r}_0|} V(\vec{r}_0) \psi(\vec{r}_0) d^3\vec{r}_0. \quad (2.25)$$

Eqn. 2.25 gives the recursive form for ψ . Let $g = -me^{ik|\vec{r}-\vec{r}_0|}/2\pi\hbar^2|\vec{r}-\vec{r}_0|$. Then Eqn. 2.25 says that

$$\psi = \psi_0 + \int gV\psi = \psi_0 + \int gV(\psi_0 + \int gV\psi).$$

Applying this recursion several times gives the Born series:

$$\psi = \psi_0 + \int gV\psi_0 + \int \int gVgV\psi_0 + \int \int \int gVgVgV\psi_0 + \dots$$

The zeroth term is exact if there is no scattering whatsoever (i.e. $V = 0$) and the first term is accurate if the scattering potential is weak. For the purposes of this derivation, first order will be a sufficient approximation for ψ . Then

$$\psi = \psi_0 + \frac{m}{2\pi\hbar^2} \int \frac{e^{ik|\vec{r}-\vec{r}_0|}}{|\vec{r}-\vec{r}_0|} V(\vec{r}_0) \psi_0(\vec{r}_0) d^3\vec{r}_0$$

Recall that the strategy was to compare this solution of the Helmholtz equation with the wavefunction from the quantum scattering model (Eqn. 2.18) in order to find the scattering amplitude, $f(\theta)$. Doing so yields

$$f(\theta) = -\frac{r}{e^{ikr}} \frac{m}{2\pi\hbar^2 A} \int \frac{e^{ik|\vec{r}-\vec{r}_0|}}{|\vec{r}-\vec{r}_0|} V(\vec{r}_0) \psi_0(\vec{r}_0) d^3\vec{r}_0.$$

The Coulomb potential goes as $1/r^2$, and as such $V(\vec{r}_0)$ is localized about $\vec{r}_0 = 0$. Since particles are observed far away from their scattering centers, it is advantageous to make use of the fact that $\vec{r} \gg \vec{r}_0$. However, caution must be taken, since one must evaluate the exponential and non-exponential terms separately, for they are of separate orders. For the non-exponential terms, this is simple, since

$$\frac{r}{|\vec{r}-\vec{r}_0|} \approx 1.$$

The exponential terms look like

$$e^{ik(|\vec{r}-\vec{r}_0|-r)},$$

and so it is useful to expand the absolute value as

$$|\vec{r} - \vec{r}_0|^2 = r^2 + r_0^2 - 2\vec{r} \cdot \vec{r}_0 \approx r^2(1 - 2\frac{\vec{r} \cdot \vec{r}_0}{r^2}),$$

or simply

$$|\vec{r} - \vec{r}_0| \approx r - \hat{r} \cdot \vec{r}_0.$$

This leaves

$$f(\theta) = \frac{m}{2\pi\hbar^2} \int e^{-ik\hat{r} \cdot \vec{r}_0} V(\vec{r}_0) e^{ik\hat{z} \cdot \vec{r}_0} d^3 \vec{r}_0, \quad (2.26)$$

where $\psi_0(\vec{r}_0) = Ae^{ik\hat{z} \cdot \vec{r}_0}$. Now define $\vec{\kappa} \equiv k(\hat{z} - \hat{r})$ such that $\kappa = 2k \sin \theta/2$. The exponential term becomes

$$e^{i\vec{\kappa} \cdot \vec{r}_0} = e^{i\kappa r_0 \cos \theta_0}.$$

Furthermore, the form of the potential V is known. Since the scattering for the low Z target happens at low temperatures, it is possible to use the Fermi-Thomas approximation for screening [21]. This modifies the first Maxwell equation to

$$(\nabla^2 - b^2)V(r) = -\frac{Q}{\epsilon_0}\delta(r),$$

which has the solution

$$V(r) = \frac{Q}{4\pi\epsilon_0} \frac{e^{-br}}{r},$$

where b is some constant, ϵ_0 is the permittivity of free space, and Q is the charge of the potential (in this case, the atomic number Z). Then the quantum scattering equation (Eqn. 2.26) becomes

$$f(\theta) \propto \int e^{i\kappa r_0 \cos(\theta_0)} e^{-bro} r_0 \sin(\theta_0) dr_0 d\theta_0 d\phi_0,$$

where the amplitude terms have been left out since $|f(\theta)|^2$ is normalized anyway. Here it is seen that there does exist some θ dependence in $f(\theta)$ (by virtue of κ). The integral over ϕ_0 is trivial, and the integral over θ_0 can be done via u substitution. This leaves

$$f(\theta) \propto \frac{1}{\kappa} \int_0^\infty e^{-bro} \sin(\kappa r_0) dr_0,$$

which has the solution

$$f(\theta) \propto \frac{1}{b^2 + \kappa^2}.$$

For classical Rutherford scattering, $b \rightarrow 0$. Recalling that $\kappa = 2k \sin \theta / 2$ yields the final Rutherford scattering distribution:

$$|f(\theta)|^2 \propto \frac{1}{\sin^4(\theta/2)} \propto \frac{1}{(1 - \cos^2 \theta)^2}. \quad (2.27)$$

Only the tail of Eqn. 2.27 should be used since it blows up at $\theta = 0$. This may seem like a contradiction, since the Born series was truncated at the weak potential term (the first nontrivial term), and hence the incoming muons should not scatter much at all! In fact, the muons are not scattering much at all for each individual atom they encounter. Over the entire absorber, however, some muons will have a net scattering angle which is small (and therefore should not be approximated by the Rutherford tail) whereas others will have a large net scattering angle (and are well represented by Eqn. 2.27). Many weak potentials can still induce a relatively large scattered angle.

CHAPTER 3
STOCHASTIC PROCESSES IN G4BEAMLINE

3.1 Straggling

G4Beamline uses the in-house straggling model in [16]. GEANT4 has determined that a “thick absorber” occurs when the following conditions are met:

$$\begin{aligned}\epsilon &= \kappa T_c \\ T_{max} &\leq 2T_c,\end{aligned}\tag{3.1}$$

where T_c is the cut kinetic energy of δ -electrons and the other symbols can be found in the Definition of Terms at the beginning of this document.

For thick absorbers, the energy loss is sampled according to a simple Gaussian distribution with average equal to the Bethe Bloch energy loss (Eqn. 2.4) and a standard deviation according to Bohr’s variance (Eqn. 2.5).

If these conditions are not met, a “thin absorber” algorithm is called. Here, atoms are assumed to only have two energy levels with binding energies E_1 and E_2 . The interacting muon can then lose energy via excitation, yielding an energy loss of E_1 or E_2 , or lose energy via δ ray production, yielding an energy loss according to $g(E) \propto 1/E^2$, or (more likely) some combination or weighted average of the two. $g(E)$ may then be normalized:

$$\int_{E_0}^{T_{up}} g(E)dE = 1 \rightarrow g(E) = \frac{E_0 T_{up}}{T_{up} - E_0} \frac{1}{E^2},\tag{3.2}$$

where E_0 is the ionization energy of the atom in question and T_{up} is some kinetic energy cutoff (either the production threshold for delta rays or the maximum transferrable energy, whichever is smaller).

The probability for obtaining any one of these energy losses is given by the macroscopic cross section, Σ_i , where $i = 1, 2, 3$. For excitation ($i = 1, 2$), the cross section has a form similar to the deterministic Bethe-Bloch equation (Eqn. 2.4):

$$\Sigma_i = C \frac{f_i}{E_i} \frac{\ln(2m_e c^2 (\beta\gamma)^2 / E_i)}{\ln(2m_e c^2 (\beta\gamma)^2 / I)} (1 - r). \quad (3.3)$$

Here, C and $r = 0.55$ are model parameters with r describing the relative contribution of excitation to ionization, f_i are the relative oscillator strengths of the energy levels of E_i , I is the average ionization energy, and the other symbols have their usual meaning. For continuous energy loss, the cross section is given by

$$\Sigma_3 = C \frac{T_{up} - E_0}{T_{up} E_0 \ln(T_{up}/E_0)} r. \quad (3.4)$$

The oscillator strengths are relative to one another and hence should satisfy

$$f_1 + f_2 = 1. \quad (3.5)$$

The next constraint comes from [22] and simply states that all the energy levels should be weighted and add logarithmically to the total ionization energy:

$$f_1 \ln E_1 + f_2 \ln E_2 = \ln I. \quad (3.6)$$

Moreover, f_1 and f_2 can be thought of as representing the relative number of loosely and tightly bound electrons. Then using the first constraint, it is easy to see that the absolute number of loosely bound electrons are $Z \cdot f_1$ and the absolute number of tightly bound electrons are $Z \cdot f_2$ (since $Z \cdot f_1 + Z \cdot f_2 = Z$). For modelling purposes, GEANT4 has placed empirical initial conditions on these parameters:

$$f_2 = 0 \quad \text{for } Z = 1, \quad (3.7)$$

$$f_2 = 2/Z \quad \text{for } Z \geq 2, \quad (3.8)$$

$$E_2 = 10 \text{ eV } Z^2, \quad (3.9)$$

$$E_0 = 10 \text{ eV}. \quad (3.10)$$

From these, f_1 and E_1 can be found from Eqns. ?? and ?? given a particular muon through a particular material (from which Z , I , β , and the like are taken).

Finally, an energy loss for a thin absorber can be sampled. For the contribution due to excitation, two numbers n_1 and n_2 are sampled randomly from a Poisson distribution. These numbers represent the relative contributions of the energy levels of E_1 and E_2 , respectively:

$$\epsilon_{exc} = n_1 E_1 + n_2 E_2.$$

The contribution due to ionization can be found by inverting the cumulative distribution function of $g(E)$:

$$G(E) = \int_{E_0}^E g(E)dE \rightarrow E = \frac{E_0}{1 - u \frac{T_{up} - E_0}{T_{up}}}.$$

However, this is only for a single ionization. For an absorber of length L , the number of ionizations n_3 is again sampled from a Poisson distribution. Then the total energy loss for thin absorbers is

$$\epsilon = n_1 E_1 + n_2 E_2 + \sum_{j=1}^{n_3} \frac{E_0}{1 - u_j \frac{T_{up} - E_0}{T_{up}}}. \quad (3.11)$$

It should be noted that [16] does make a brief mention of a width correction algorithm. This algorithm allegedly decreases the dependence of the results on kinetic energy cuts and stepsizes and works for any thickness of material. However, the section in the manual is less than a page long and purely conceptual without any mathematics or data on which to elaborate.

Finally, the GEANT4 straggling routine can be summarized as such:

1. Determine if absorber is “thick” via Eqn. 3.1.
2. If absorber is “thick”, use Gaussian distribution with mean $\mu = \langle dE/dx \rangle$ (from Eqn. 2.4) and standard deviation from Eqn. ??.

3. If absorber is “thin”, use Eqn. 3.11.

- Select n_1 , n_2 , and n_3 from a Poisson distribution.
- Select u_j from a uniform distribution on $[0, 1]$ (where $j = 1 \dots n_3$).
- Find E_2 , f_2 , and E_0 from Eqn. 3.7.
- Find E_1 from Eqns. 3.5 and 3.6.

4. Apply width correction algorithm.

3.2 Scattering

The G4Beamline scattering model in [23] uses the GEANT4 Urbán model [16], and again parameterizes according to experimental data and Lewis theory [24]. Based on the models available, it can be inferred that the function responsible for the sampling of the angular distribution, $g(u)$, is based off [25] and Rutherford scattering, which was derived in Section ?? and resulted in Eqn. 2.27. It should be noted that the shape of $g(u)$ was chosen empirically, and is

$$g(u) = q_g[p_g g_1(u) + (1 - p_g)g_2(u)] + (1 - q_g)g_3(u), \quad (3.12)$$

where $0 \leq p_g, q_g \leq 1$ and

$$\begin{aligned} g_1(u) &= C_1 e^{-a(1-u)} & -1 \leq u_0 \leq u \leq 1 \\ g_2(u) &= C_2 \frac{1}{(b_r - u)^{d_r}} & -1 \leq u \leq u_0 \leq 1 \\ g_3(u) &= C_3 & -1 \leq u \leq 1 \end{aligned}$$

are normalized over $[-1, 1]$, where C_i are normalization constants and a , b_r , d_r , and u_0 are empirical parameters. Here [16] points out that for small angles, $g(u)$ is nearly Gaussian since $\exp(1 - u) = \exp(1 - \cos \theta) \approx \exp(\theta^2/2)$ and for large angles $g(u)$ resembles the Rutherford dependence of Eqn. 2.27 for $b_r \approx 1$ and d_r close to 2.

While Eqn. 3.12 is the main point of this section, it would be incomplete without shedding some light on the six parameters mentioned. a , u_0 , and d_r are chosen based off theoretical and experimental data and p_g , q_g , and b_r satisfy constraints. The form of a is chosen by comparing the modified Highland-Lynch-Dahl formula for the width of the angular distribution to that of $g_1(u)$. If θ_0 is the Highland-Lynch-Dahl width of the (approximate) Gaussian distribution then it follows that on one hand

$$\exp\left(-\frac{\theta^2}{2\theta_0^2}\right) \approx \exp\left(\frac{1}{2} \cdot \frac{1 - \cos \theta}{1 - \cos \theta_0}\right),$$

and on the other

$$g_1(u) \propto \exp(-a(1-u)).$$

Therefore, it is reasonable to choose a as

$$a = \frac{0.5}{1 - \cos \theta_0} \quad (3.13)$$

so that

$$g_1(u) \propto \exp\left(-\frac{\theta^2}{2\theta_0^2}\right).$$

For heavy charged particles (such as muons), the model for θ_0 has been chosen as

$$\theta_0 = \frac{13.6 \text{ MeV}}{\beta cp} z_{ch} \sqrt{\frac{t}{X_0} \left[1 + 0.105 \ln\left(\frac{t}{X_0}\right) + 0.0035 \left(\ln\left(\frac{t}{X_0}\right) \right)^2 \right]} \left(1 - \frac{0.24}{Z(Z+1)} \right).$$

It is reasonable to demand that $g(u)$ be continuous and smooth on $[-1, 1]$. Taking these conditions at $u = u_0$ yields the following constraints:

$$\begin{aligned} p_g g_1(u_0) &= (1 - p_g) g_2(u_0) \\ a \cdot p_g g_1(u_0) &= (1 - p_g) g_2(u_0) \cdot \frac{d_r}{b_r - u_0}. \end{aligned}$$

From the first equation, it is simple to see that

$$p_g = \frac{g_2(u_0)}{g_1(u_0) + g_2(u_0)} \quad (3.14)$$

and that

$$a = \frac{d_r}{b_r - u_0}.$$

Here, apparently

$$u_0 = 1 - \frac{3}{a} \quad (3.15)$$

and (for heavy particles like muons)

$$d_r = 2.40 - 0.027Z^{\frac{2}{3}}. \quad (3.16)$$

[16] does not elaborate on this parameterization, but validation in Section ?? will show that these are reasonable. Moving forward, this yields

$$b_r = \frac{a}{d_r} + u_0. \quad (3.17)$$

Lastly, q_g is found by knowing that $g(u)$ must give the same mean value as Lewis theory. While complicated, q_g is shown here for completion's sake. [16] shows that

$$q_g = \frac{(1 - \frac{\lambda_{10} - \lambda_{11}}{\lambda_{10}})^{\frac{t}{\lambda_{10} - \lambda_{11}}}}{p_g \langle u \rangle_1 + (1 - p_g) \langle u \rangle_2}, \quad (3.18)$$

where λ_{10} is the value of the first transport free mean path at the beginning of the step and λ_{11} is this value at the end of the step.

In summary, the scattering model used by G4Beamline is based on the Geant4 model, which includes Lewis theory. The full form of the scattering equation is given by Eqn. 3.12. This model has 9 parameters:

Parameter	Found Via	Equation Number
C_1 , C_2 , and C_3	Normalization	N/A
a	Relating the Gaussian-like behavior of g to Highland-like theory [12]	3.13
p_g and b_r	Demanding continuity and smoothness	3.14 and 3.17
u_0 and d_r	Emperical parameterization	3.15 and 3.16
q_g	Demanding that g gives the same mean value as Lewis theory	3.18

CHAPTER 4
STOCHASTIC PROCESSES IN COSY INFINITY

4.1 Straggling

COSY uses Landau theory [17] to describe the straggling distribution. This theory is discussed in detail in Section 2.1.2. Other straggling models which were investigated were

- Functionalization
- Urbán model [16]
- Vavilov theory [20]
- Edgeworth series [26]
- Convolution method (compound Poisson method) [27]
- Landau/Gaussian convolution [28]
- Blunck-Liesegang theory [29]

However, Landau theory proved to be the best fit. It was chosen over the Vavilov distribution in particular due to a complication where the Vavilov tail was abruptly cut off under certain circumstances.

The average of the Landau distribution is infinity, which is clearly nonphysical. Given the universal Landau parameter (Eqn. 2.16),

$$\lambda = \frac{\epsilon - \langle \epsilon \rangle}{\xi} - (1 - C_{Euler}) - \beta^2 - \ln(\xi/T_{max}),$$

fluctuations about the mean energy loss $\langle \epsilon - \langle \epsilon \rangle \rangle$ will also be divergent given enough samples. This results in a sensitivity to stepsize. In order to combat this, an artificial cutoff is given to λ such that the average Landau ϵ is equal to the average Bethe-Bloch energy loss $\langle \epsilon \rangle$. That is, it is required that

$$\begin{aligned}\langle \lambda \rangle &= \left\langle \frac{\epsilon - \langle \epsilon \rangle}{\xi} \right\rangle - (1 - C_{Euler}) - \beta^2 - \ln(\xi/T_{max}) \\ &= -(1 - C_{Euler}) - \beta^2 - \ln(\xi/T_{max}).\end{aligned}$$

If this cutoff is λ_{max} , then $\langle \lambda \rangle$ can be calculated as

$$\langle \lambda \rangle = \frac{\int_0^{\lambda_{max}} \lambda * f(\lambda) d\lambda}{\int_0^{\lambda_{max}} f(\lambda) d\lambda}.$$

The task then is to numerically find λ_{max} such that it satisfies

$$\frac{\int_0^{\lambda_{max}} \lambda * f(\lambda) d\lambda}{\int_0^{\lambda_{max}} f(\lambda) d\lambda} = -(1 - C_{Euler}) - \beta^2 - \ln(\xi/T_{max}).$$

Geant version 3.21 [30] suggests the following form for λ_{max} :

$$\lambda_{max} = 0.60715 + 1.1934 \langle \lambda \rangle + (0.67794 + 0.052382 \langle \lambda \rangle) \exp[0.94753 + 0.74442 \langle \lambda \rangle] \quad (4.1)$$

(note that Geant 4 does not have a section on the Landau cutoff since the Urbán model is used instead). However, a plot of required cutoffs (λ_{max}) vs. desired means ($\langle \lambda \rangle$) was plotted independently in this work with muon ionization cooling parameters in mind. The results are shown in Figure 4.1, and the determined form of the function is

$$\lambda_{max} = 0.517891 + 1.17765 \langle \lambda \rangle + (0.476074 + 0.00880733 \langle \lambda \rangle) \exp[1.15467 + 0.984008 \langle \lambda \rangle]. \quad (4.2)$$

This may be easily interpreted into some ϵ_{max} using Eqn. 2.16:

$$\epsilon_{max} = \xi[\lambda_{max} + (1 - C_{Euler}) + \beta^2 + \ln(\xi/T_{max})] + \langle \epsilon \rangle.$$

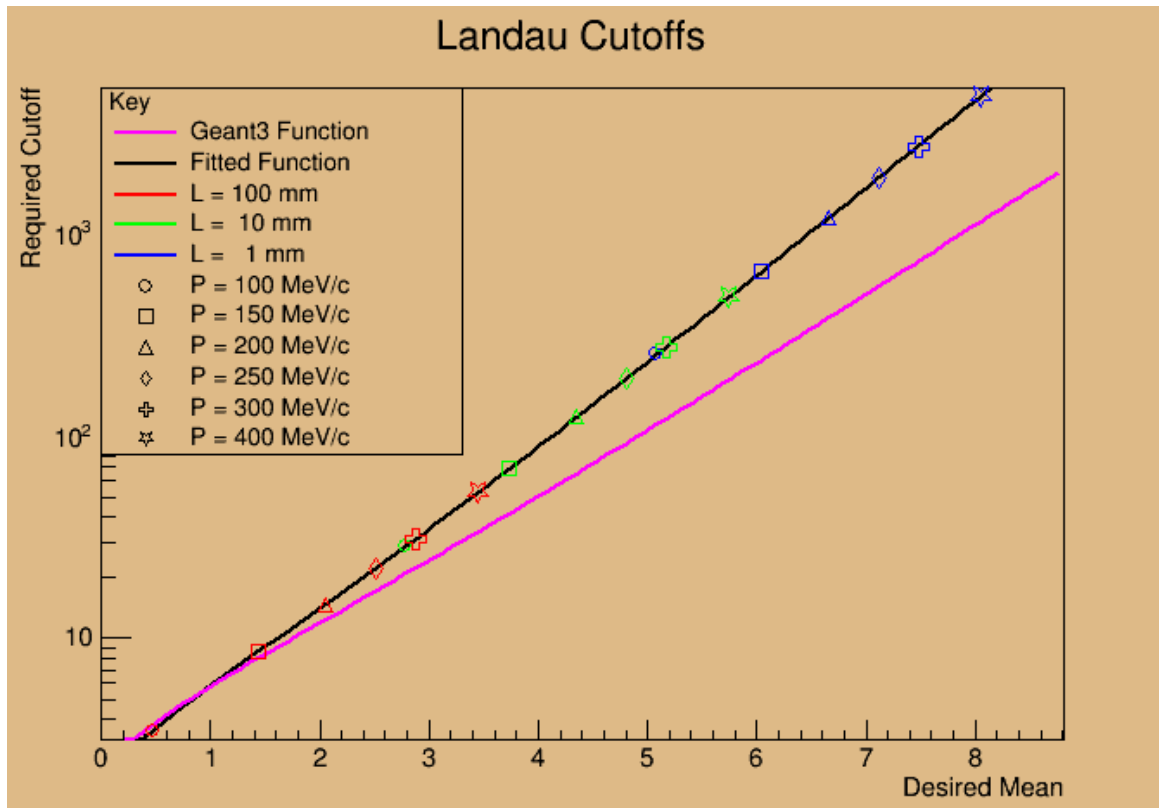


Figure 4.1: λ_{max} vs. $\langle \lambda \rangle$ over a variety of liquid hydrogen absorber lengths and initial beam momenta. The black line is the fitted curve (see Eqn. 4.2) and the pink line is the form given by Geant 3 (see Eqn. 4.1).

Therefore, during the energy loss sampling, if any energy loss ϵ is selected which is greater than ϵ_{max} it is thrown out and the sampling is performed again. However, if the result has been thrown out 100 times, the particle is assumed to have lost too much energy and is considered lost.

4.2 Scattering

Similar to ICOOL’s fifth method of scattering, the Rutherford model (see Sec. 2.2), COSY utilizes a piecewise distribution function which is Gaussian at small angles (as Goudsmit and Saunderson suggested [25]) and Rutherford-like at large angles. This Rutherford-like tail is derived in Sec. 4.2.1 and yields the Mott scattering cross section in Eqn. 4.4. The practical implementation of this probability distribution function is then discussed in Sec. 4.2.2.

4.2.1 Theoretical Derivation.

Electron-muon scattering is a textbook scattering problem following Feynman rules [1]. Similar to both Secs. 2.2 and 2.1, either the collision time of the muon and electron is assumed to be very small compared to the electron orbital time or the electron is initially at rest. The z-axis is aligned with the muon’s velocity such that $v_x = v_y = 0$. The reference frame is the lab frame. Please refer to the Supplemental Information in Section 6.1 for a review on symbols and methods.

To find the scattering cross section, it is necessary to have both the scattering amplitude \mathcal{M} (sometimes also called the ‘matrix element’, although this is a little ambiguous) and the available phase space over which to integrate. However, [1] notes that the integration over the available phase space is simply a constant. Since this cross section is the tail of a piecewise function, all multiplicative constants will be

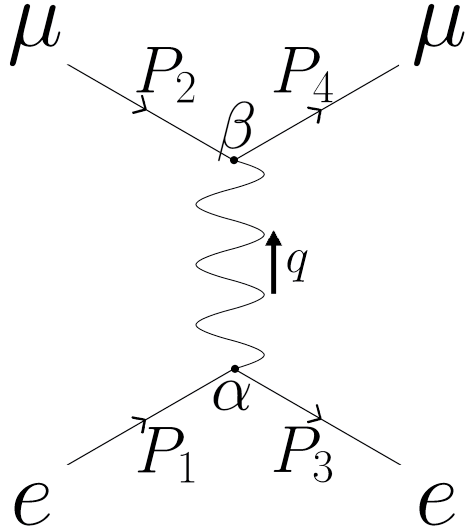


Figure 4.2: Feynman diagram for electron-muon scattering. P_1 and P_2 are the incoming four-momenta for the electron and muon and P_3 and P_4 are the outgoing four-momenta. Q represents the four-momentum carried by the virtual photon.

thrown out since these functions will have to be renormalized anyway. Then

$$\frac{d\sigma}{d\Omega} \propto |\mathcal{M}|^2.$$

Section 6.4 elaborates on the process of determining \mathcal{M} from Figure 4.2. This results in the scattering amplitude found in Eqn. 6.15, reproduced here by doing away with the constants:

$$\mathcal{M} \propto \bar{U}_4 \gamma^\beta U_2 * \frac{1}{q^2} (-\eta_{\alpha\beta} + \frac{q_\alpha q_\beta}{q^2}) * \bar{U}_3 \gamma^\alpha U_1.$$

Taking the second term in parenthesis, observe that it is proportional to $\bar{U}_4 \gamma^\beta U_2 q_\beta$. By conservation of P_β at vertex β , it can be seen that $P_{2\beta} + q_\beta = P_{4\beta}$. Then

$$\begin{aligned} \bar{U}_4 \gamma^\beta U_2 q_\beta &= \bar{U}_4 (\gamma^\beta (P_{4\beta} - P_{2\beta})) U_2 \\ &= \bar{U}_4 (\gamma^\beta P_{4\beta} - \gamma^\beta P_{2\beta}) U_2. \end{aligned}$$

Eqn. 6.2 states that $\gamma^\alpha P_\alpha - m = 0$ for particles, and so

$$\bar{U}_4 \gamma^\beta U_2 q_\beta = \bar{U}_4 (m_\mu - m_\mu) U_2 = 0.$$

For this reason, the second term in parenthesis vanishes entirely, leaving

$$\mathcal{M} \propto \bar{U}_4 \gamma^\beta U_2 * \frac{\eta_{\alpha\beta}}{q^2} * \bar{U}_3 \gamma^\alpha U_1,$$

or propagating the $\eta_{\alpha\beta}$ through,

$$\mathcal{M} \propto \bar{U}_4 \gamma^\beta U_2 * \frac{1}{q^2} * \bar{U}_3 \gamma_\beta U_1.$$

The final cross section is proportional to $|\mathcal{M}|^2$, and so

$$|\mathcal{M}|^2 \propto \frac{1}{q^4} * \bar{U}_4 \gamma^\beta U_2 [\bar{U}_4 \gamma^\delta U_2]^* * \bar{U}_3 \gamma_\beta U_1 [\bar{U}_3 \gamma_\delta U_1]^*.$$

Since $\bar{U}_4 \gamma^\beta U_2$ is the same as $\bar{U}_3 \gamma_\beta U_1$ except for notation, from here the quantity $\bar{U}_4 \gamma^\beta U_2 [\bar{U}_4 \gamma^\delta U_2]^*$ will be reduced and the same treatment will be applied to $\bar{U}_3 \gamma_\beta U_1 [\bar{U}_3 \gamma_\delta U_1]^*$.

Since $\bar{U}_4 \gamma^\delta U_2 \in \mathbb{C}$ in Dirac space,

$$\begin{aligned} [\bar{U}_4 \gamma^\delta U_2]^* &= [\bar{U}_4 \gamma^\delta U_2]^\dagger \\ &= U_2^\dagger \gamma^{\delta\dagger} \bar{U}_4^\dagger. \end{aligned}$$

Observe that since γ^δ has the form

$$\gamma^\delta = \begin{pmatrix} A & B \\ -B & -A \end{pmatrix}$$

then

$$\begin{aligned} \gamma^0 \gamma^\delta \gamma^0 &= \begin{pmatrix} I_2 & 0 \\ 0 & I_2 \end{pmatrix} \begin{pmatrix} A & B \\ -B & -A \end{pmatrix} \begin{pmatrix} I_2 & 0 \\ 0 & I_2 \end{pmatrix} \\ &= \begin{pmatrix} A & -B \\ B & -A \end{pmatrix} \\ &= \gamma^{\delta\dagger}, \end{aligned}$$

and so

$$[\bar{U}_4 \gamma^\delta U_2]^* = U_2^\dagger [\gamma^0 \gamma^\delta \gamma^0] \bar{U}_4^\dagger.$$

Recall the definition of the spinor adjoint in Eqn. 6.3:

$$\bar{U} = U^\dagger \gamma^0.$$

Then

$$\begin{aligned} \bar{U}_4^\dagger &= (U_4^\dagger \gamma^0)^\dagger \\ &= \gamma^{0\dagger} U_4^{\dagger\dagger} \\ &= \gamma^0 U_4, \end{aligned}$$

which results in

$$[\bar{U}_4 \gamma^\delta U_2]^* = U_2^\dagger [\gamma^0 \gamma^\delta \gamma^0] [\gamma^0 U_4],$$

or more suggestively,

$$\begin{aligned} [\bar{U}_4 \gamma^\delta U_2]^* &= [U_2^\dagger \gamma^0] \gamma^\delta [\gamma^0 \gamma^0] U_4 \\ &= \bar{U}_2 \gamma^\delta U_4. \end{aligned}$$

This results in

$$|\mathcal{M}|^2 \propto \frac{1}{q^4} * \bar{U}_4 \gamma^\beta U_2 \bar{U}_2 \gamma^\delta U_4 * \bar{U}_3 \gamma_\beta U_1 \bar{U}_1 \gamma_\delta U_3. \quad (4.3)$$

In principle, if the spinors of the muons were known (e.g. the muons were part of a polarized beam) this could be evaluated directly. However, in general the spinors are not known. As an approximation, it is necessary to average the spinors over their spins. Again, starting with the muons and extrapolating the treatment to the electrons,

$$\begin{aligned} \langle \bar{U}_4 \gamma^\beta U_2 \bar{U}_2 \gamma^\delta U_4 \rangle_{\text{spin } 2} &= \frac{1}{2} \sum_{s_2=1}^2 \bar{U}_4 \gamma^\beta U_2^{(s_2)} \bar{U}_2^{(s_2)} \gamma^\delta U_4 \\ &= \frac{1}{2} \bar{U}_4 \gamma^\beta \left[\sum_{s_2=1}^2 U_2^{(s_2)} \bar{U}_2^{(s_2)} \right] \gamma^\delta U_4. \end{aligned}$$

Recall the completeness property of spinors (Eqn. 6.4):

$$\sum_s U^{(s)} \bar{U}^{(s)} = \gamma^\alpha P_\alpha + m$$

then

$$\langle \bar{U}_4 \gamma^\beta U_2 \bar{U}_2 \gamma^\delta U_4 \rangle_{\text{spin } 2} = \frac{1}{2} \bar{U}_4 \gamma^\beta (\gamma^\epsilon P_{2\epsilon} + m_\mu) \gamma^\delta U_4.$$

Averaging similarly over the spin for particle #4 yields

$$\langle \bar{U}_4 \gamma^\beta U_2 \bar{U}_2 \gamma^\delta U_4 \rangle_{\text{spin } 2, \text{ spin } 4} = \frac{1}{2} \frac{1}{2} \sum_{s_4=1}^2 \bar{U}_4^{(s_4)} [\gamma^\beta (\gamma^\epsilon P_{2\epsilon} + m_\mu) \gamma^\delta] U_4^{(s_4)}.$$

Now, spinors do not generally commute, but their components (which are scalars) do.

Observing that \bar{U} is a 1x4 row vector, the bracketed term is a 4x4 matrix, and U is a 4x1 column vector, it is possible to write out the matrix multiplication as an explicit double sum over the indices i, j :

$$\begin{aligned} \langle \bar{U}_4 \gamma^\beta U_2 \bar{U}_2 \gamma^\delta U_4 \rangle_{s_2, s_4} &= \frac{1}{4} \sum_{s_4=1}^2 \sum_{i,j=1}^4 \bar{U}_{4i}^{(s_4)} [\gamma^\beta (\gamma^\epsilon P_{2\epsilon} + m_\mu) \gamma^\delta]_{ij} U_{4j}^{(s_4)} \\ &= \frac{1}{4} \sum_{i,j=1}^4 \left([\gamma^\beta (\gamma^\epsilon P_{2\epsilon} + m_\mu) \gamma^\delta]_{ij} \left[\sum_{s_4=1}^2 \bar{U}_4^{(s_4)} U_4^{(s_4)} \right]_{ij} \right) \end{aligned}$$

Spinor completeness (Eqn. 6.4) requires a summation over $U \bar{U}$, not $\bar{U} U$. However, $\bar{U} U$ is still useful. Since $A^T + B^T = [A + B]^T$,

$$\begin{aligned} \sum \bar{U} U &= \left[\sum (\bar{U} U)^T \right]^T \\ &= \left[\sum U^T \bar{U}^T \right]^T. \end{aligned}$$

Again explicitly writing the matrix multiplication,

$$\begin{aligned}
\sum \bar{U}U &= \left[\sum_{k,l} \left(\sum_{k,l}^4 (U_k)^T (\bar{U}_l)^T \right) \right]^T \\
&= \left[\sum_{k,l}^4 \left(\sum_{k,l} (U_k)^T (\bar{U}_l)^T \right) \right]^T \\
&= \left[\sum_{k,l}^4 \left(\sum_{k,l} U_l \bar{U}_k \right) \right]^T \\
&= \left[\sum_{k,l}^4 \left(\sum_{k,l} U \bar{U} \right) \right]_{l,k}^T.
\end{aligned}$$

Now it is possible to use spinor completeness (Eqn. 6.4):

$$\begin{aligned}
\sum \bar{U}U &= \left[\sum_{k,l} (\gamma^\alpha P_\alpha + m)_{l,k} \right] \\
&= (\gamma^\alpha P_\alpha + m)^T.
\end{aligned}$$

Conclusively, if the i - j^{th} component of $\sum \bar{U}U$ is desired, then the indices of Eqn. 6.4 must be exchanged:

$$\begin{aligned}
\left[\sum \bar{U}U \right]_{i,j} &= [(\gamma^\alpha P_\alpha + m)^T]_{i,j} \\
&= [(\gamma^\alpha P_\alpha + m)_{i,j}]^T \\
&= [\gamma^\alpha P_\alpha + m]_{j,i}.
\end{aligned}$$

This results in

$$\langle \bar{U}_4 \gamma^\beta U_2 \bar{U}_2 \gamma^\delta U_4 \rangle_{s2, s4} = \frac{1}{4} \sum_{i,j=1}^4 ([\gamma^\beta (\gamma^\epsilon P_{2\epsilon} + m_\mu) \gamma^\delta]_{ij} [\gamma^\kappa P_{4\kappa} + m_\mu]_{j,i}).$$

Upon the concatenation of the subscripts i, j and j, i , it can be seen that

$$\langle \bar{U}_4 \gamma^\beta U_2 \bar{U}_2 \gamma^\delta U_4 \rangle_{s2, s4} = \frac{1}{4} \sum_{i=1}^4 ([\gamma^\beta (\gamma^\epsilon P_{2\epsilon} + m_\mu) \gamma^\delta] (\gamma^\kappa P_{4\kappa} + m_\mu))_{ii}.$$

This is now the definition of a trace ($\sum_i M_{ii} \equiv \text{Tr}(M)$). Then

$$\langle \bar{U}_4 \gamma^\beta U_2 \bar{U}_2 \gamma^\delta U_4 \rangle_{s2, s4} = \frac{1}{4} \text{Tr}[\gamma^\beta (\gamma^\epsilon P_{2\epsilon} + m_\mu) \gamma^\delta (\gamma^\kappa P_{4\kappa} + m_\mu)].$$

Using the addition property of traces, it is clear that there are four terms to evaluate:

$$i) \quad \text{Tr}(\gamma^\beta \gamma^\epsilon P_{2\epsilon} \gamma^\delta \gamma^\kappa P_{4\kappa})$$

$$ii) \quad \text{Tr}(\gamma^\beta \gamma^\epsilon P_{2\epsilon} \gamma^\delta m_\mu)$$

$$iii) \quad \text{Tr}(\gamma^\beta m_\mu \gamma^\delta \gamma^\kappa P_{4\kappa})$$

$$iv) \quad \text{Tr}(\gamma^\beta m_\mu \gamma^\delta m_\mu).$$

The derivations for the solutions to these traces can be found in Sec. 6.3. The first term is the trace of four γ matrices and can be solved by using Eqn. 6.14:

$$\begin{aligned} \text{Tr}(\gamma^\beta \gamma^\epsilon P_{2\epsilon} \gamma^\delta \gamma^\kappa P_{4\kappa}) &= P_{2\epsilon} P_{4\kappa} \text{Tr}(\gamma^\beta \gamma^\epsilon \gamma^\delta \gamma^\kappa) \\ &= 4P_{2\epsilon} P_{4\kappa} (\eta^{\beta\epsilon} \eta^{\delta\kappa} - \eta^{\beta\delta} \eta^{\epsilon\kappa} + \eta^{\beta\kappa} \eta^{\epsilon\delta}) \\ &= 4(P_2^\beta P_4^\delta - P_2 \cdot P_4 \eta^{\beta\delta} + P_2^\delta P_4^\beta). \end{aligned}$$

The second term is the trace of an odd number of γ matrices, and is equal to zero via Eqn. 6.11:

$$\begin{aligned} \text{Tr}(\gamma^\beta \gamma^\epsilon P_{2\epsilon} \gamma^\delta m_\mu) &= P_{2\epsilon} m_\mu \text{Tr}(\gamma^\beta \gamma^\epsilon \gamma^\delta) \\ &= 0. \end{aligned}$$

The third term is also a trace of an odd number of γ matrices:

$$\begin{aligned} \text{Tr}(\gamma^\beta m_\mu \gamma^\delta \gamma^\kappa P_{4\kappa}) &= m_\mu P_{4\kappa} \text{Tr}(\gamma^\beta \gamma^\delta \gamma^\kappa) \\ &= 0. \end{aligned}$$

The final term is the trace of two γ matrices, and results in the Minkowski metric via Eqn. 6.13:

$$\begin{aligned} \text{Tr}(\gamma^\beta m_\mu \gamma^\delta m_\mu) &= m_\mu^2 \text{Tr}(\gamma^\beta \gamma^\delta) \\ &= 4m_\mu^2 \eta^{\beta\delta}. \end{aligned}$$

Putting it all together results in

$$\langle \bar{U}_4 \gamma^\beta U_2 \bar{U}_2 \gamma^\delta U_4 \rangle_{s2, s4} = P_2^\beta P_4^\delta - P_2 \cdot P_4 \eta^{\beta\delta} + P_2^\delta P_4^\beta + m_\mu^2 \eta^{\beta\delta}.$$

The electron portion is mathematically the same. Symbolically, contravariant indices become covariant (e.g. γ^β becomes γ_β), the mass is now the electron mass (i.e. m_μ becomes m_e), and the even subscripts become odd (i.e. P_2, P_4 become P_1, P_3). Explicitly, Eqn. 4.3 becomes

$$\begin{aligned} \langle |\mathcal{M}|^2 \rangle &\propto \frac{1}{q^4} * \langle \bar{U}_4 \gamma^\beta U_2 \bar{U}_2 \gamma^\delta U_4 \rangle_{s2, s4} * \langle \bar{U}_3 \gamma_\beta U_1 \bar{U}_1 \gamma_\delta U_4 \rangle_{s1, s3} \\ &\propto \frac{1}{q^4} * (P_2^\beta P_4^\delta - P_2 \cdot P_4 \eta^{\beta\delta} + P_2^\delta P_4^\beta + m_\mu^2 \eta^{\beta\delta}) * (P_{1\beta} P_{3\delta} - P_1 \cdot P_3 \eta_{\beta\delta} + P_{1\delta} P_{3\beta} + m_e^2 \eta_{\beta\delta}) \end{aligned}$$

Explicitly, the algebra is

$$\begin{aligned} \langle |\mathcal{M}|^2 \rangle &\propto \frac{1}{q^4} * [(P_1 \cdot P_2)(P_3 \cdot P_4) - (P_1 \cdot P_3)(P_2 \cdot P_4) + (P_1 \cdot P_4)(P_2 \cdot P_3) + m_e^2(P_2 \cdot P_4) \\ &\quad - (P_1 \cdot P_3)(P_2 \cdot P_4) + 4(P_1 \cdot P_3)(P_2 \cdot P_4) - (P_1 \cdot P_3)(P_2 \cdot P_4) - 4m_e^2(P_2 \cdot P_4) \\ &\quad + (P_1 \cdot P_4)(P_2 \cdot P_3) - (P_1 \cdot P_3)(P_2 \cdot P_4) + (P_1 \cdot P_2)(P_3 \cdot P_4) + m_e^2(P_2 \cdot P_4) \\ &\quad + m_\mu^2(P_1 \cdot P_3) - 4m_\mu^2(P_1 \cdot P_3) + m_\mu^2(P_1 \cdot P_3) + 4m_\mu^2 m_e^2], \end{aligned}$$

with $\eta^{\alpha\beta} \eta_{\alpha\beta} = 4$. Gathering the like terms, this reduces to

$$\langle |\mathcal{M}|^2 \rangle \propto \frac{1}{q^4} [2(P_1 \cdot P_4)(P_2 \cdot P_3) + 2(P_1 \cdot P_2)(P_3 \cdot P_4) - 2m_e^2(P_2 \cdot P_4) - 2m_\mu^2(P_1 \cdot P_3) + 4m_\mu^2 m_e^2].$$

Up until here, this is a quite general expression for two particles interacting via virtual photon exchange. For COSY, straggling and scattering are mutually exclusive processes: first the straggling routine is called and then the scattering routine is called. Therefore, for this model it must be assumed that there is no energy exchange between the muon and electron. Consequently, since the electron is bound it will remain fixed and the muon will scatter. This can be seen diagrammatically in Figure 4.3.

Now it is clear that $P_1 = P_3 = (m_e, 0, 0, 0)$. Furthermore, since the total energy of the muon is conserved $E_2 = E_4 = E_\mu$ and $P_2 = (E_\mu, \vec{p}_2)$ and $P_4 = (E_\mu, \vec{p}_4)$

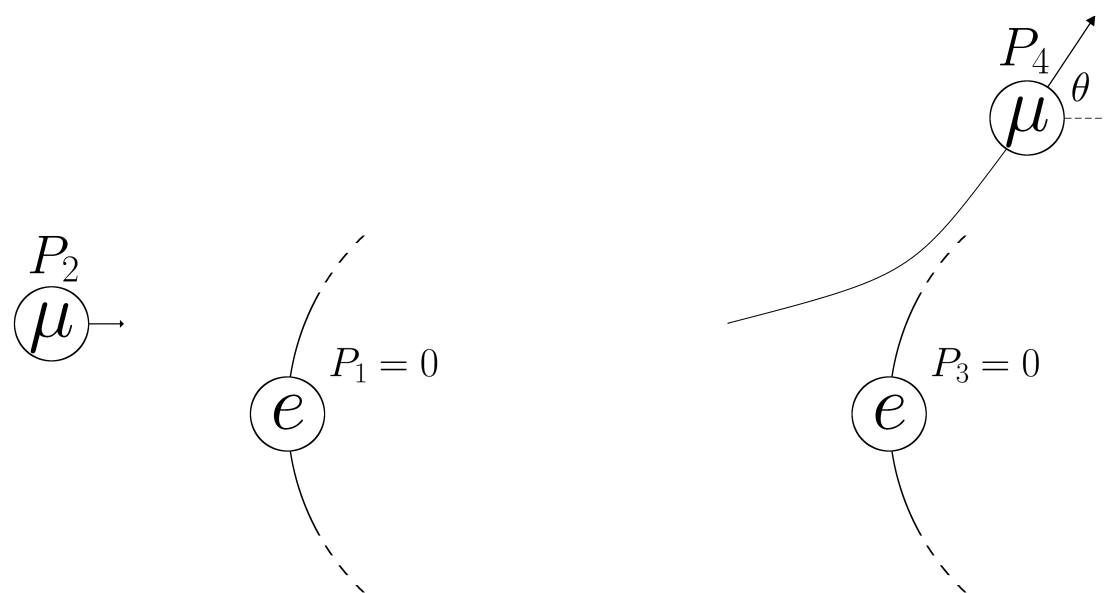


Figure 4.3: COSY treatment of muon-electron scattering. Since the routines are called separately, the model assumes no straggling while scattering.

and so

$$\begin{aligned}
 P_1 \cdot P_2 &= E_\mu m_e & P_1 \cdot P_3 &= m_e^2 \\
 P_1 \cdot P_4 &= E_\mu m_e & P_2 \cdot P_3 &= E_\mu m_e \\
 P_2 \cdot P_4 &= E_\mu^2 - \vec{p}_2 \cdot \vec{p}_4 & &= E_\mu^2 - p_\mu^2 \cos \theta \\
 P_3 \cdot P_4 &= E_\mu m_e.
 \end{aligned}$$

Then

$$\langle |\mathcal{M}|^2 \rangle \propto \frac{1}{q^4} [2(E_\mu m_e)(E_\mu m_e) + 2(E_\mu m_e)(E_\mu m_e) - 2m_e^2(E_\mu^2 - p_\mu^2 \cos \theta) - 2m_\mu^2 m_e^2 + 4m_\mu^2 m_e^2].$$

Factoring out the term $2m_e^2$,

$$\begin{aligned}
 \langle |\mathcal{M}|^2 \rangle &\propto \frac{1}{q^4} (E_\mu^2 + E_\mu^2 - E_\mu^2 + p_\mu^2 \cos \theta - m_\mu^2 + 2m_\mu^2) \\
 &\propto \frac{1}{q^4} (E_\mu^2 + p_\mu \cos \theta + m_\mu^2) \\
 &\propto \frac{1}{q^4} (p_\mu + m_\mu + p_\mu \cos \theta + m_\mu^2) \\
 &\propto \frac{1}{q^4} (2m_\mu^2 + p_\mu(1 + \cos \theta)).
 \end{aligned}$$

Factoring out $2m_\mu^2$ and observing that $p/m = \beta\gamma$ yields

$$\langle |\mathcal{M}|^2 \rangle \propto \frac{1 + \frac{(\beta\gamma)^2}{2}(1 + \cos \theta)}{q^4}.$$

Again using conservation of P_β at vertex β , it can be seen that

$$P_{2\beta} + q_\beta = P_{4\beta} \rightarrow q_\beta = P_{4\beta} - P_{2\beta}$$

. Then

$$\begin{aligned}
 q^2 &= (P_{4\beta} - P_{2\beta})^2 \\
 &= ((E_4, \vec{p}_4) - (E_2, \vec{p}_2))^2 \\
 &= ((0, \vec{p}_4 - \vec{p}_2))^2 \\
 &= -(p_4^2 + p_2^2 - p_4 p_2 \cos \theta) \\
 &= -2p_\mu(1 - \cos \theta).
 \end{aligned}$$

Squaring q^2 and throwing out the constant p_μ ,

$$\langle |\mathcal{M}|^2 \rangle \propto \frac{1 + \frac{(\beta\gamma)^2}{2}(1 + \cos\theta)}{(1 - \cos\theta)^2}.$$

Finally, the Mott cross section is obtained:

$$\frac{d\sigma}{d\Omega} \propto \frac{1 + \frac{(\beta\gamma)^2}{2}(1 + \cos\theta)}{(1 - \cos\theta)^2}. \quad (4.4)$$

Observe that for a non-relativistic beam of muons, $\beta\gamma \rightarrow 0$ and this reduces to the Rutherford cross section (Eqn. 2.27).

4.2.2 Implementation.

Now that the scattering cross sections have been obtained, implementation of these cross sections will be discussed. In COSY, when a particle passes through matter, the change in angle of this particle will be selected from a probability distribution. For $u = \cos\theta$, this distribution should be Gaussian at small angles [25] and follow the Mott cross section at large angles. Therefore, the distribution has been chosen as

$$g(u) = \begin{cases} e^{-a(1-u)} & u_0, \leq u \\ \zeta \frac{1+\frac{1}{2}(\beta\gamma)^2(1+u-b_c)}{(1-u+b_c)^2} & u \leq u_0 \end{cases}. \quad (4.5)$$

The parameter a is an empirical parameter, based off Highland theory [12], and can be found in Eqn. 3.13, which is reproduced here

$$a = \frac{0.5}{1 - \cos\theta_0}.$$

In [12], Highland remarks that θ_0 should have the form

$$\theta_0 = \frac{E_s}{p\beta} \sqrt{\frac{L}{X_0}}.$$

However, this definition has been extended in this work to include empirical corrections

$$\theta_0 = \frac{13.6 \text{ eV}}{\beta p} \sqrt{\frac{L}{X_0} \left[1 + h_1 \ln \frac{L}{X_0} + h_2 \left(\ln \frac{L}{X_0} \right)^2 \right]}, \quad (4.6)$$

where the Highland correction terms have been chosen novelly in this work as $h_1 = 0.103$ and $h_2 = 0.0038$.

u_0 is the point at which the Gaussian term meets the Mott tail. This has been chosen empirically as

$$u_0 = 1 - \frac{4.5}{a}. \quad (4.7)$$

This parameter was fitted alongside the Highland correction terms to match the experimental results in [31].

ζ and b_c are the angular scattering distribution's amplitude and offset for the tail. These are found by demanding continuity and smoothness at u_0 :

$$\begin{aligned} e^{-a(1-u_0)} &= \zeta \frac{1 + \frac{1}{2}(\beta\gamma)^2(1+u_0-b_c)}{(1-u_0+b_c)^2} \\ ae^{-a(1-u_0)} &= \zeta \frac{1 + \frac{1}{2}(\beta\gamma)^2(1+u_0-b_c)}{(1-u_0+b_c)^2} \left(\frac{2}{1-u_0+b_c} + \frac{(\beta\gamma)^2}{2+(\beta\gamma)^2(1+u_0-b_c)} \right). \end{aligned}$$

Then

$$a = \frac{2}{1-u_0+b_c} + \frac{(\beta\gamma)^2}{2+(\beta\gamma)^2(1+u_0-b_c)}.$$

Solving this for the quantity $(u_0 - b_c)$ yields a quadratic with the solution

$$\begin{aligned} A_1 &= -a(\beta\gamma)^2 \\ b_c &= u_0 + \frac{A_2 + \sqrt{A_2^2 - 4A_1A_3}}{2A_1}, \quad A_2 = -(\beta\gamma)^2 - 2a \\ A_3 &= (\beta\gamma)^2(a-3) + 2a - 4. \end{aligned} \quad (4.8)$$

Continuity for $g(u_0)$ can now be solved to find ζ :

$$\zeta = \frac{e^{-a(1-u_0)}(1-u_0+b_c)^2}{1 + \frac{1}{2}(\beta\gamma)^2(1+u_0-b_c)}. \quad (4.9)$$

Now that the distribution function has a concrete form, it will be implemented by inverting the cumulative distribution function (CDF). Let $G(u)$ be the integral of $g(u)$. Then the variable G will be uniformly sampled over the region $[0, G_{max}]$. If

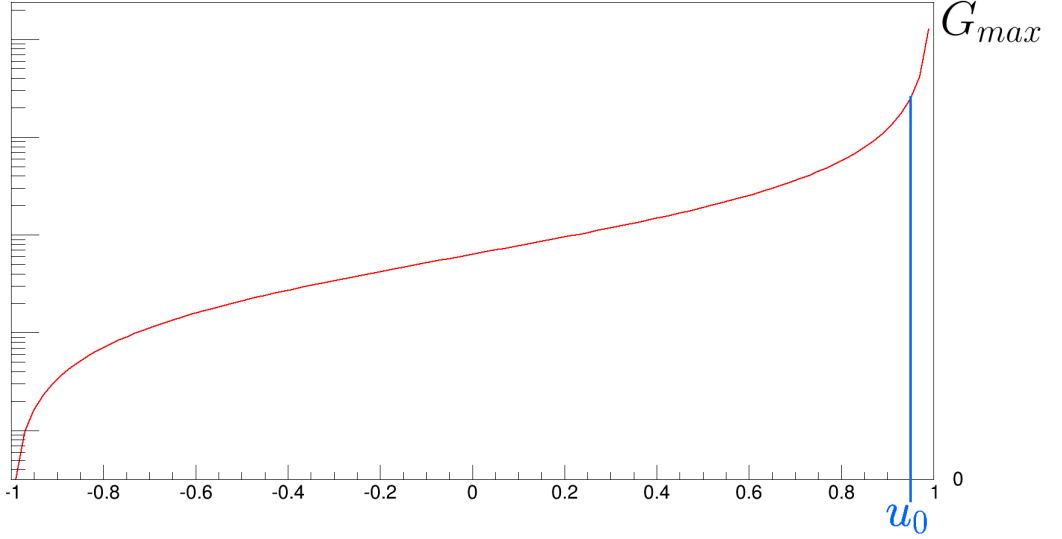


Figure 4.4: Example of the cumulative angular distribution function for muons of 200 MeV/c through 1 mm of liquid hydrogen. Note that the y-axis is log scaled due to the very sharp peak. Furthermore, note that u_0 is greatly exaggerated, since its actual value for these parameters is 0.9999992.

$G \geq G(u_0) \equiv G_0$ then the Gaussian part of the distribution is used to generate u (i.e. $G(u \geq u_0)$). Otherwise, the tail of the distribution will be used. Figure 4.4 shows $G(u)$ for $L = 1$ mm, $p = 200$ MeV/c, and a radiation length of $X_0 = 8.66$ m (to simulate liquid hydrogen).

However, since this is a piecewise function the CDF will be inverted in pieces. The CDF begins on the negative limit, and so the tail of the CDF will be found first:

$$G(u \leq u_0) = \int_{-1}^u \zeta \frac{1 + \frac{1}{2}(\beta\gamma)^2(1 + u - b_c)}{(1 - u + b_c)^2} du.$$

This integral may be solved by substituting $v = 1 - u + b_c$ and simply splitting the numerator into separate parts:

$$\begin{aligned} G(u \leq u_0) &= -\zeta(1 + \frac{1}{2}(\beta\gamma)^2(1 - b_c)) \int v^{-2} dv - \zeta \frac{(\beta\gamma)^2}{2} \int (v^{-2} - v^{-1} + b_c v^{-2}) dv \\ G(u \leq u_0) &= \zeta(1 + (\beta\gamma)^2) \left(\frac{1}{1 - u + b_c} - \frac{1}{2 + b_c} \right) + \zeta \frac{(\beta\gamma)^2}{2} \ln \left(\frac{1 - u + b_c}{2 + b_c} \right) \end{aligned} \quad (4.10)$$

In order to invert the CDF given in Eqn. 4.10, one must find $u(G)$. However, for the tail this is extremely difficult and involves special functions. Therefore, it is more prudent to generate u via bisection method (see Figure 4.5). In this method, the true G is sampled uniformly on the range $[0, G_{max}]$, where $G_{max} \equiv G(1)$ and can be found via Eqn. 4.11. If $G < G_0$, then the tail is sampled. A trial u called \bar{u} (as in ‘average’) is selected from some range which is known to contain the actual u . The range is described as $[u_{min}, u_{max}]$, and $\bar{u} = (u_{min} + u_{max})/2$.

Initially, the range is chosen as $u_{min} = -1$ and $u_{max} = u_0$ (since that is the largest range on which $G(u \leq u_0)$ is valid). $\bar{G} \equiv G(\bar{u})$ is found using Eqn. 4.10, and then the routine is subject to the following conditionals:

- If $\bar{G} \in [G - \delta G, G + \delta G]$ then $u = \bar{u}$, return value.
- If $\bar{G} < G - \delta G$ then $u_{min} = \bar{u}$, rerun with new u_{min} .
- If $\bar{G} > G + \delta G$ then $u_{max} = \bar{u}$, rerun with new u_{max} .

δG is a precision, and has been chosen for this work as $\delta G = 10^{-8}$. However, it is conceded that in the future δG should be a percentage of G_{max} rather than an absolute number.

For the peak, $u_0 \leq u$ and so the CDF becomes

$$G(u_0 \leq u) = \int_{-1}^{u_0} g(u) du + \int_{u_0}^u e^{-a(1-u)} du.$$

The first term is simply G_0 , the cumulative distribution function at u_0 . The second term is easily integrable and yields

$$G(u_0 \leq u) = G_0 + \frac{e^{-a(1-u)} - e^{-a(1-u_0)}}{a}. \quad (4.11)$$

Now explicitly,

$$G_{max} \equiv G(1) = G_0 + \frac{1}{a} - \frac{e^{-a(1-u_0)}}{a}.$$

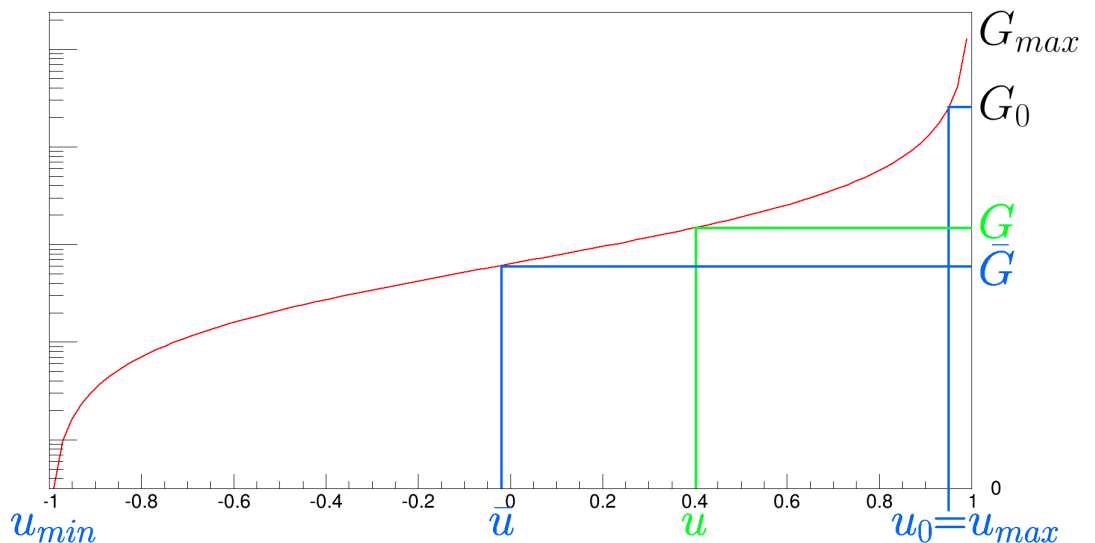


Figure 4.5: Example of the first iteration of the algorithm to obtain the true u (in green). The true G is chosen uniformly from $G \in [0, G_{max}]$. If $G < G_0$, then the tail is sampled via bisection method. In this case, since $\bar{G} < G$, \bar{u} is the new u_{min} and \bar{u} is calculated again.

The inversion of this function is quite simple, and is

$$u(G_0 \leq G) = 1 + \frac{1}{a} \ln(a[G - G_0] + e^{-a(1-u_0)}). \quad (4.12)$$

Therefore, if $G \in [0, G_{max}]$ is greater than or equal to G_0 , then it is simply inserted into Eqn. 4.12 and the true u is obtained.

It is a subtle yet important point to note that the Mott cross section (Eqn. 4.4), upon which the probability distribution function $g(u)$ in Eqn. 4.5 is based, assumes an on-axis straight line trajectory (that is, $x = y = p_x = p_y = 0$). The treatment of this subtlety will be discussed here.

The routine which uses the scattering distribution $g(u)$ is called SCATDIST and takes two arguments: θ_0 (Eqn. 4.6) and p , the momentum. θ_0 includes not only the material parameters (L, X_0) but also energy terms ($1/\beta p$), and p is the momentum *after* the straggling routine has been called. SCATDIST returns not the scattered angle, but the new z-momentum $p_z = pu = p \cos \theta$.

This new z-momentum is in the rotated frame, i.e. the frame at which $p_x = p_y = 0$ (see Figure 4.6), and so is called $p_{z,R}$. The transverse momentum in the rotated frame, $p_{T,R}$, can be found via $p_{T,R} = \sqrt{p^2 - p_{z,R}^2}$, but this is the total transverse momentum ($\theta_o + \theta_s$), which includes the original momentum (θ_o), not simply the transverse momentum which was gained via scattering (θ_s). Rotation back into the lab frame is given by

$$\begin{pmatrix} P_z \\ P_T \end{pmatrix} = \begin{pmatrix} \cos \theta_o & -\sin \theta_o \\ \sin \theta_o & \cos \theta_o \end{pmatrix} \begin{pmatrix} P_{z,R} \\ P_{T,R} \end{pmatrix}.$$

Note that at this point one must not uniformly distribute P_T into p_x and p_y . This is because, for example, if p_x was positive before scattering it should have a strong probability of being positive after scattering. If one were to distribute P_T uniformly

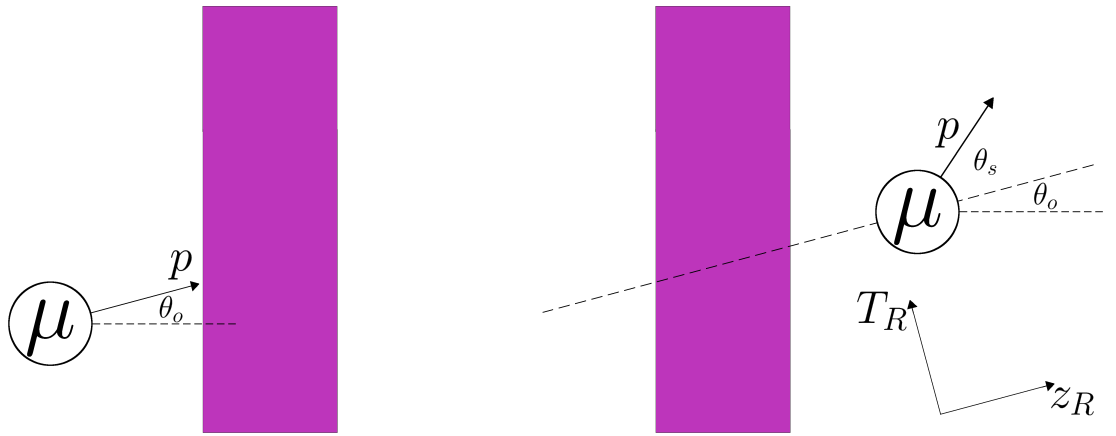


Figure 4.6: Example of a muon entering an absorber (purple) with some nonzero initial angle θ_o . The muon then scatters an angle θ_s with respect to its initial momentum \vec{p} . The scattering distribution $g(u)$ assumes a straight, on-axis particle ($x = y = p_x = p_y = 0$), and so is in the rotated frame, represented by T_R, z_R .

then p_x would have a 50/50 chance of being negative. While the histogram of p_x may not be affected, the transverse phase space would certainly not be correct. For this reason, only the transverse momentum gained via scattering should be uniformly distributed into p_x and p_y .

Let the original momenta (after straggling but before scattering) be denoted with o in the same fashion that θ_o is the angle before scattering. Then the amount of transverse momentum which was gained via scattering is $P_T - P_{T,o}$. This new amount of transverse momentum must be added to the original $p_{x,o}$ and $p_{y,o}$ uniformly. Consequently, let ϕ be an angle chosen from $[0, 2\pi]$. Then the final p_x and p_y are

$$p_x = p_{x,o} + (P_T - P_{T,o}) \cos \phi$$

$$p_y = p_{y,o} + (P_T - P_{T,o}) \sin \phi.$$

In summation, the angular distribution used by COSY Infinity is based on a piecewise function which is Gaussian for small angles [25] and has a Mott tail for large angles. This distribution is represented by $g(u)$ in Eqn. 4.5, where $u \equiv \cos \theta$. $g(u)$ has four parameters: a , an emperical parameter which is based on Highland theory [12] and is dependent on some critical angle θ_0 , defined in Eqn. 4.6; u_0 , the emperical cutoff angle which distinguishes which angles are Gaussian and which are not, found by Eqn. 4.7; b_c , a parameter derivable from smoothness of g at u_0 , which represents the offset of the Mott tail, found in Eqn. 4.8; and ζ , a parameter derivable from continuity of g at u_0 which represents the amplitude of the Mott tail, found in Eqn. 4.9. From $g(u)$, its antiderivative $G(u)$ may be found and a particular G may be picked from the range $[0, G_{max}]$. If $G < G_0 \equiv G(u_0)$, then u comes from the Mott tail and a bisection method is used to find u . If $G_0 \leq G$ then u comes from the Gaussian peak and $G(u)$ may be inverted to find $u(G)$. This scattered angle must then be rotated into the lab frame and the additional transverse momentum must be uniformly distributed into p_x and p_y .

4.3 Transverse Displacement

When a particle traverses matter, because of the multiple scattering events a direct correlation between the particle's transverse position and scattered angle is not always clear. Two identical particles with identical initial conditions may end up with identical scattered angles but different transverse positions (see Figure 4.7). This is because these two particles may take slightly different paths through the absorber. While both of these paths may lead to a similar final angle with respect to the z-axis, the positions will likely be different due to their trajectories.

For this reason, emperical corrections have been made to COSY which reflect these transverse corrections. While there is no real data on the transverse position of muons before and after they traverse a medium, it is reasonable that very small step

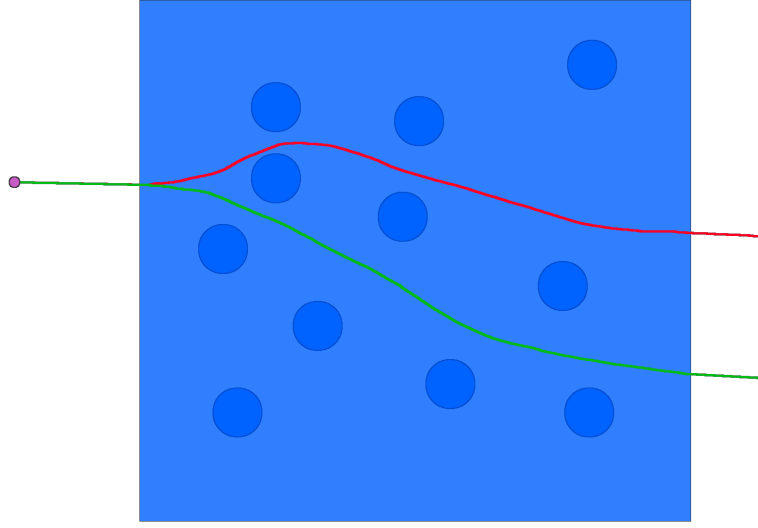


Figure 4.7: Two examples of true paths which a particle might take when traversing a medium. Note that both the red path and green path have the same final scattered angle but different transverse positions.

sizes (very short true paths) should be more realistic than large step sizes. Therefore, COSY was matched ‘empirically’ with G4Beamline across several initial momenta and absorber lengths. The result was

$$x = x_o + x_D + \text{Gaus}(\theta_{diff} * L/2, \theta_c/(2\sqrt{3})), \quad (4.13)$$

where x_o is the original x position, $x_D = L * P_{x,o}/P_{z,o}$ is the deterministic gain in x , and $\text{Gaus}(\mu, \sigma)$ is a randomly selected number from a Gaussian distribution with mean μ and standard deviation σ . The forms of μ and σ were selected based off [32]. $\theta_{diff} = \theta_{final} - \theta_o$ is the amount of deflection which occurred due to scattering and $\theta_c = 13.6 \text{ eV}/\beta p \cdot \sqrt{1/X_0}$ is the coefficient from Highland theory [12].

4.4 Temporal Displacement

For the time-of-flight offset, both the deterministic and stochastic processes are handled in the same routine. At first order, the particle decelerates at some constant

(or average) value through an absorber of length L . If a is the constant acceleration then

$$v_f = v_o + a\Delta t,$$

or

$$a = \frac{v_f - v_o}{\Delta t}.$$

At the same time,

$$v_f^2 = v_o^2 + 2aL,$$

and so

$$a = \frac{v_f^2 - v_o^2}{2L}.$$

Then

$$\Delta t = \frac{(v_f - v_o)2L}{v_f^2 - v_o^2}.$$

Given

$$\begin{aligned}\beta &= \frac{p}{E} && \text{and} \\ v &= \beta c\end{aligned}$$

then

$$\Delta t = \frac{\left(\frac{p_f}{E_f} - \frac{p_o}{E_o}\right)2L}{\left(\frac{p_f^2}{E_f^2} - \frac{p_o^2}{E_o^2}\right)c}. \quad (4.14)$$

However, COSY does not have a time variable, but rather a time-like variable ℓ , which is described as the time-of-flight in units of length. In [4], this is defined as

$$\ell = \frac{-(t - t_0)v_0\gamma}{1 + \gamma},$$

where the subscript 0 signifies the reference particle. Let the time before a step be denoted with 1 and the time after a step denoted with 2. Then to find ℓ_2 given ℓ_1 and Δt from Eqn. 4.14, observe that

$$\begin{aligned}\ell_1 &= \frac{(t_{01} - t_1)v_{01}\gamma_1}{1 + \gamma_1} = (t_{01} - t_1)A_1 \\ \ell_1 &= \frac{(t_{02} - t_2)v_{02}\gamma_2}{1 + \gamma_2} = (t_{02} - t_2)A_2,\end{aligned}\tag{4.15}$$

where

$$A_n \equiv v_{0n}\gamma_n/(1 + \gamma_n).\tag{4.16}$$

Then

$$\begin{aligned}\ell_2 - \ell_1 &= ([t_{02}] - [t_2])A_2 - (t_{01} - t_1)A_1 \\ &= [(t_{02} - t_{01}) + t_{01}] - [(t_2 - t_1) + t_1]A_2 - (t_{01} - t_1)A_1 \\ &= (\Delta t_0 - \Delta t)A_2 + (t_{01} - t_1)A_2 - (t_{01} - t_1)A_2 \\ &= (\Delta t_0 - \Delta t)A_2 + (t_{01} - t_1)(A_2 - A_1).\end{aligned}$$

Eqn. 4.15 says that $t_{01} - t_1 = \ell_1/A_1$. Moving ℓ_1 to the right hand side,

$$\begin{aligned}\ell_2 &= (\Delta t_0 - \Delta t)A_2 + \frac{\ell_1}{A_1}(A_2 - A_1) + \ell_1 \\ &= (\Delta t_0 - \Delta t)A_2 + \ell_1\left(\frac{A_2 - A_1}{A_1} + \frac{A_1}{A_1}\right) \\ &= (\Delta t_0 - \Delta t)A_2 + \ell_1\frac{A_2}{A_1}.\end{aligned}$$

Resubstituting for A_n via Eqn. 4.16 yields the final result

$$\ell_2 = \frac{(\Delta t_0 - \Delta t)v_{02}\gamma_2}{1 + \gamma_2} + \ell_1\frac{v_{02}\gamma_2(1 + \gamma_1)}{v_{01}\gamma_1(1 + \gamma_2)}.\tag{4.17}$$

Using Eqn. 4.17, the Δt from Eqn. 4.14 can be directly input into the new COSY variable for time-of-flight in units of length.

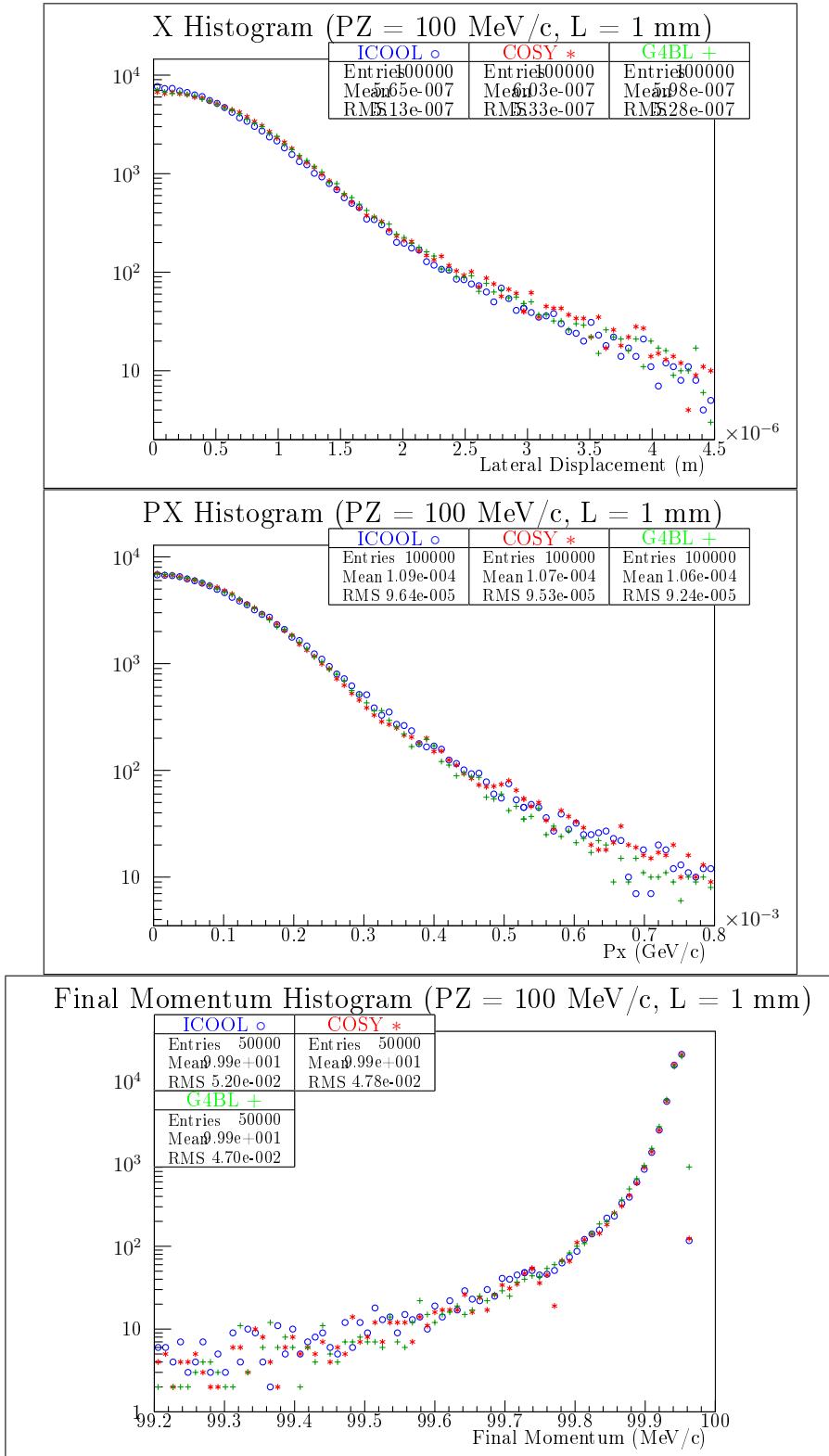
CHAPTER 5

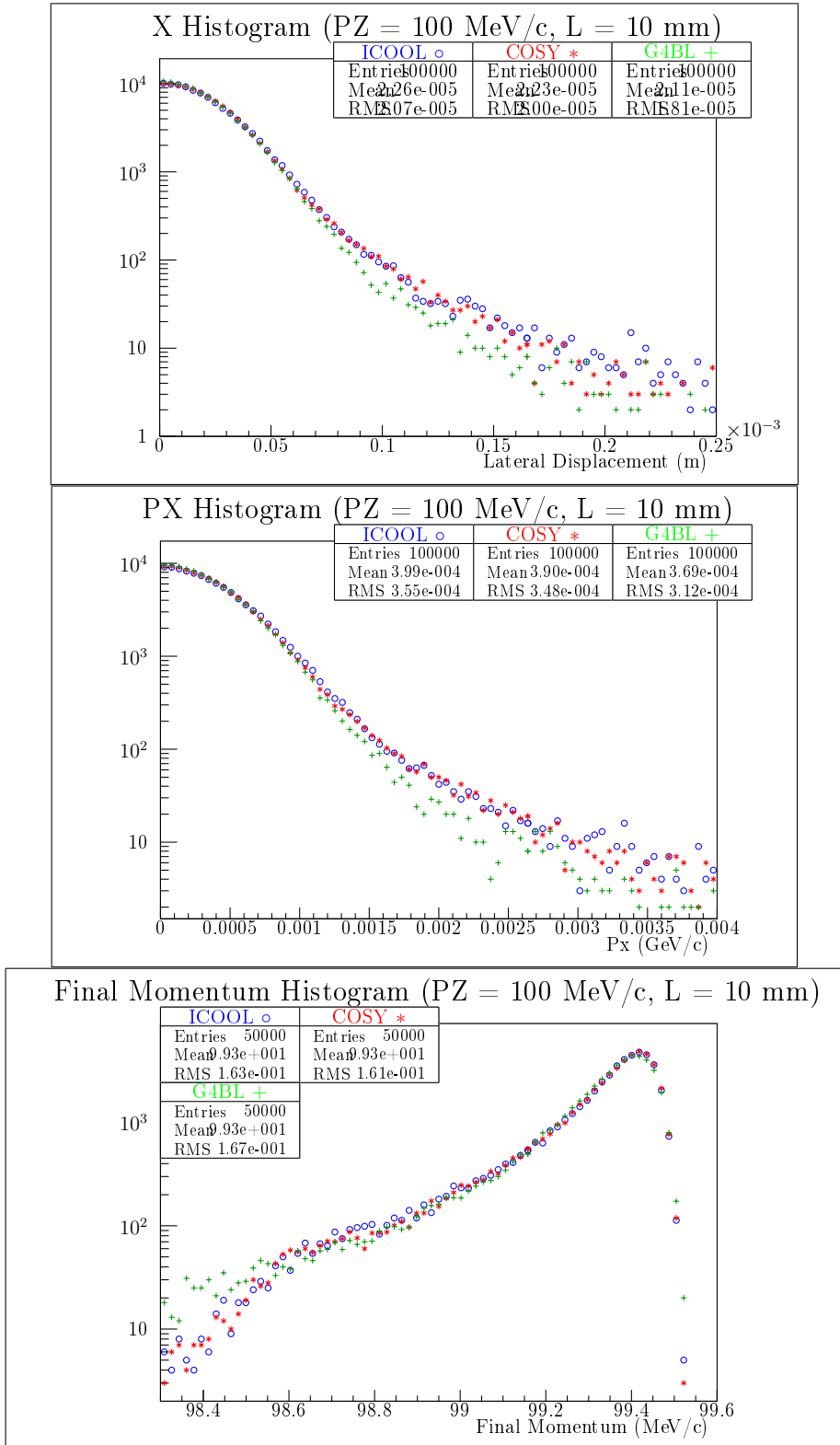
RESULTS

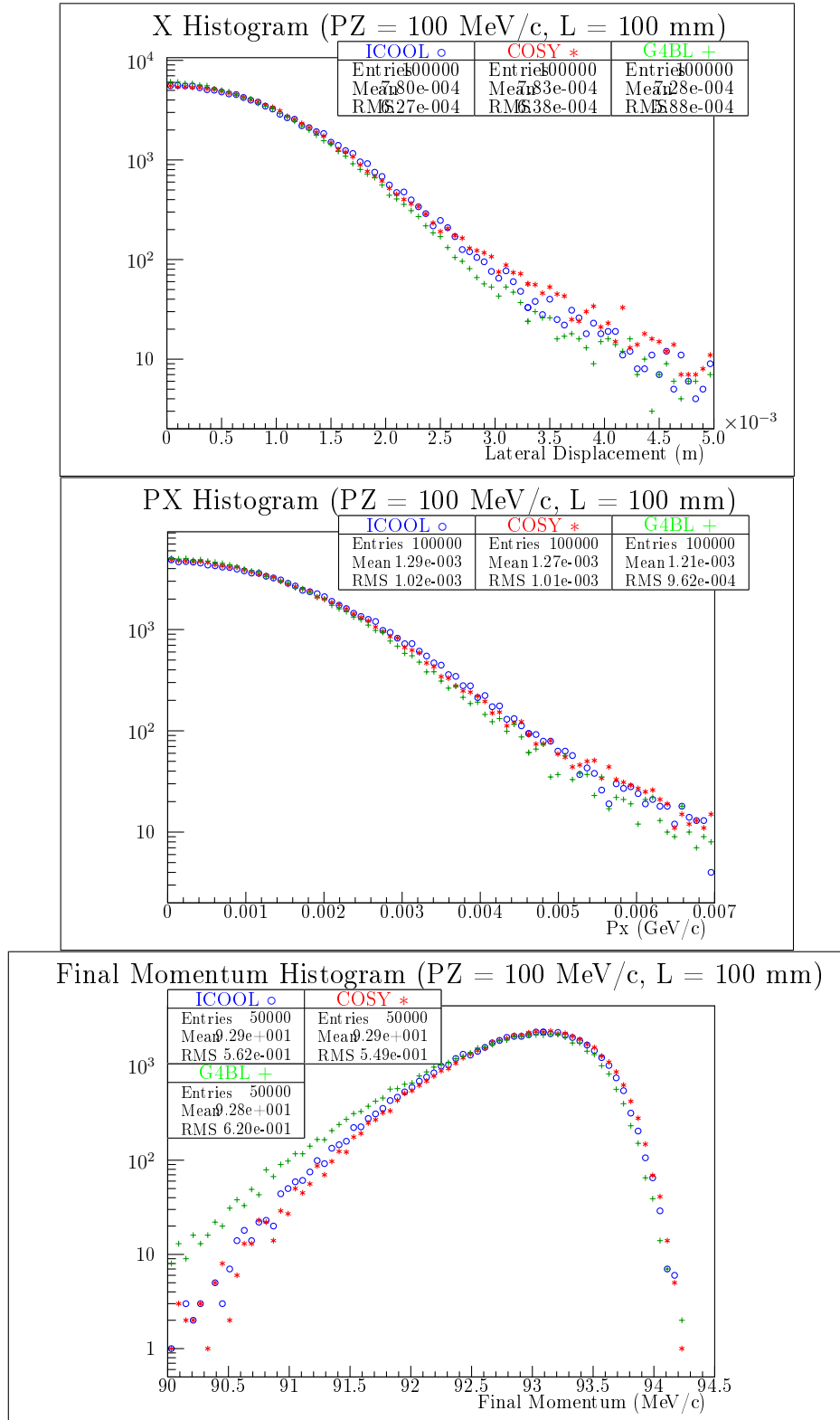
In this chapter, comparison of the new COSY routines will be benchmarked against both ICOOL and G4Beamline for pencil beams through. Moreover, both validation against past experiments and predictions of future experiments will be shown.

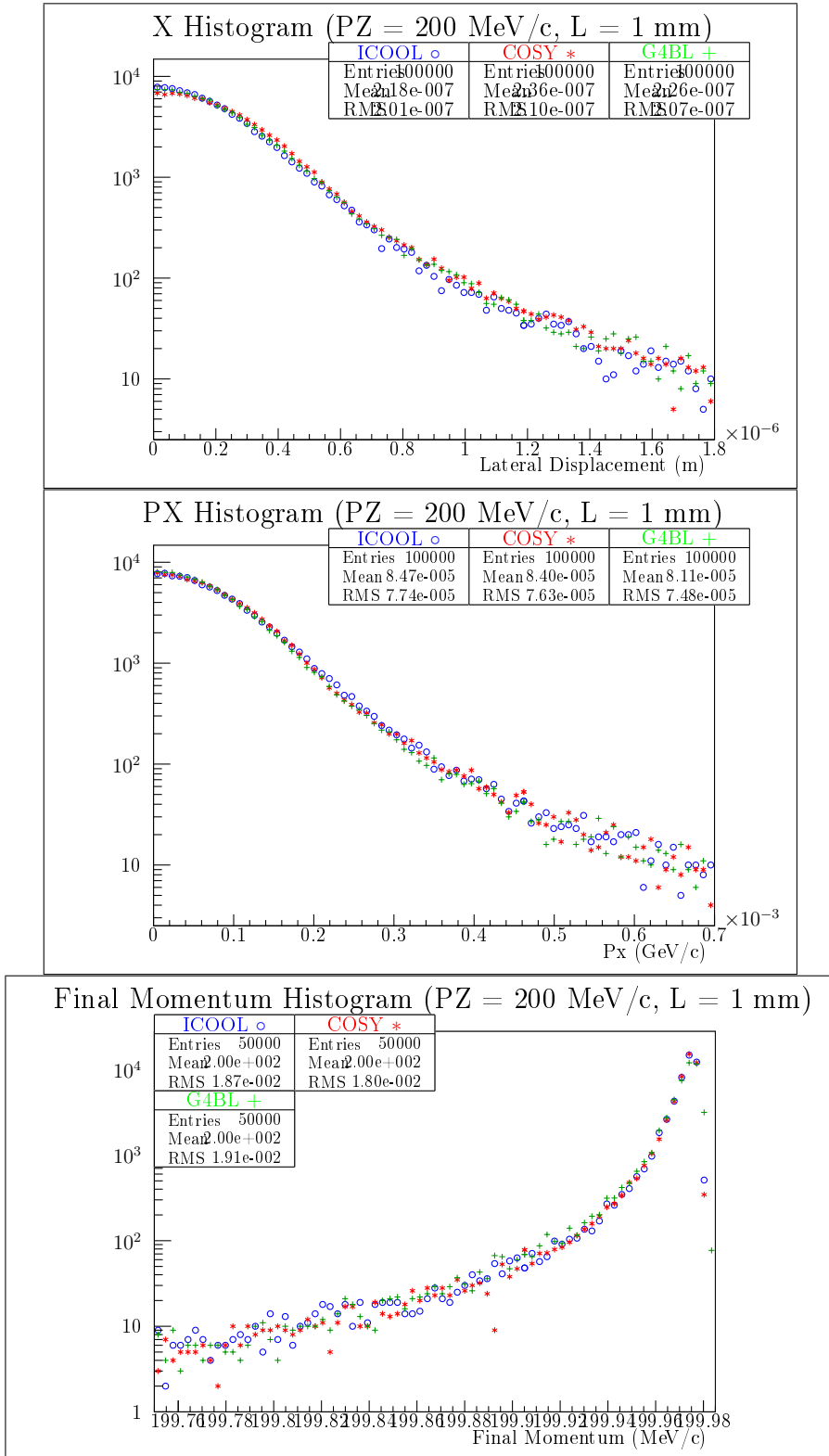
5.1 Benchmark Against Other Codes

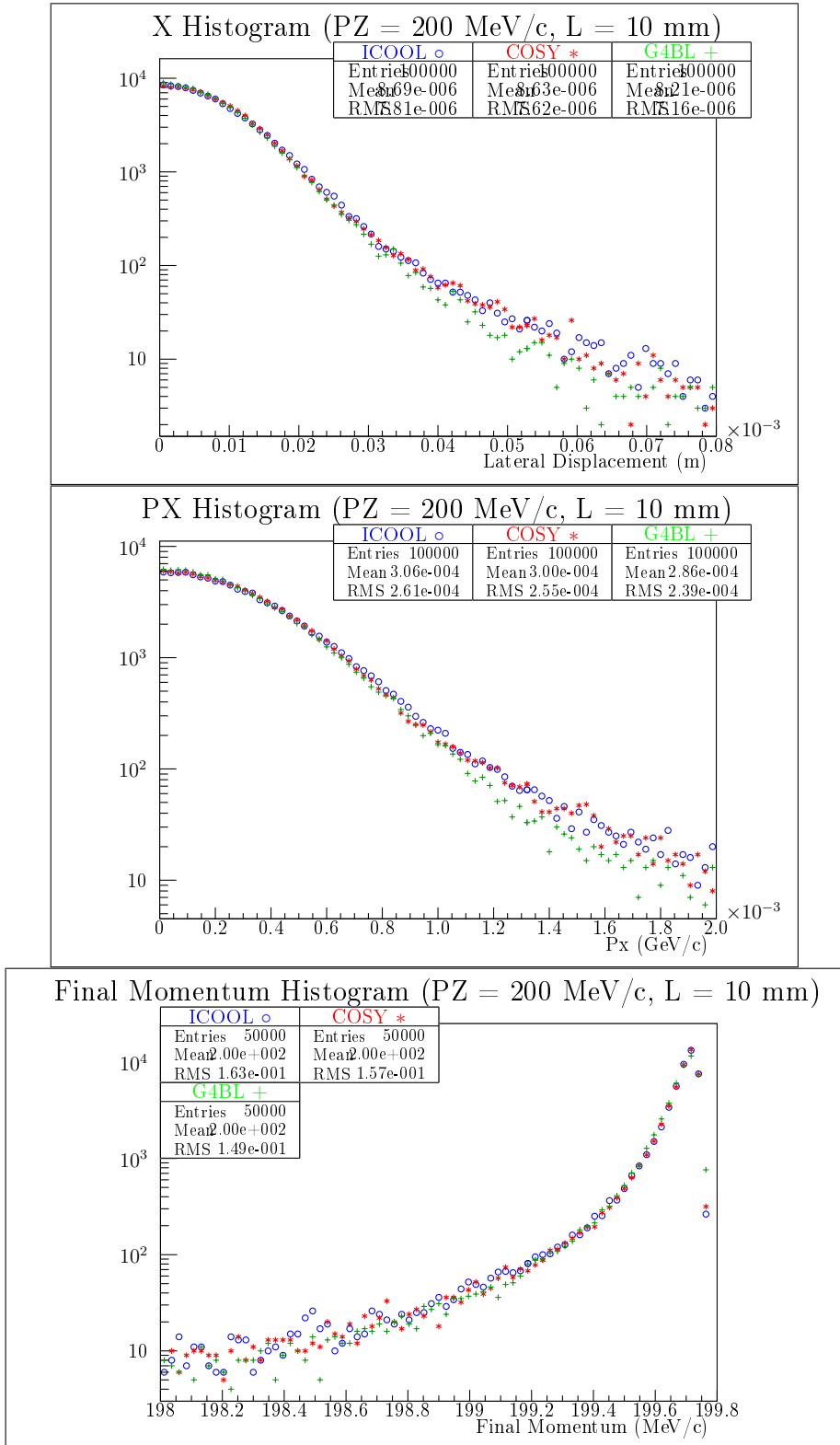
This section shows the comparison of the new COSY routines with those of two other codes, ICOOL [15] and G4Beamline [23]. The comparisons are done over both the momentum range of cooling channels (100, 200, 300, and 400 MeV/ c) and various absorber lengths or stepsizes (1, 10, and 100 mm). These simulations were performed using a pencil beam of the aforementioned momenta through liquid hydrogen. Both lithium hydride and beryllium were also tested with similar results.

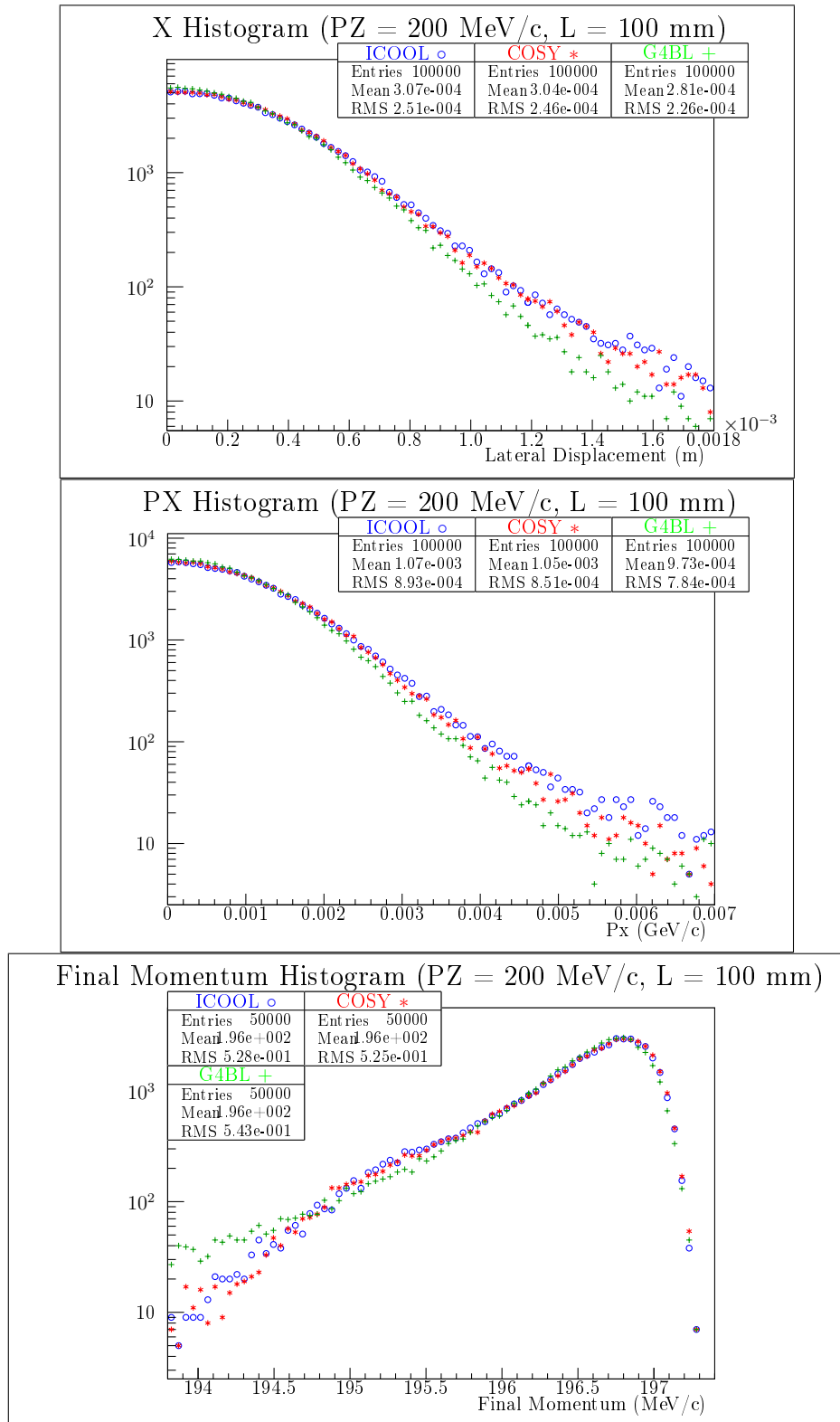


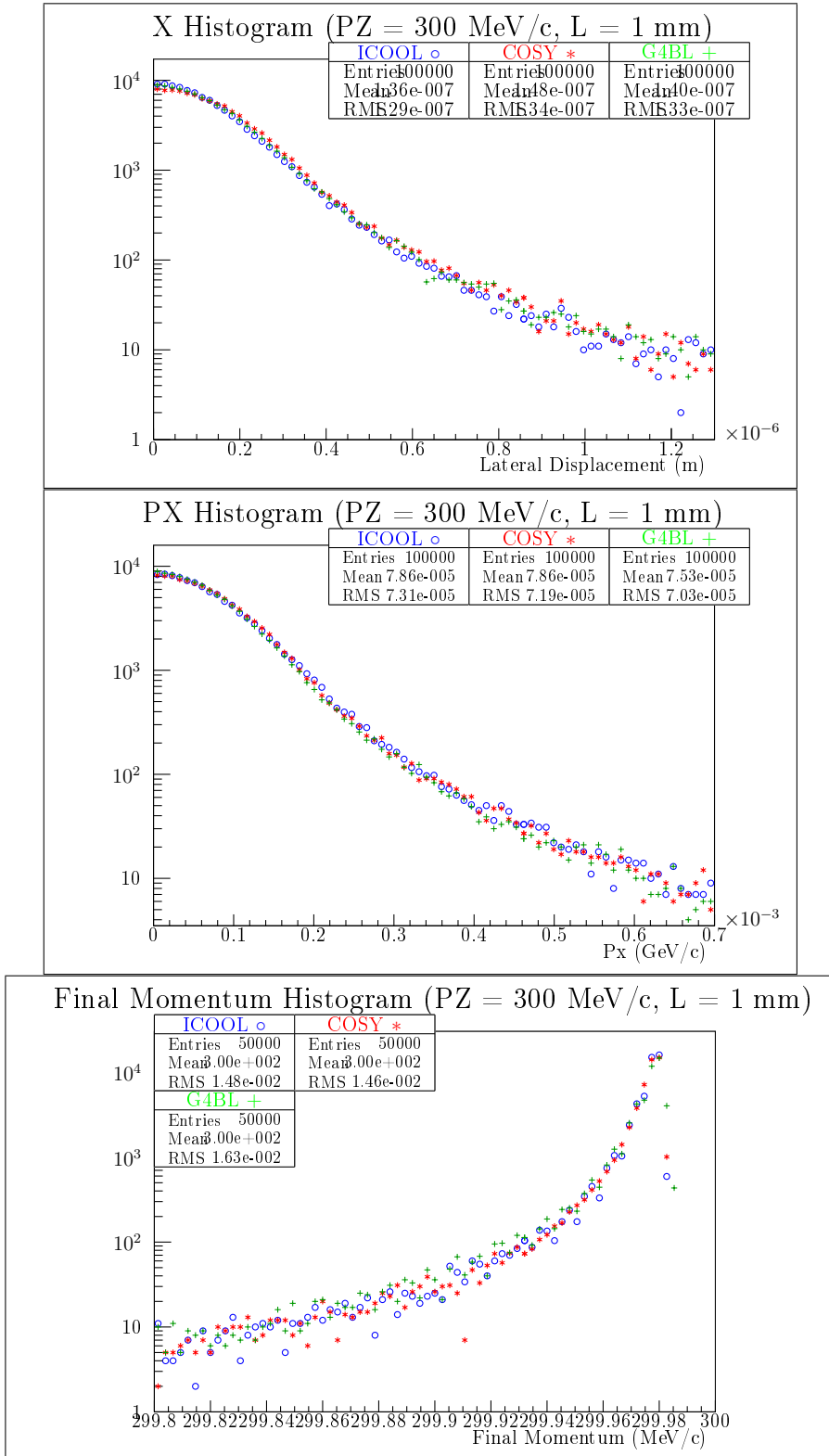


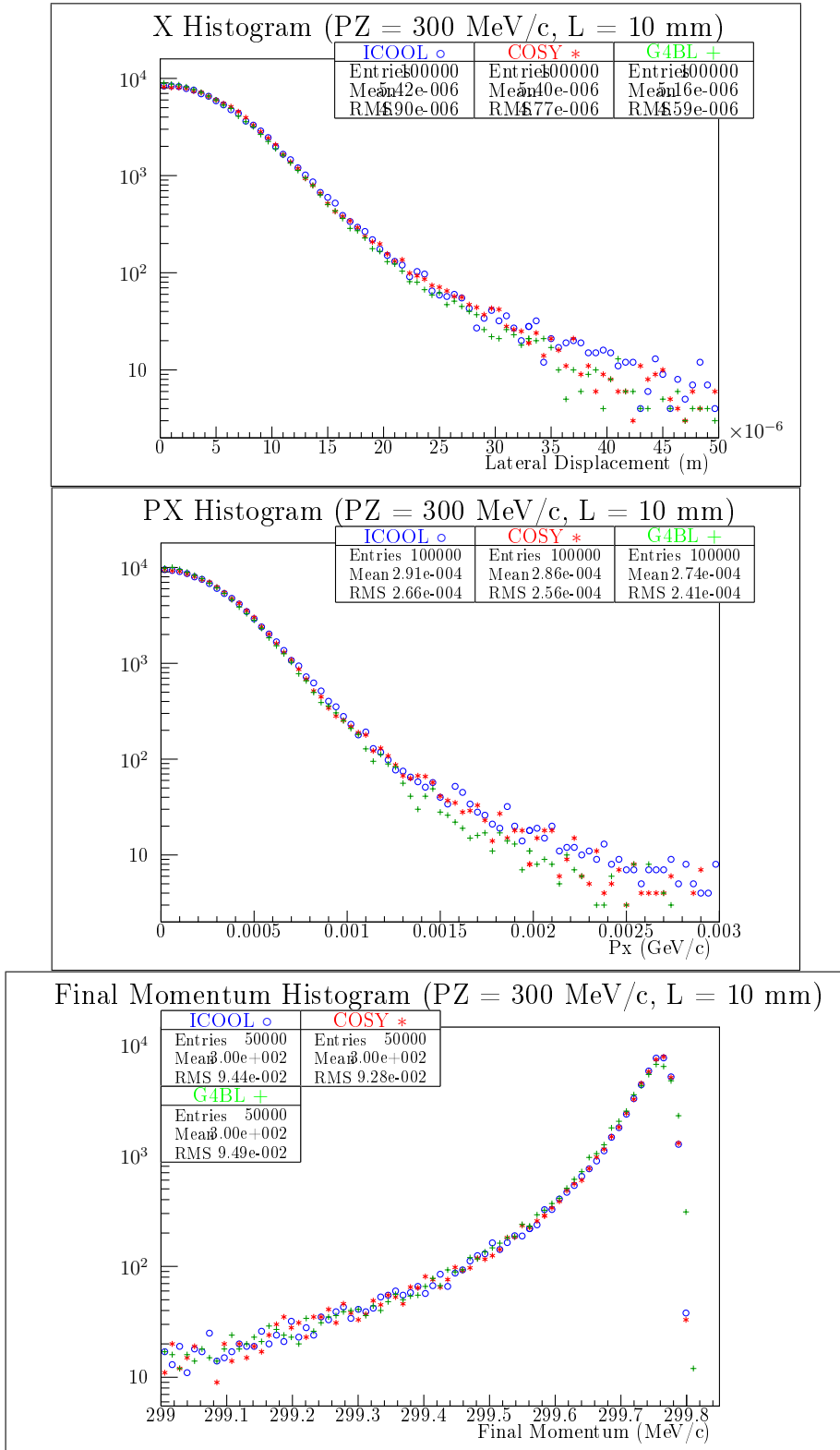


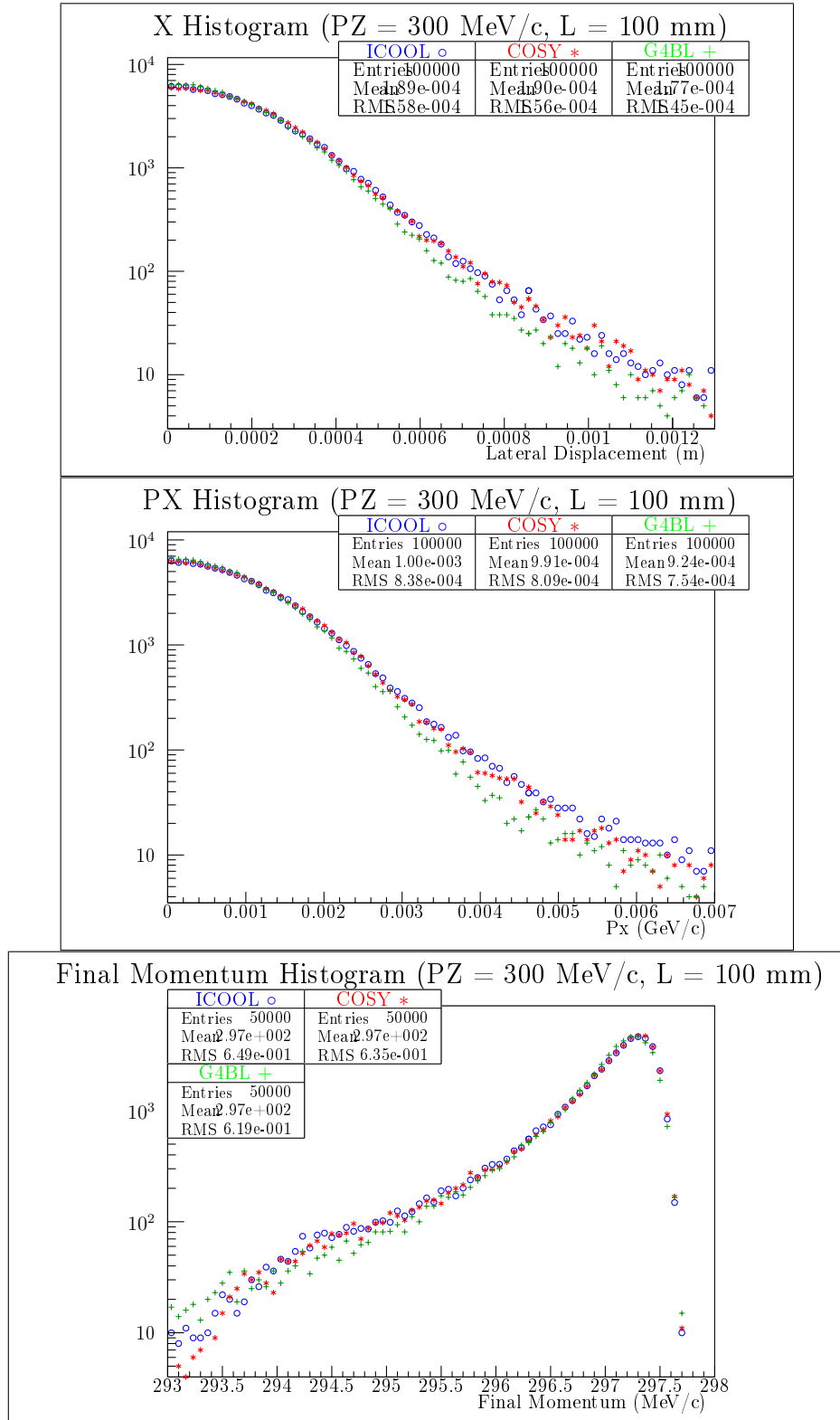


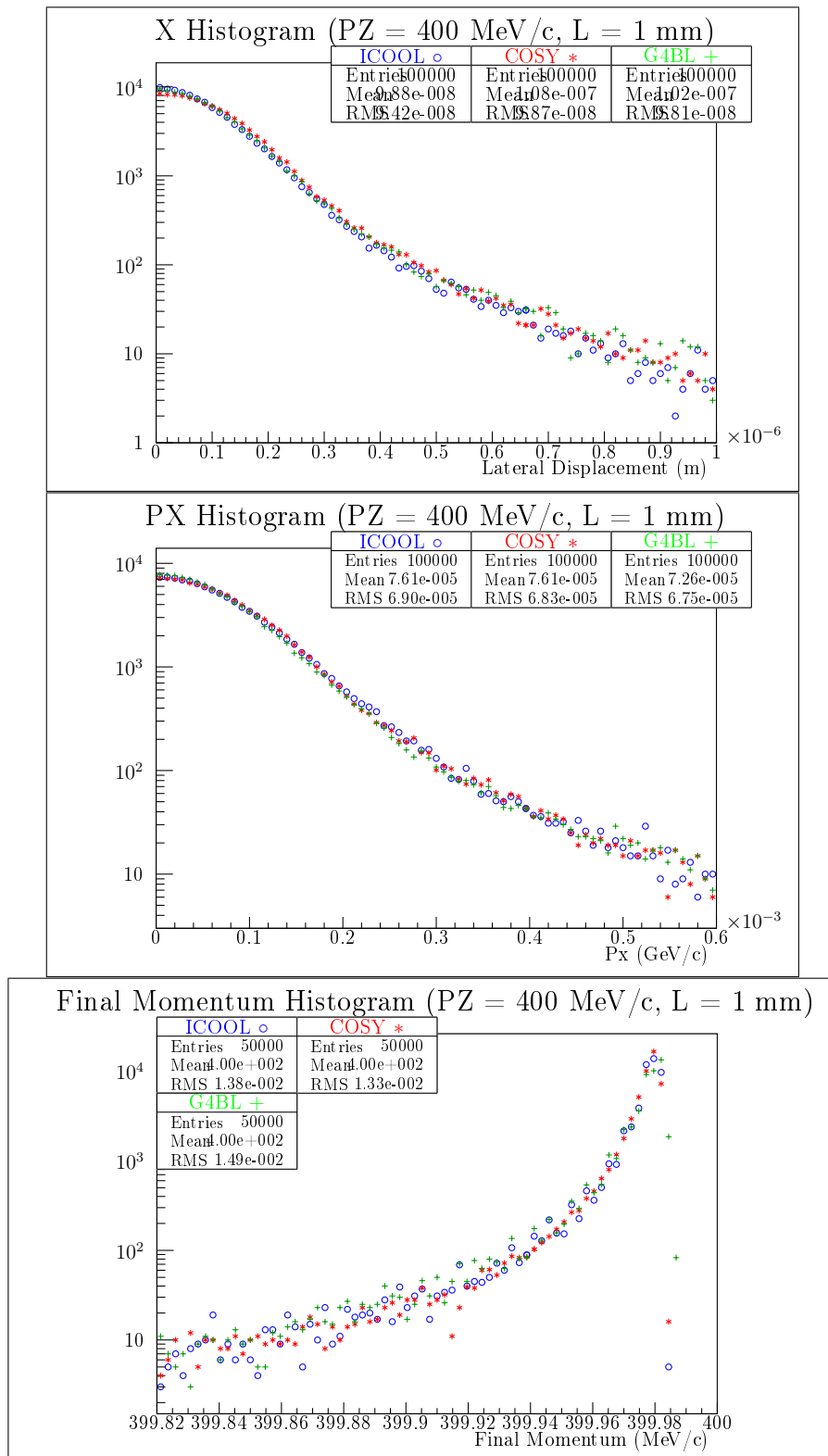


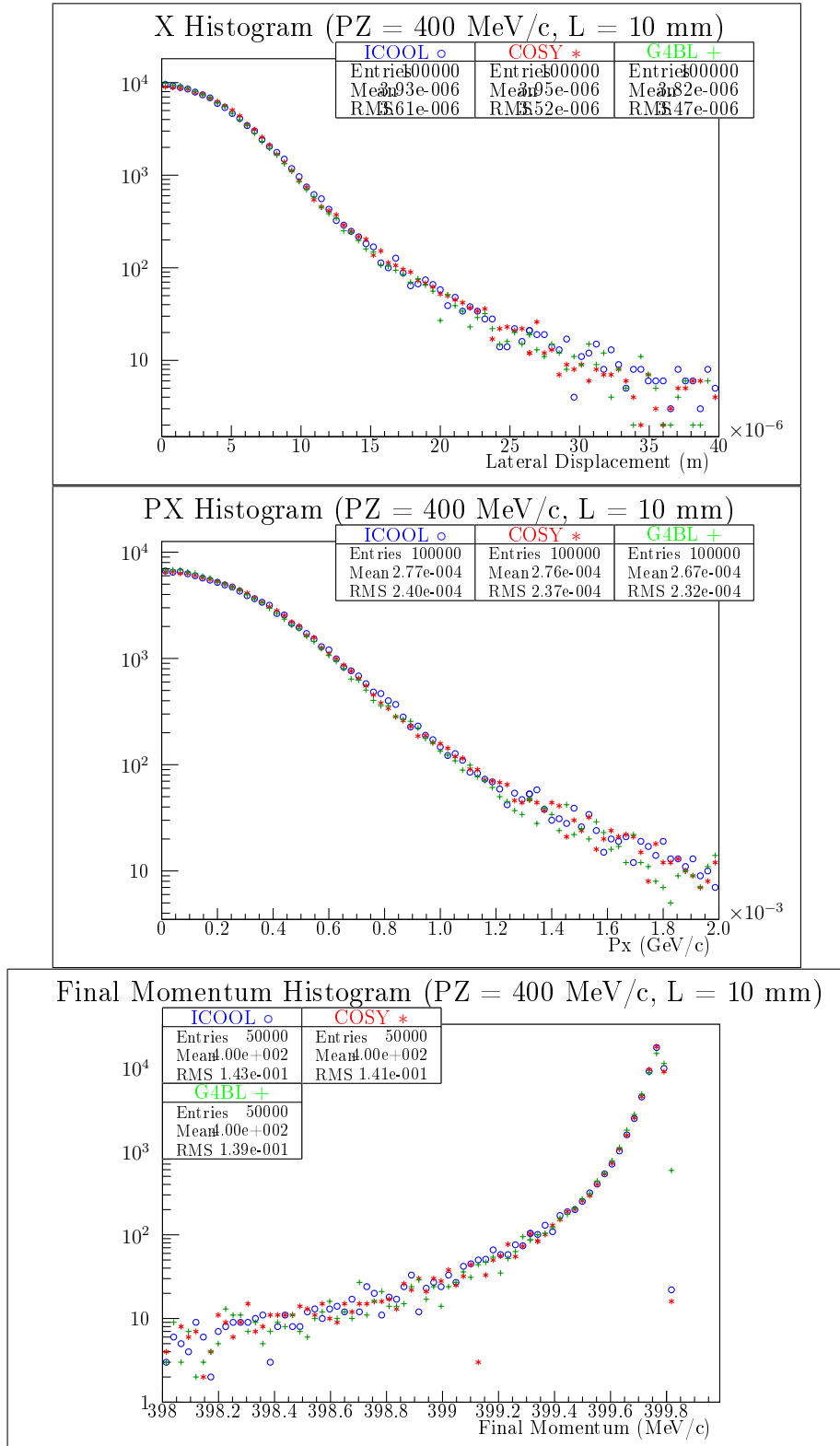


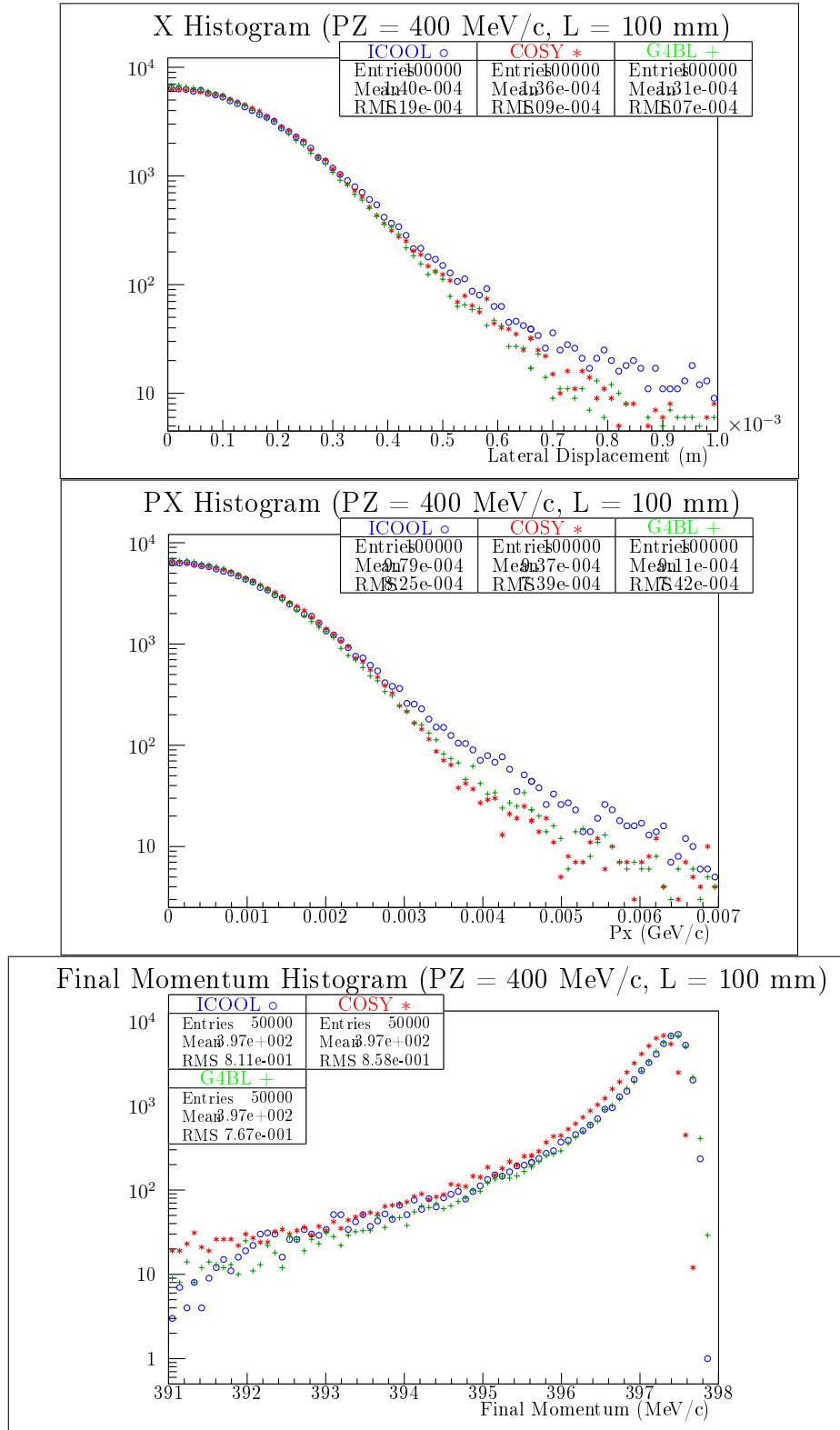












5.2 Validation

The new COSY routines were also compared to [31], often referred to as MuScat. This experiment measured the scattering of a beam of collimated muons through seven materials. To emulate this, pencil beams with $P = 172 \text{ MeV}/c$ were created in COSY, G4Beamline, and ICOOL. The pencil beam consisted of 10,000 particles and was propagated through 109 mm of liquid hydrogen, 159 mm of liquid hydrogen, and 3.73 mm of beryllium. COSY took a single step through the absorbers while G4BL and ICOOL took their respective default step sizes. The results are shown below.

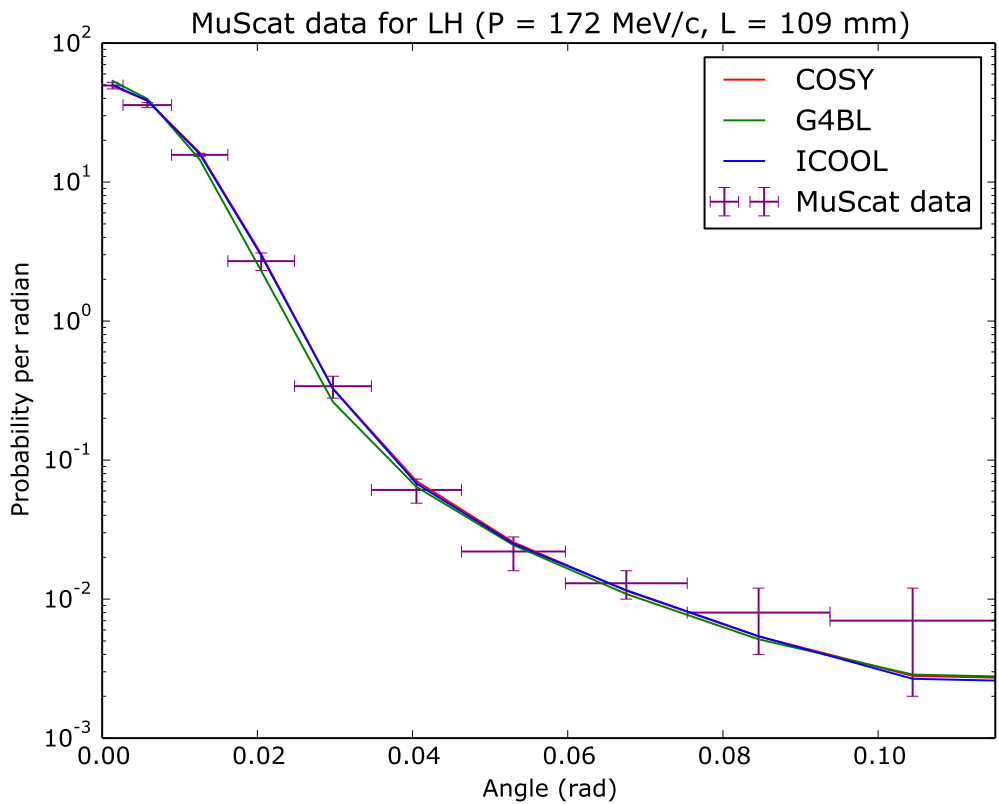


Figure 5.1: MuScat results for 109 mm of liquid hydrogen compared against COSY (red), G4BL (green), and ICOOL (blue).

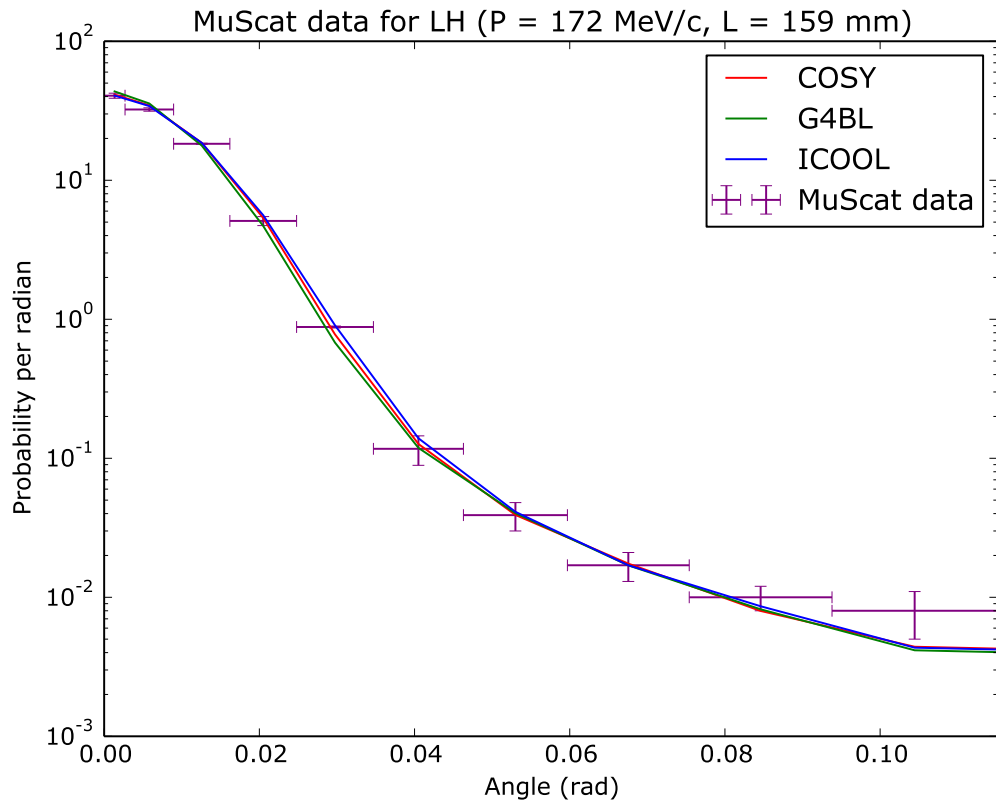


Figure 5.2: MuScat results for 159 mm of liquid hydrogen compared against COSY (red), G4BL (green), and ICOOL (blue).

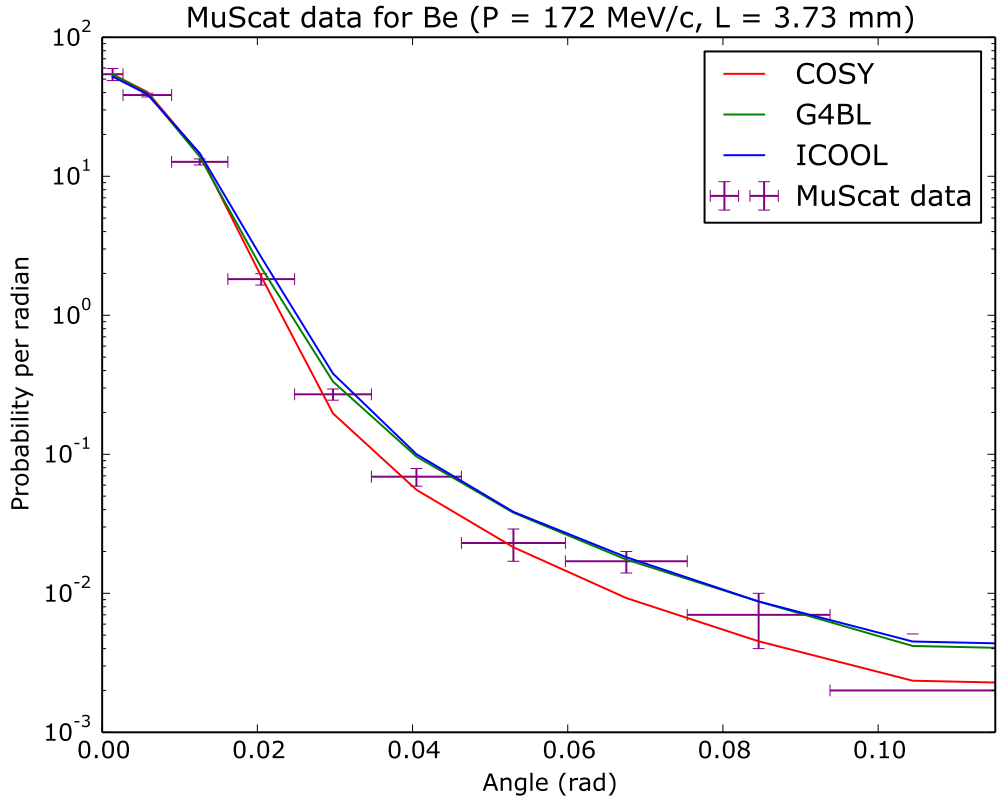


Figure 5.3: MuScat results for 3.73 mm of beryllium compared against COSY (red), G4BL (green), and ICOOL (blue).

In the liquid hydrogen cases, COSY appears to match both G4Beamline and ICOOL very well, as well as the MuScat data points. In the case of beryllium, COSY matches the MuScat points slightly better than G4Beamline and ICOOL, particularly for the two data points between 0.04 and 0.06 radians.

5.3 The Muon Ionization Cooling Experiment

This section introduces the Muon Ionization Cooling Experiment (MICE, [33]), a practical application for the new absorber routines in COSY. Next, new non-absorber subroutines added to COSY specifically for MICE will be briefly discussed.

Finally, the results of the MICE simulations in both G4Beamline and COSY will be examined.

5.3.1 Introduction to MICE.

The Muon Ionization Cooling Experiment (MICE [33]) is an experiment currently being developed at the Rutherford Appleton Laboratory in Oxfordshire, U.K. Its goal is to show a proof-of-principle demonstration of muon ionization cooling which should result in a high brilliance beam. While there are six stages, this work is demonstrated via Step III. The cell of Step III involves four tilted coils positioned among a liquid hydrogen absorber and a radio frequency cavity, shown in Figure 5.4. Furthermore, an empty cell containing only the coils was positioned before and after the entire cell chain.

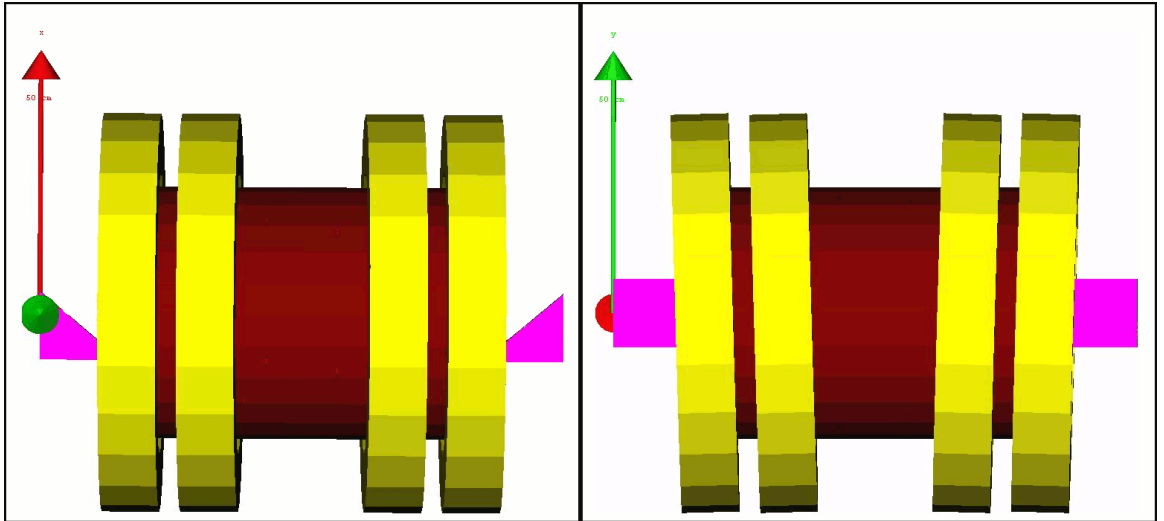


Figure 5.4: MICE Stage III cell. Left: rotated such that the y-axis points out of the page. Right: rotated such that the x-axis points into the page.

5.3.2 Non-absorber Routines in COSY for MICE.

For this work, COSY was compared to G4Beamline for 1,000,000 particles through 50 cells. This was a challenge in COSY because COSY includes neither

a tilted coil element nor an arbitrary way to superimpose maps on one another. Moreover, while COSY does have a method to read from and write to a file, these methods are particularly slow for 1,000,000 particles.

The tilted coil routine is intrinsically dependent on the straight coil routine in COSY, **CMSTP**. The tilted coil routine, named **CMSTPT**, uses the following algorithm:

1. Drift to the center of the coil
2. Tilt the reference axis using **TA**
3. Drift back to the start of the cell
4. Run **CMSTP**
5. Drift back to the center of the coil
6. Tilt the axis back into the lab frame
7. Drift to the end of the cell

In order to superimpose coils of different tilt angles, the user must make an approximation. To acquire a map which represents a propagation of an amount **STEP** through several superimposed tilted coils,

1. Choose a step size **STEP**
2. Step through the first **CMSTPT** by an amount **STEP**
3. Drift back by an amount **STEP**
4. Repeat steps 2 for all remaining coils and step 3 for all remaining coils except for the last one

Finally, the read and write routines needed to be optimized. Rather than using COSYScript, the new routines should use the underlying FORTRAN instead.

A routine called `WRITE_ICOOL` was written in order to take a COSY vector (see, e.g., Figure 1.2) and write an ICOOL-style `for009` file. To do this, on the COSYScript level the vector was converted from (X, A, Y, B, L, D) to (X, PX, Y, PY, ToF, E) . This vector was then passed on to the FORTRAN level, where a simple loop wrote the information to a file.

Instead of reading a file, both COSY and G4Beamline were modified to generate a beam of particles. In COSY, this meant first initializing a 1D vector using `IN1DVE` on the COSYScript level. In COSY, this means returning a vector `V:=0&0...&0`. However, looping as follows has been shown to be computationally expensive:

```
V:=0 ;
LOOP I 0 SIZE ;
V:=V&0 ;
ENDLOOP ;
```

Instead, the routine should make use of the power of 2^n (i.e. `V:=V&V`). However, since typically `SIZE` $\neq 2^n$ for $n \in \mathbb{Z}$, this will greatly under- or over-shoot the value of `SIZE`. In this case, the algorithm is split into pieces (see Figure 5.5).

The first task is to ensure that n is the integer closest to `SIZE` while maintaining $2^n \leq \text{SIZE}$. This is done via

$$\text{SIZE} \geq 2^n \rightarrow n = \text{INT}\left[\frac{\ln \text{SIZE}}{\ln 2}\right],$$

where `INT` is the COSYScript routine for floor (not the nearest integer, which in COSY is `NINT`). Now it is possible to fill the temporary vector `TV` up until 2^n via

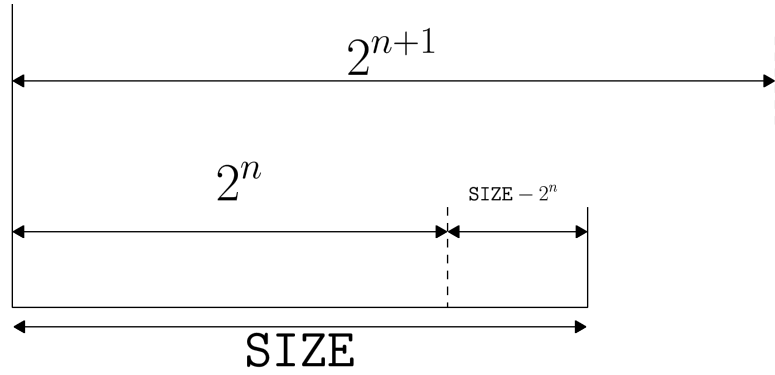


Figure 5.5: Diagram of obtaining a vector of rank **SIZE** via 2^n method. Typically 2^n is either much less than or much greater than the intended **SIZE**.

```

TV:=0 ;
LOOP I 1 N ;
    TV:=TV&TV ;
ENDLOOP ;
V:=V&TV ;

```

The remaining amount is now **SIZE**– 2^n . This entire process is then repeated, with the new **SIZE** as the remaining **SIZE**– 2^n . This is done until the length of **V** is equal to the original **SIZE**. This process may be generalized to fill a vector with some value other than zero if desired.

5.3.3 Results of the MICE Simulation.

enter data here!

CHAPTER 6
SUPPLEMENTAL INFORMATION

6.1 A Brief Review of Particle Physics

Since this dissertation concerns only muons interacting with electrons, this brief review will only cover particles with spin 1/2. This review follows [1]. Particles of four-momentum $P = (E, \vec{p}) = (E, p_x, p_y, p_z)$ must satisfy the relativistic energy-momentum relation:

$$P^\alpha P_\alpha - m^2 = 0, \quad (6.1)$$

since

$$\begin{aligned} P^\alpha P_\alpha - m^2 &= E^2 - p^2 - m^2 \\ &= E^2 - (p^2 + m^2) \\ &= E^2 - E^2 = 0. \end{aligned}$$

For particles at rest (i.e. $\vec{p} = 0$), this can be written as:

$$P^\alpha P_\alpha - m^2 = (p^0 + m)(p^0 - m) = 0,$$

and so clearly the energy $p^0 = E$ has to be either the rest mass or the negative of the rest mass (for antiparticles). However, for particles which are not at rest, if this same form is desired then it should look something like

$$P^\alpha P_\alpha - m^2 = (\gamma^\beta P_\beta + m)(\gamma^\delta P_\delta - m).$$

One may solve this equation for the coefficients $\gamma^\beta = (\gamma^0, \gamma^1, \gamma^2, \gamma^3)$, but no scalars solve this complex system. Dirac proposed that the various γ s were actually matrices, not scalars. This approach has the solution:

$$\gamma^0 = \begin{pmatrix} I_2 & 0 \\ 0 & -I_2 \end{pmatrix} \quad \gamma^j = \begin{pmatrix} 0 & \sigma^j \\ -\sigma^j & 0 \end{pmatrix},$$

where σ^j are the Pauli matrices. This leads to the Dirac equation for particles (for antiparticles, simply switch the sign of the mass):

$$\gamma^\alpha P_\alpha - m = 0. \quad (6.2)$$

These particles can be represented by the wavefunctions for free particles,

$$\psi(x) = C e^{-(i/\hbar)p \cdot x} U^{(s)}(P),$$

where C is some amplitude, U is the spinor, and s is the spin state of the particle (in this case $s = 1, 2$). Antiparticle spinors are represented by V (unused in this work). Spinor adjoints are defined by

$$\bar{U} = U^\dagger \gamma^0 = U^{*T} \gamma^0, \quad (6.3)$$

where $*$ represents the complex conjugate and T the transpose. These spinors satisfy the Diracequation:

$$(\gamma^\alpha P_\alpha - m)U = 0,$$

they are orthogonal:

$$\bar{U}^{(1)} U^{(2)} = 0,$$

and they are normalized:

$$\bar{U} U = 2m,$$

and they are complete:

$$\sum_{s=1}^2 U^{(s)} \bar{U}^{(s)} = (\gamma^\alpha P_\alpha + m). \quad (6.4)$$

These spinors are four-component column vectors, and spinors describing particles (U) and antiparticles (V) for spin 1/2 particles could be represented as, for instance

$$U^{(1)} = \begin{pmatrix} 1 \\ 0 \\ 0 \\ 0 \end{pmatrix} \quad U^{(2)} = \begin{pmatrix} 0 \\ 1 \\ 0 \\ 0 \end{pmatrix}$$

$$V^{(1)} = \begin{pmatrix} 0 \\ 0 \\ 1 \\ 0 \end{pmatrix} \quad V^{(2)} = \begin{pmatrix} 0 \\ 0 \\ 0 \\ 1 \end{pmatrix},$$

but are usually more complicated if unpolarized.

6.2 Explicit Forms of the Dirac Gamma Matrices and Pauli Matrices

From the conventions in [1] it is observed that the Pauli matrices are defined as:

$$\sigma^1 = \begin{pmatrix} 0 & 1 \\ 1 & 0 \end{pmatrix} \quad \sigma^2 = \begin{pmatrix} 0 & -i \\ i & 0 \end{pmatrix} \quad \sigma^3 = \begin{pmatrix} 1 & 0 \\ 0 & -1 \end{pmatrix}.$$

Then the Dirac matrices follow as:

$$\gamma^0 = \begin{pmatrix} 1 & 0 & 0 & 0 \\ 0 & 1 & 0 & 0 \\ 0 & 0 & -1 & 0 \\ 0 & 0 & 0 & -1 \end{pmatrix} \quad \gamma^1 = \begin{pmatrix} 0 & 0 & 0 & 1 \\ 0 & 0 & 1 & 0 \\ 0 & -1 & 0 & 0 \\ -1 & 0 & 0 & 0 \end{pmatrix} \quad (6.5)$$

$$\gamma^2 = \begin{pmatrix} 0 & 0 & 0 & -i \\ 0 & 0 & i & 0 \\ 0 & i & 0 & 0 \\ -i & 0 & 0 & 0 \end{pmatrix} \quad \gamma^3 = \begin{pmatrix} 0 & 0 & 1 & 0 \\ 0 & 0 & 0 & -1 \\ -1 & 0 & 0 & 0 \\ 0 & 1 & 0 & 0 \end{pmatrix}.$$

6.3 Proofs of Useful Dirac Gamma Matrix Trace Identities

6.3.1 Proof of $(\gamma^5)^2 = I_4$.

Let $\gamma^5 \equiv i\gamma^0\gamma^1\gamma^2\gamma^3$. Then explicitly carrying out the multiplication yields

$$\gamma^5 = i \begin{pmatrix} 0 & 0 & 0 & 1 \\ 0 & 0 & 1 & 0 \\ 0 & 1 & 0 & 0 \\ 1 & 0 & 0 & 0 \end{pmatrix} \cdot -i \begin{pmatrix} 0 & 1 & 0 & 0 \\ 1 & 0 & 0 & 0 \\ 0 & 0 & 0 & 1 \\ 0 & 0 & 1 & 0 \end{pmatrix}$$

$$\gamma^5 = \begin{pmatrix} 0 & 0 & 1 & 0 \\ 0 & 0 & 0 & 1 \\ 1 & 0 & 0 & 0 \\ 0 & 1 & 0 & 0 \end{pmatrix}. \quad (6.6)$$

Then

$$(\gamma^5)^2 = I_4. \quad (6.7)$$

6.3.2 Proof of $\gamma^5\gamma^\alpha = -\gamma^\alpha\gamma^5$.

Let the form of γ^α be represented as

$$\begin{pmatrix} A & B \\ -B & -A \end{pmatrix}$$

(i.e. for $\alpha = 0$, $A = I_2$ and $B = 0$; otherwise $A = 0$ and $B = \sigma^\alpha$). Then using the explicit form of γ^5 in Eqn. 6.6:

$$\begin{pmatrix} 0 & I_2 \\ I_2 & 0 \end{pmatrix} \begin{pmatrix} A & B \\ -B & -A \end{pmatrix} + \begin{pmatrix} A & B \\ -B & -A \end{pmatrix} \begin{pmatrix} 0 & I_2 \\ I_2 & 0 \end{pmatrix} = \begin{pmatrix} 0 & 0 \\ 0 & 0 \end{pmatrix}.$$

Therefore,

$$\gamma^5\gamma^\alpha = -\gamma^\alpha\gamma^5. \quad (6.8)$$

6.3.3 Proof of $\text{Tr}(\text{odd number of } \gamma \text{ matrices}) = 0$.

Let there be the trace of an arbitrary odd number of γ matrices

$$\text{Tr}(\gamma^{\alpha_1}\gamma^{\alpha_2}\dots\gamma^{\alpha_n}),$$

such that n is odd. Now insert into the beginning of the trace $\gamma^5\gamma^5$,

$$\text{Tr}(\gamma^5\gamma^5\gamma^{\alpha_1}\gamma^{\alpha_2}\dots\gamma^{\alpha_n}),$$

and there are two cases. The first makes use of $(\gamma^5)^2 = I_4$ (Eqn. 6.7), and results in

$$\begin{aligned} \text{Tr}(\gamma^5\gamma^5\gamma^{\alpha_1}\gamma^{\alpha_2}\dots\gamma^{\alpha_n}) &= \text{Tr}(I_4\gamma^{\alpha_1}\gamma^{\alpha_2}\dots\gamma^{\alpha_n}) \\ \text{Tr}(\gamma^5\gamma^5\gamma^{\alpha_1}\gamma^{\alpha_2}\dots\gamma^{\alpha_n}) &= \text{Tr}(\gamma^{\alpha_1}\gamma^{\alpha_2}\dots\gamma^{\alpha_n}) \end{aligned} \quad (6.9)$$

The next case uses the cyclic property of traces, which is $\text{Tr}(ABCD) = \text{Tr}(BCDA) = \text{Tr}(CDAB) = \dots$. Then

$$\text{Tr}(\gamma^5 \gamma^5 \gamma^{\alpha_1} \gamma^{\alpha_2} \dots \gamma^{\alpha_n}) = \text{Tr}(\gamma^5 \gamma^{\alpha_1} \gamma^{\alpha_2} \dots \gamma^{\alpha_n} \gamma^5).$$

Now using $\gamma^5 \gamma^\alpha = -\gamma^\alpha \gamma^5$ (Eqn. 6.8):

$$\text{Tr}(\gamma^5 \gamma^5 \gamma^{\alpha_1} \gamma^{\alpha_2} \dots \gamma^{\alpha_n}) = \text{Tr}(\gamma^5 \gamma^{\alpha_1} \gamma^{\alpha_2} \dots \gamma^5 \gamma^{\alpha_n})(-1)^1.$$

Applying this n times yields

$$\text{Tr}(\gamma^5 \gamma^5 \gamma^{\alpha_1} \gamma^{\alpha_2} \dots \gamma^{\alpha_n}) = \text{Tr}(\gamma^5 \gamma^5 \gamma^{\alpha_1} \gamma^{\alpha_2} \dots \gamma^{\alpha_n})(-1)^n.$$

Since n is negative, $(-1)^n = -1$. Again using $(\gamma^5)^2 = I_4$ (Eqn. 6.7), this yields

$$\text{Tr}(\gamma^5 \gamma^5 \gamma^{\alpha_1} \gamma^{\alpha_2} \dots \gamma^{\alpha_n}) = -\text{Tr}(\gamma^{\alpha_1} \gamma^{\alpha_2} \dots \gamma^{\alpha_n}). \quad (6.10)$$

Combining Eqns. 6.9 and 6.10:

$$\text{Tr}(\gamma^5 \gamma^5 \gamma^{\alpha_1} \gamma^{\alpha_2} \dots \gamma^{\alpha_n}) = \text{Tr}(\gamma^{\alpha_1} \gamma^{\alpha_2} \dots \gamma^{\alpha_n})$$

$$\text{Tr}(\gamma^5 \gamma^5 \gamma^{\alpha_1} \gamma^{\alpha_2} \dots \gamma^{\alpha_n}) = -\text{Tr}(\gamma^{\alpha_1} \gamma^{\alpha_2} \dots \gamma^{\alpha_n}).$$

Since this trace is both positive and negative the only conclusion is that it must be zero:

$$\text{Tr}(\gamma^{\alpha_1} \gamma^{\alpha_2} \dots \gamma^{\alpha_n}) = 0 \quad \text{for odd } n. \quad (6.11)$$

6.3.4 Proof of $\text{Tr}(\gamma^\alpha \gamma^\beta) = 4\eta^{\alpha\beta}$.

$\eta^{\alpha\beta}$ is an element of the Minkowski metric, which is defined here as

$$\eta = \begin{pmatrix} 1 & 0 & 0 & 0 \\ 0 & -1 & 0 & 0 \\ 0 & 0 & -1 & 0 \\ 0 & 0 & 0 & -1 \end{pmatrix}.$$

Unlike γ^α , $\eta^{\alpha\beta}$ is simply a number. For example, if $\alpha \neq \beta$ then $\eta^{\alpha\beta} = 0$, if $\alpha = \beta = 0$ then $\eta^{\alpha\beta} = 1$, and so on. While it can be shown explicitly, it will be treated as fact that the defining algebra is

$$\gamma^\alpha \gamma^\beta + \gamma^\beta \gamma^\alpha = 2\eta^{\alpha\beta} I_4, \quad (6.12)$$

which is simply to say that

$$\begin{aligned} (\gamma^0)^2 &= I_4 \\ (\gamma^{1,2, \text{ or } 3})^2 &= -I_4 \\ \gamma^\alpha \gamma^\beta &= 0 \quad \text{for } \alpha \neq \beta. \end{aligned}$$

Now, concerning the problem at hand

$$\text{Tr}(\gamma^\alpha \gamma^\beta) = \frac{1}{2}(\text{Tr}(\gamma^\alpha \gamma^\beta) + \text{Tr}(\gamma^\beta \gamma^\alpha)).$$

Using first the cyclic property of traces, the addition of two traces, and the defining algebra (Eqn. 6.12)

$$\begin{aligned} \text{Tr}(\gamma^\alpha \gamma^\beta) &= \frac{1}{2}(\text{Tr}(\gamma^\alpha \gamma^\beta) + \text{Tr}(\gamma^\beta \gamma^\alpha)) \\ &= \frac{1}{2}\text{Tr}(\gamma^\alpha \gamma^\beta + \gamma^\beta \gamma^\alpha) \\ &= \frac{1}{2}\text{Tr}(2\eta^{\alpha\beta} I_4). \end{aligned}$$

Finally,

$$\text{Tr}(\gamma^\alpha \gamma^\beta) = 4\eta^{\alpha\beta}. \quad (6.13)$$

6.3.5 Proof of $\text{Tr}(\gamma^\alpha \gamma^\beta \gamma^\delta \gamma^\epsilon) = 4(\eta^{\alpha\beta} \eta^{\delta\epsilon} - \eta^{\alpha\delta} \eta^{\beta\epsilon} + \eta^{\alpha\epsilon} \eta^{\beta\delta})$.

Using the defining algebra (Eqn. 6.12), commuting α and β yields that

$$\begin{aligned} \text{Tr}(\gamma^\alpha \gamma^\beta \gamma^\delta \gamma^\epsilon) &= \text{Tr}((2\eta^{\alpha\beta} - \gamma^\beta \gamma^\alpha) \gamma^\delta \gamma^\epsilon) \\ &= \text{Tr}(2\eta^{\alpha\beta} \gamma^\delta \gamma^\epsilon - \gamma^\beta \gamma^\alpha \gamma^\delta \gamma^\epsilon). \end{aligned}$$

Using the same method first for α and δ and then α and ϵ ,

$$\begin{aligned}\text{Tr}(\gamma^\alpha \gamma^\beta \gamma^\delta \gamma^\epsilon) &= \text{Tr}(2\eta^{\alpha\beta} \gamma^\delta \gamma^\epsilon - \gamma^\beta(2\eta^{\alpha\delta} - \gamma^\delta \gamma^\alpha) \gamma^\epsilon) \\ &= \text{Tr}(2\eta^{\alpha\beta} \gamma^\delta \gamma^\epsilon - 2\eta^{\alpha\delta} \gamma^\beta \gamma^\epsilon + \gamma^\beta \gamma^\delta \gamma^\alpha \gamma^\epsilon) \\ &= \text{Tr}(2\eta^{\alpha\beta} \gamma^\delta \gamma^\epsilon - 2\eta^{\alpha\delta} \gamma^\beta \gamma^\epsilon + \gamma^\beta \gamma^\delta (2\eta^{\alpha\epsilon} - \gamma^\beta \gamma^\delta \gamma^\epsilon \gamma^\alpha)) \\ &= \text{Tr}(2\eta^{\alpha\beta} \gamma^\delta \gamma^\epsilon - 2\eta^{\alpha\delta} \gamma^\beta \gamma^\epsilon + 2\eta^{\alpha\epsilon} \gamma^\beta \gamma^\delta - \gamma^\beta \gamma^\delta \gamma^\epsilon \gamma^\alpha).\end{aligned}$$

Recalling the addition properties of traces and observing Eqn. 6.13,

$$\begin{aligned}\text{Tr}(\gamma^\alpha \gamma^\beta \gamma^\delta \gamma^\epsilon) &= 2\eta^{\alpha\beta} \text{Tr}(\gamma^\delta \gamma^\epsilon) - 2\eta^{\alpha\delta} \text{Tr}(\gamma^\beta \gamma^\epsilon) + 2\eta^{\alpha\epsilon} \text{Tr}(\gamma^\beta \gamma^\delta) - \text{Tr}(\gamma^\beta \gamma^\delta \gamma^\epsilon \gamma^\alpha) \\ &= 8\eta^{\alpha\beta} \eta^{\delta\epsilon} - 8\eta^{\alpha\delta} \eta^{\beta\epsilon} + 8\eta^{\alpha\epsilon} \eta^{\beta\delta} - \text{Tr}(\gamma^\beta \gamma^\delta \gamma^\epsilon \gamma^\alpha).\end{aligned}$$

Now recalling the cyclic permutative properties of traces, it can be seen that $\text{Tr}(\gamma^\beta \gamma^\delta \gamma^\epsilon \gamma^\alpha) = \text{Tr}(\gamma^\alpha \gamma^\beta \gamma^\delta \gamma^\epsilon)$. Then it is possible to move the last term on the right side to the left side, yielding the desired outcome

$$\text{Tr}(\gamma^\alpha \gamma^\beta \gamma^\delta \gamma^\epsilon) = 4\eta^{\alpha\beta} \eta^{\delta\epsilon} - 4\eta^{\alpha\delta} \eta^{\beta\epsilon} + 4\eta^{\alpha\epsilon} \eta^{\beta\delta}. \quad (6.14)$$

6.4 Scattering Amplitude from Figure 4.2

Figure 4.2, which is reproduced here for convenience, represents a muon-electron interaction via exchange of a virtual photon from the electron vertex α to the muon vertex β .

The fermion flow is the path which goes along the directions of the arrows. For example, the first fermion flow which is observed is the muon flow: a muon enters from the left, there is an interaction at the propagator vertex β , and a muon exits from the right. Each muon contributes its spinor, and the outgoing muon and incoming muon are adjoints of one another (i.e. if the spinor of P_2 is $U(P_2)$ then the spinor of P_4 is $\bar{U}(P_4)$). The propagator vertex contributes a factor of $-ieQ_\mu \gamma^\beta$. Since matrices compound right-to-left, it is necessary to start at the end of the fermion flow and work backwards. Then the scattering amplitude is

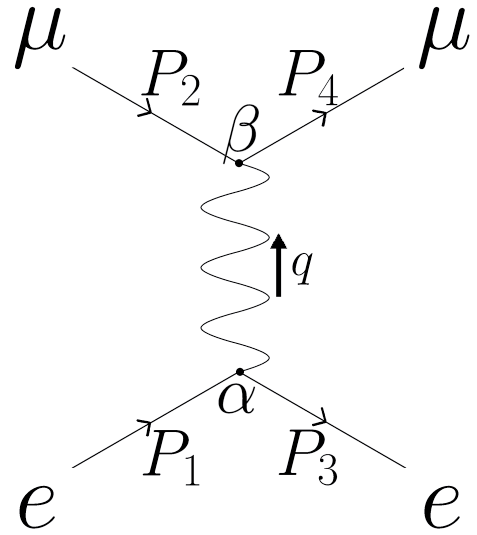


Figure 6.1: Feynman diagram for electron-muon scattering. P_1 and P_2 are the incoming four-momenta for the electron and muon and P_3 and P_4 are the outgoing four-momenta. Q represents the four-momentum carried by the virtual photon.

$$\begin{aligned}
 & \mu \quad P_2 \quad P_4 \quad \mu = \bar{U}_4(-ieQ_e\gamma^\beta)U_2 \\
 & \text{---} \\
 & \quad \quad \quad \quad \quad \quad \quad \quad \quad = \frac{i}{q^2}(-\eta_{\alpha\beta} + \frac{q_\alpha q_\beta}{q^2}) \\
 & \text{---} \\
 & e \quad P_1 \quad P_3 \quad e = \bar{U}_3(-ieQ_e\gamma^\alpha)U_1
 \end{aligned}$$

Figure 6.2: Mathematical interpretation the three branches of the Feynman diagram in Figure 6.1. The top part is the muon flow, the middle is the virtual photon, and the bottom is the electron flow.

$$i\mathcal{M} = \bar{U}_4(-ieQ_\mu\gamma^\beta)U_2 \cdot \frac{i}{q^2}(-\eta_{\alpha\beta} + \frac{q_\alpha q_\beta}{q^2}) \cdot \bar{U}_3(-ieQ_e\gamma^\alpha)U_1. \quad (6.15)$$

BIBLIOGRAPHY

- [1] D. Griffiths. *Introduction to Elementary Particles*. 2nd edition, 2008.
- [2] Pauline Gagnon. The standard model: A beautiful but flawed theory. <http://www.quantumdiaries.org>, 2014.
- [3] A.C. Melissinos. An unpublished note. Available online at "<http://www.hep.princeton.edu/mumu/physics/>", 1960.
- [4] M. Berz and K. Makino. *COSY Infinity Beam Physics Manual*, 2013. Version 9.1.
- [5] J. Nielsen and D. McMorrow. *Elements of Modern X-ray Physics*. 2nd edition, 2011.
- [6] D. Griffiths. *Introduction to Quantum Mechanics*. 2nd edition, 2005.
- [7] J. V. José and E. J. Saletan. *Classical Dynamics: A Contemporary Approach*. 1998.
- [8] G. K. O'Neill. Storage-ring synchrotron: Device for high-energy physics research. *Phys. Rev.*, 102, 1956.
- [9] P. Stehle D.B. Lichtenberg and K. R. Symon. Symon. modifications of liouville's theorem required by the presence of dissipative forces. *MURA*, 126, 1956.
- [10] Yu.M. Ado and V.I. Balbekov. Use of ionization friction in the storage of heavy particles. *Sov. Atomic Energy*, 31, 1971.
- [11] R. Fernow *et al.* Muon muon collider: A feasibility study. In *Snowmass96 workshop proceedings, chpt. 6*, 1997.
- [12] V. Highland. Some practical remarks on multiple scattering. *NIM*, 129, 1975.
- [13] J. Beringer *et al.* (PDG) PR D86, 010001 chpt. 31, 2013.
- [14] Particle Data Group Atomic Nuclear Properties. <http://pdg.lbl.gov/2014/AtomicNuclearProperties/>, 2014.
- [15] R.C. Fernow *et. al.* Icool. <http://www.cap.bnl.gov/ICOOL/fernnow/readme.html>, 2012. Version 3.30.
- [16] CERN. *GEANT4 Physics Reference Manual*, 2011. Version 9.5.0.
- [17]
- [18] Robert L. Borrelli and Courtney S. Coleman. *Differential Equations: A Modeling Perspective*. 2nd edition, 2004.
- [19] M. S. Livingston and H. A. Bethe. Chapter xvi: Auxiliary data for the evaluation of experiments. *Reviews of Modern Physics*, 9, 1937. Section C: Nuclear Dynamics, Experimental.
- [20] P. V. Vavilov. Ionization losses of high energy heavy particles. *Soviet Physics JETP*, 5, 1957.

- [21] N.W. Ashcroft and N.D. Mermin. *Solid State Physics, HRW International Editions.* 1976.
- [22] H. Bichsel. Straggling in thin silicon detectors. *Rev. Mod. Phys.*, 60, 1988.
- [23] Tom Roberts. G4beamline. <http://www.muonsinternal.com/muons3/G4beamline>, 2014. Version 2.15w.
- [24] H.W. Lewis. Multiple scattering in an infinite medium. *Phys. Rev.*, 78, 1950.
- [25] S. Goudsmit and J.L. Saunderson. Multiple scattering of electrons. *Phys. Rev.*, 57, 1939.
- [26] A. Van Ginneken. Edgeworth series for collision energy loss and multiple scattering. *NIM*, 160, 2000.
- [27] A. M. Kellerer. Calculation of energy deposition spectra. In *Proceedings of the Symposium on Microdosimetry*, 1967.
- [28] S. Hancock *et al.* Energy loss and energy straggling of protons and pions in the momentum range 0.7 to 115 gev/*c*. *Phys. Rev. A*, 28, 1983.
- [29] O. Blunck and S. Leisegang. Zum energieverlust schneller elektronen in d unnen schichten. *Z. Physik*, 128, 1950.
- [30] CERN. *GEANT - Detector Description and Simulation Tool*, 1993. Version 3.21.
- [31] D. Attwood *et al.* The scattering of muons in low z materials. *NIM*, 251, 2006.
- [32] R. Fernow and J. C. Gallardo. Muon transverse ionization cooling: Stochastic approach. *Phys. Rev. E*, 52, 1995.
- [33] U. Bravar *et at.* Mice: The muon ionization cooling experiment. In *Proceedings of the DPF-2011 Conference*, 2011.